DEVELOPMENT OF TANDEM TIME-OF-FLIGHT INSTRUMENTATION FOR THE EXAMINATION OF PROMPT PHOTODISSOCIATION OF PEPTIDES USING 193-nm RADIATION

A Dissertation

by

JOSEPH WILLIAM MORGAN

Submitted to the Office of Graduate Studies of
Texas A&M University
in partial fulfillment of the requirements for the degree of

DOCTOR OF PHILOSOPHY

December 2005

Major Subject: Chemistry

DEVELOPMENT OF TANDEM TIME-OF-FLIGHT INSTRUMENTATION FOR THE EXAMINATION OF PROMPT PHOTODISSOCIATION OF PEPTIDES USING 193-nm RADIATION

A Dissertation

by

JOSEPH WILLIAM MORGAN

Submitted to the Office of Graduate Studies of
Texas A&M University
in partial fulfillment of the requirements for the degree of

DOCTOR OF PHILOSOPHY

Approved by:

Chair of Committee,	David H. Russell
Committee Members,	D. Wayne Goodman
	Max D. Summers
	Gyula Vigh
Head of Department,	Emile A. Schweikert

December 2005

Major Subject: Chemistry

ABSTRACT

Development of Tandem Time-of-Flight Instrumentation for the Examination of Prompt Photodissociation of Peptides Using 193-nm Radiation. (December 2005)

Joseph William Morgan, B.S., Truman State University

Chair of Advisory Committee: Dr. David H. Russell

The design and incorporation of a decelerating/accelerating cell into a reflectron time-of-flight mass spectrometer is described for the examination of promptly-formed photodissociation products of peptide ions. The analytical utility of prompt 193-nm photodissociation was investigated for model peptides that resemble tryptic digest products, as well as for two sets of homologous peptides. The first of these sets include bradykinin, several bradykinin fragments, and two bradykinin mutants with substituted amino acids. Fragment ion spectra of $[M + H]^+$, $[M + Na]^+$, and $[M + Cu]^+$ were collected for each of these peptides. The second set of homologous peptides has the sequence XVGVAZG, where variable amino acid X was either arginine, histidine, or lysine, and amino acid Z was either proline, serine, or glycine. Photofragment ion spectra obtained using the new mass spectrometer are compared to results of high energy collision induced dissociation (CID) acquired on a high performance commercial instrument. The advantages and disadvantages of prompt photodissociation relative to CID are discussed, as well as the advantages of photodissociation using the modified instrument geometry versus that of the post-source decay focusing method.

DEDICATION

To my wife, Jacinda, for unconditional love and support and for making life worth living. To my parents for their assistance, faith, and encouragement.

ACKNOWLEDGMENTS

I thank my advisor, Dr. David H. Russell for providing the opportunity, tools, and latitude to perform this research and present my findings to the American Society for Mass Spectrometry at national conferences. I thank Dr. Damon C. Barbacci for the design and construction of the high performance mass spectrometer that was the template for the instrument described herein. I thank Dr. Justin M. Hettick for his promotion of this project, my training, as well as for friendship and for many invitations to partake in his culinary works. I also thank J. Garrett Slaton for synthesizing and sharing peptide samples.

For useful discussions and guidance, I appreciate Dr. Kent Gillig, Dr. John A. McLean, and Dr. William K. Russell. Special thanks to the machinists in the Texas A&M Chemistry Department, Kenneth Greer and Anthony Montalbano, for quality construction of instrument parts from my designs. Thanks to the sponsors of this work, the Department of Energy, Division of Chemical Sciences for support of photodissociation studies, the Robert A. Welch Foundation for support of metal ion studies, and The National Science Foundation Major Research Instruments Grant for funding the development of advanced time-of-flight instrumentation.

TABLE OF CONTENTS

CHAPTER Page

LIST OF FIGURES

FIGURE Page

FIGURE Page

FIGURE Page

LIST OF TABLES

CHAPTER I

INTRODUCTION

Determination of molecular structure using tandem mass spectrometry (MS) is based upon unimolecular fragmentation of the gas-phase ion [1,2]. In a tandem MS analysis, ions are formed in the mass spectrometer source then separated on the basis of mass-to-charge (m/z) ratios in a first stage mass analyzer (MS^1). Subsequent to separation, ions within a desired m/z range are isolated such that the unimolecular fragmentation product ions from a precursor of interest may be observed without contributions from undesirable precursors. The ions of interest are then subjected to excitation of internal energy modes in sufficient quantity to cause bond dissociations. Fragment ions and remaining precursor ions are then mass analyzed by using a second stage of mass analysis (MS^2). Differences in fragment ion m/z are then used to determine the composition of the selected ions of interest through identification of the neutral molecules that have been lost. A block diagram of this process is displayed in Figure 1.

Various mass spectrometer designs have been utilized for tandem MS analysis which may be categorized as either tandem-in-time or tandem-in-space [3]. Tandem-in-time designs, such as a Fourier-transform ion cyclotron resonance (FTICR) mass spectrometer [4] or a quadrupole ion trap (QIT) mass spectrometer [5], perform the

---

This dissertation follows the style and format of the *Journal of the American Society for Mass Spectrometry*.

stepwise processes mentioned above in the same space within the instrument (*e.g.* within an FTICR trapping cell). Tandem-in-space designs include triple quadrupole [6], sector [7-9], and tandem time- of-flight (TOF) [10] mass spectrometers. Instruments of this nature transmit a beam of ions to perform excitation and detection in separate areas of the mass spectrometer.

Figure 1. Block diagram of the tandem mass spectrometry experiment.

Time-of-Flight Mass Spectrometry

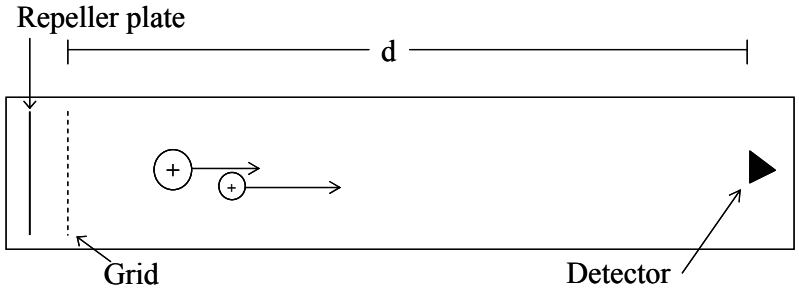

Figure 2. Simple time-of-flight mass spectrometer.

The most simple of mass analyzers is the linear TOFMS (Figure 2), consisting of an evacuated flight tube, source acceleration optics, and a detector. An electric field is created between a repeller plate and a wire mesh grid to accelerate the ions to uniform kinetic energy (*KE*). The velocity (*v*) of an ion of given m/z (*m*) is determined using Equation 1, where *e* is the charge on an electron, *z* is the number of charges on the ion,

$$v = \left(\frac{2KE}{m}\right)^{1/2} = \left(\frac{2zeV}{m}\right)^{1/2} \quad (1)$$

and V is the electric potential between the source repeller and grid. As can be seen from Equation 1, ions having low m/z values travel with greater velocities than ions of high m/z, and thus arrive at the detector with shorter times-of-flight. The TOF of an ion is simply the distance traveled in the field-free drift region (d) divided by the velocity, plus the time required for the ion to traverse the source, t_s (Equation 2).

$$t = d\left(\frac{m}{2ze}\right)^{1/2} + t_s \quad (2)$$

Although early TOF mass spectrometers were limited in the range of detectable m/z and mass resolution [11], many improvements have been made over the years. Factors that influence resolution in a TOF analysis include temporal and spatial variations in ionization and variations in initial ion velocity [12]. Time-lag focusing (*i.e.*, delayed extraction (DE)) introduced by Wiley and McLaren improves resolution for ions having the same m/z but are formed in the source at different positions or with different initial velocities [13]. Barbacci *et al*. have recently described the variables that affect resolution in a DE-TOF experiment [14]. Another major improvement in TOFMS was the development of the reflectron, or ion mirror [15]. The reflectron in a DE-RTOFMS (Figure 3) compensates for variations in kinetic energy of ions of similar m/z. Ions of higher kinetic energy penetrate the reflectron to a greater depth and have longer residence times. Ions travel a greater total distance, increasing separation of ions of

different m/z without an increase in separation of isomass ions of differing kinetic energies [16].

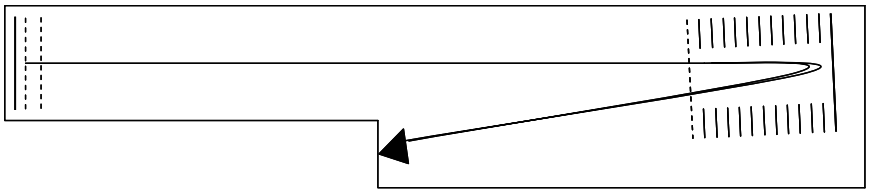

Figure 3. Schematic of a delayed extraction reflectron TOFMS.

Improvements in ionization methods have led to enhanced TOFMS performance, particularly those in which ions are formed at a surface. Early examples include fast atom bombardment (FAB) [17] and secondary ion mass spectrometry (SIMS) [18]. These desorption/ionization methods utilize projectiles having keV kinetic energies that impinge on a sample surface to cause translational and vibrational excitation at the sample-vacuum interfacial region. Neutral molecules and ions are subsequently ejected from the excited medium. The inherent nature of vibrational excitation leads to fragmentation during desorption and unimolecular decay following ion extraction from the source, placing a limit on the maximum ion m/z that may be detected. Higher m/z ions are detected in plasma desorption MS experiments [19] where spontaneous fission fragments of ^{252}Cf having MeV kinetic energies are used as projectiles; however, extensive fragmentation is still observed [20].

In recent years, the most commonly used methods for the ionization of large biological analytes such as peptides and proteins are electrospray ionization (ESI) [21] and matrix-assisted laser desorption/ionization (MALDI) [22,23]. ESI results in a wide

distribution of charge states (*e.g.*, $[M + nH]^{n+}$, where n=1,2,3…), whereas MALDI yields predominantly singly charged ions. Both are considered relatively "soft" ionization techniques, as they result in ions having low internal energies and cause very little fragmentation during the ionization process. These conditions are ideal for tandem MS experiments for the purpose of transmitting a maximum number of intact ions through MS^1 prior to excitation. An initially low and narrow internal energy distribution is desired such that the internal energy of the activated complex may be carefully controlled.

The advantages of MALDI-TOFMS are numerous. The ionization efficiency of MALDI combined with the high transmission of the TOFMS has allowed detection of attomole quantities of biomolecules [24,25]. Of all mass spectrometers, TOFMS has the highest mass range, the lowest cost, and the shortest acquisition time [26]. These properties have led MALDI-TOFMS to become the primary tool for proteomics, the analysis of the full complement of cellular proteins [27].

Biological Mass Spectrometry

Characterization of expressed proteins is routinely performed using gel or liquid separation methods, followed by enzymatic digestion and mass analysis of the resulting peptides [28,29]. The data obtained through the mass analysis step is used to identify proteins present by comparison to genomic and protein databases. This peptide mass fingerprinting (PMF) experiment, however, does not provide information necessary for the elucidation of the amino acid sequence of a peptide or protein that has not yet been entered into the database. *De novo* sequencing of peptides is also necessary when the

number of observed peptides in the PMF is too small for a database match or in the case of a post-translationally modified peptide appearing without the unmodified counterpart [30]. Fragment data obtained for peptides by tandem mass spectrometry methods may be used to further interrogate protein databases to identify the intact protein, resulting in increased confidence levels [31].

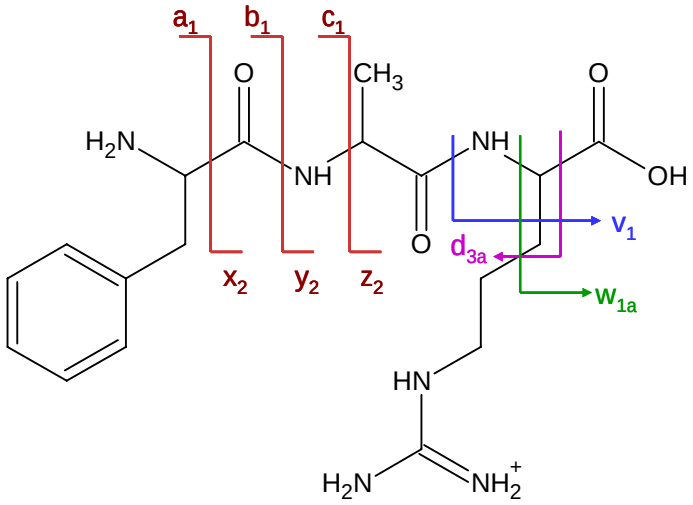

Figure 4. Fragmentation of tripeptide FAR.

Peptide ions fragment in a predictable manner following excitation, making manual amino acid sequence determination possible. Figure 4 shows examples of peptide fragmentation for the tripeptide Phe-Ala-Arg. Designations for fragment ions are given by Roepstorff and Fohlman [32], modified by Biemann [33]. Cleavages of peptide backbone bonds yield a_i, b_i, and c_i type ions when charge is retained on the N-terminal side of the dissociating bond, and x_i, y_i, and z_i type ions when charge is retained on the C-terminal side of the dissociating bond. Once identified, backbone cleavage

product ions are used to reconstruct the amino acid sequence based on the masses of the twenty common amino acid residues [34,35].

A side chain loss from an a_i-type ion yields a d_{ia}-type ion, while a side chain loss from a z_i-type ion results in a w_{ia}-type ion. These cleavages occur between the α- and β-carbons of the amino acid side chains. A side chain loss from a y_i-type ion yields a v_i-type ion. Bond cleavage to form the v_i ion occurs between the α-carbon of the amino acid side chain and the peptide backbone. Side chain cleavage product ions are useful for confirmation of backbone cleavage product ion assignments. Side chain cleavage products of type d_{ia} and w_{ia} are particularly useful for differentiating between isomass amino acid residues leucine (loss of 42 Da) and isoleucine (loss of 28 Da).

Ion Activation

The excitation step of the tandem mass spectrometry experiment is omitted when examining the products of metastable decay, utilizing only the internal energy acquired during ionization. This method is typically used only in transmitted ion beam experiments such as magnetic sector MS [36] and TOFMS [37]. A variety of excitation methods have been used within various tandem mass spectrometer designs. For example, collision induced dissociation (CID) [38,39], surface induced dissociation (SID) [40], electron capture dissociation (ECD) [41-51], and photodissociation [52-56] have all been utilized in conjunction with tandem mass spectrometry. Each excitation method has advantages and limitations which are discussed in the following paragraphs.

Collisional activation is performed by accelerating ions into a neutral background gas. CID may be performed with either multiple low energy (several eV) collisions [57]

or a single high energy (keV) collision [58]. Regardless of the ion kinetic energy the desired result is a fraction of the translational energy of the colliding ion is partitioned into its vibrational and/or electronic internal energy modes. The maximum quantity of energy that can be imparted to the ion occurs through a center-of-mass collision (E_{com}), which can be calculated using Equation 3, where m_N is the mass of the inert gas molecule or atom, m_i is the mass of the impinging ion, and E_{lab} is the kinetic energy of the ion.

$$E_{com} = \left(\frac{m_N}{m_N + m_i} \right) E_{lab} \tag{3}$$

Note that as the mass of the ion increases, the maximum quantity of energy that may be deposited decreases for a given ion kinetic energy [59,60]. A higher mass target gas (*e.g.* Ar rather than He) may be used to compensate for this effect to a small degree. Polyatomic molecules are not good candidates for target gases, as collision will result in vibrational activation of the target. Another disadvantage of CID is the loss of ion kinetic energy due to the inherent nature of partitioning this energy into internal energy through inelastic collision, as well as through elastic scattering [61,62]. Variation in the extent of conversion of kinetic energy into internal energy causes an increase in the distribution width of ion velocities, which negatively influences mass measurement accuracy and resolution in a tandem TOFMS experiment by increasing the widths of arrival time distributions. Likewise, collisional activation results in a wide distribution

of ion internal energies, ranging from a few meV to several eV, with a maximum internal energy resulting from a center-of-mass collision [57].

Energy deposition is more efficient when using a surface as the neutral target, as all ions collide with the target and unlike collision with a gas, energy is not significantly partitioned into translation of the target [63]. In the SID experiment, ions inelastically collide with a surface (optimally a self-assembled monolayer on a noble metal substrate [57,64]). A fraction of the kinetic energy that is lost by the impinging ions during the collision is partitioned into internal energy modes, the newly acquired internal energy is redistributed among all available oscillators, then ions dissociate subsequent to leaving the surface [65]. At low ion-surface collision energies, trapping-desorption occurs [66]. Trapping-desorption is the process of ions sticking to the surface for a finite length of time, followed by release of the activated ions. The ion-surface interaction time is not constant for all ions, and desorption occurs in a wide distribution of angles and kinetic energies. As the projectile kinetic energy is increased, prompt fragmentation during ion-surface interaction becomes competitive with unimolecular decay following ion recoil [67-73], causing variation in fragment ion formation times. Levine, Futrell, Hanley, Hase and their coworkers have chosen the term "shattering" to describe prompt fragmentation in the SID experiment. Unfortunately, the term "shattering" implies the absence of intramolecular vibrational energy redistribution prior to fragmentation, which has not been well established by experiments reported. Quasi-equilibrium theory [1] describes prompt fragmentation in terms of simple bond cleavages. At high internal energies, simple bond cleavage is kinetically favored over rearrangement reactions that

involve a coordinated, or "tight", transition state [1]. Although fragmentation via a tight transition state may be lower in enthalpy, the simple bond cleavage is entropically favored for ions having high internal energies. Trapping-desorption and prompt fragmentation in the SID experiment are incompatible with most tandem mass spectrometer designs and result in decreases in resolution and accuracy.

Photodissociation

A more precise method of ion fragmentation in a tandem MS experiment is photodissociation. Photodissociation may be performed by using various sources of light. The earliest photodissociation experiments were performed in an FTICR-MS and utilized a broadband xenon arc lamp with a monochromator for wavelength selection [74-77]. The development of lasers over the last three decades provides a wide selection of wavelengths to best fit the requirements of tandem MS experiments. For example, continuous wave CO_2 lasers are commonly employed for infrared multiphoton dissociation (IRMPD) in QIT mass spectrometers [54] and in FTICR-MS [78,79]. Ion trapping is required for the IRMPD experiment, as significant time is necessary to absorb a sufficient number of photons to achieve a critical internal energy for dissociation. Infrared photons having wavelengths of approximately 10 μm (0.12 eV) [80] deposit energy into vibrational modes of the ion and no transition from the electronic ground state (S_0) occurs. Dissociation of the lowest energy bonds takes place when a vibrational energy level above the thermodynamic threshold is reached. This process, shown in the potential energy diagram in Figure 5, is similar to that of dissociation via multiple low energy collisions [81,82].

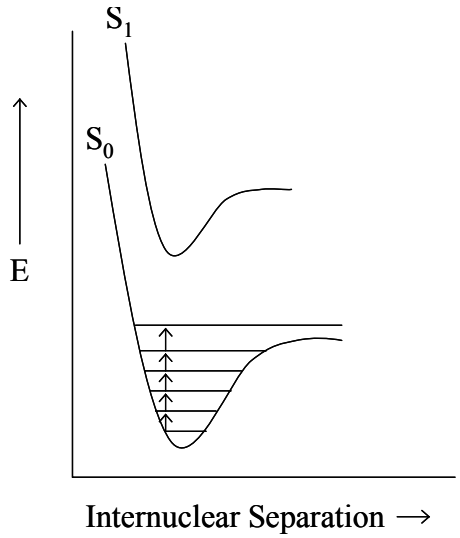

Figure 5. Potential energy diagram of IRMPD.

Pulsed ultraviolet (UV) lasers such as a frequency quadrupled neodymium: yttrium aluminum garnet (Nd:YAG) [83] or an excimer [84,85] are more compatible with transmitted ion beam mass spectrometers. Interaction time between the ion packet and the laser beam is relatively short, so photon energy and density must be sufficiently high to induce fragmentation. The excimer laser operates through the radiative decay of an excited dimer created through the association of a halogen anion and a rare gas cation, as shown in Figure 6.

The quantity of energy, E (eV), imparted to an ion absorbing a photon having wavelength λ (m) may be calculated using Equation 4. In this equation, *h* represents Planck's constant, *c* is the speed of light, and *e* is the charge on an electron.

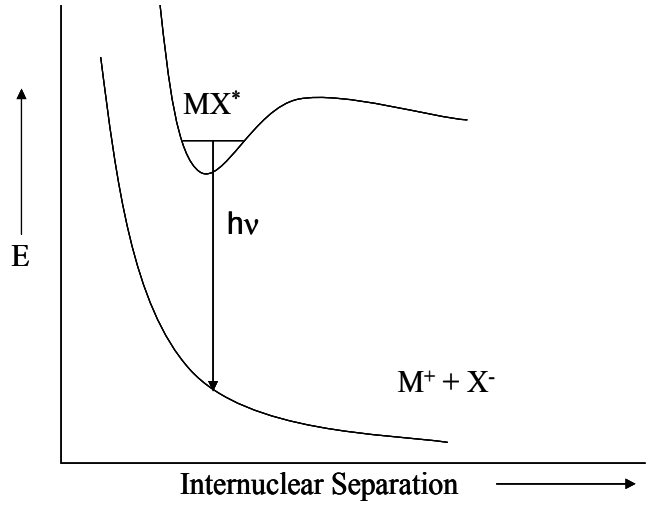

Figure 6. Potential energy diagram of excimer radiative decay.

$$E = \frac{hc}{e\lambda} \tag{4}$$

Emission wavelengths and calculated energies per photon for selected excimer laser systems are shown in Table 1 [86,87]. The ArF excimer laser is an attractive choice for photodissociation studies of peptide ions [88], because amide linkages in peptide and protein molecules act as chromophores for 193-nm radiation [89], allowing activation between each amino acid residue. Aromatic amino acid side chains strongly absorb UV light as well [90]. Absorption of a 193-nm photon increases the ion internal energy by 6.43 eV, which is in excess of the enthalpies of the carbon-carbon and carbon-nitrogen bonds (3.61 eV and 3.16 eV, respectively) that comprise the peptide backbone [91]. An additional advantage of the ArF excimer laser for UV photodissociation is that 193-nm light is absorbed by molecular oxygen in the atmosphere to a much lower degree

than shorter wavelength radiation, eliminating the necessity for vacuum containment of the laser beam [92].

Table 1. Wavelengths and photon energies for excimer species.

Excimer	Wavelength (nm)	Energy (eV)
HgCl	558	2.2
HgBr	503	2.5
HgI	444	2.8
XeF	351	3.5
XeCl	308	4.0
XeBr	292	4.3
KrF	248	5.0
KrCl	222	5.6
KrBr	203	6.1
KrI	185	6.7
ArF	193	6.4
ArCl	172	7.2
ArBr	161	7.7
F_2	157	7.9
NeF	107	11.6

Several processes may occur subsequent to UV photon absorption that lead to bond dissociation [93]. Direct photodissociation occurs either upon excitation to a region of a potential energy surface that is greater than the dissociation limit or excitation to a repulsive potential energy surface (Figure 7). Photodissociation may also occur via indirect processes, as shown in Figure 8. In the first example, the activated ion releases a photon to decay from a bound excited state to an upper vibrational level of the electronic ground state having sufficient energy for dissociation. A second indirect

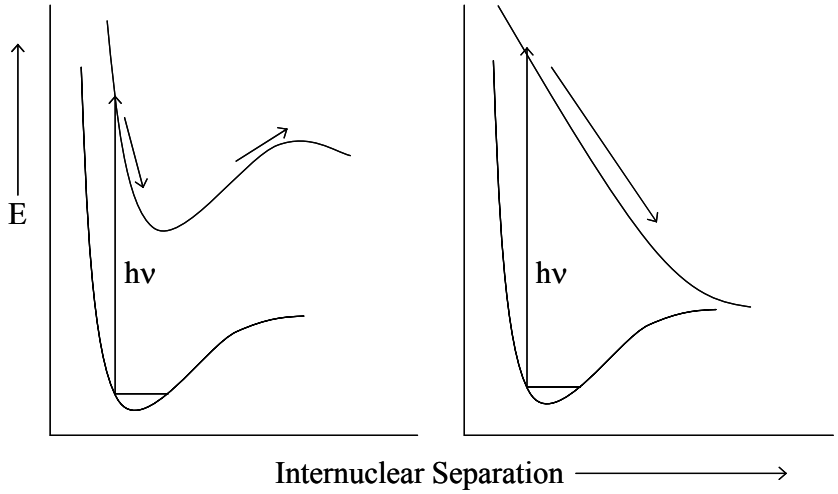

Figure 7. Examples of direct photodissociation.

photodissociation mechanism, known as "predissociation", occurs when a bound excited state undergoes an intersystem crossing to a dissociative state or through internal conversion to a lower electronic state with sufficient vibrational energy for dissociation.

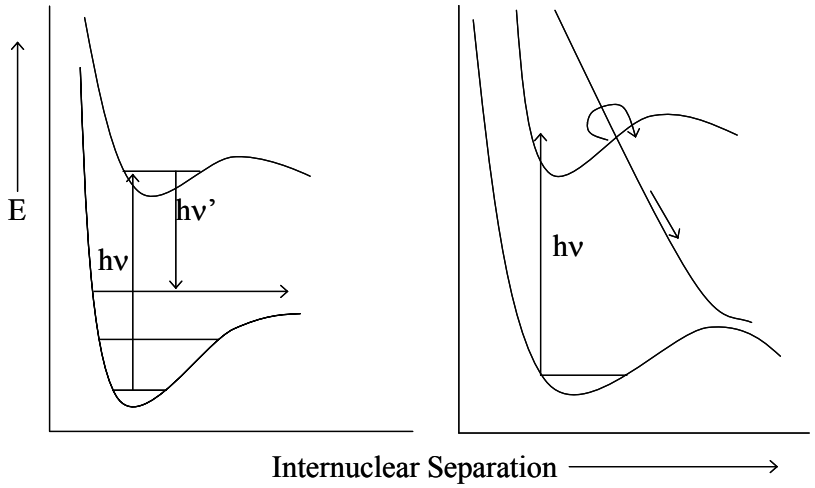

Figure 8. Examples of indirect photodissociation.

Direct photodissociation processes occur promptly (on the timescale of a few vibrations) whereas indirect photodissociation occurs subsequent to intramolecular

vibrational energy redistribution [93,94]. The dissociation mechanism that dominates is dependent upon the quanta of energy deposited by the photon and the vibrational energy level of the electronic excited state that is populated by the Franck-Condon (*i.e.* vertical) transition [95]. For non-rigid molecules such as peptides and proteins, indirect dissociation processes are more likely because many oscillators are present in which to redistribute vibrational energy [96,97].

$$k(E) = \nu\left(\frac{E - E_0}{E}\right)^{s-1} \tag{5}$$

The rate of dissociation at a given internal energy, k(E), of an ion in a bound electronic excited state may be calculated using statistical rate theory as described by Rice, Ramsperger, and Kassel [98]. In Equation 5, E_0 is the energy required for the dissociation of a particular bond, ν is the vibrational frequency of that oscillator, E is the total internal energy, and s is the total number of oscillators present in the molecule. The rate of dissociation decreases as the number of oscillators (*i.e.* degrees of freedom) is increased, and dissociation rate increases as internal energy increases.

The relationship between unimolecular dissociation rate and activation energy is illustrated by the Wahrhaftig diagram in Figure 9 (adapted from [1]). As the precursor ion internal energy increases, the formation of a different set of fragmentation products may become kinetically favored. In the general example shown, the rate of dissociation of M^+ to form products C^+ and D becomes greater than the rate of dissociation to form A^+ and B as the internal energy of M^+ increases. In this example, C^+ and D may result

from an entropically favored simple bond cleavage while A^+ and B may be produced following a rearrangement. The rearrangement reaction may have a lower enthalpy, but the dissociation rate is limited by a tight transition state [1].

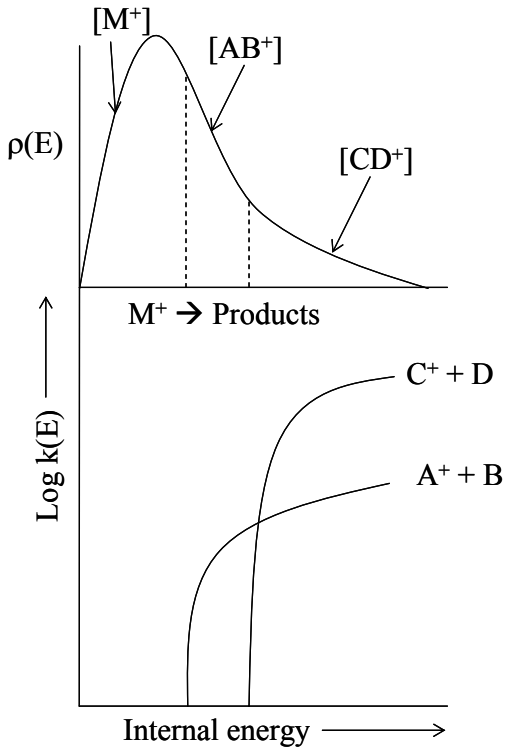

Figure 9. Wahrhaftig diagram of the relationship between unimolecular dissociation rate (k(E)) and precursor ion internal energy.

Early photodissociation experiments in our laboratory were aimed at establishing the utility of this activation method in conjunction with transmitted ion beam tandem mass spectrometers. Tecklenburg *et al.* utilized a sector instrument with a biased activation cell to investigate the fragmentation of dinitrophenyl (DNP) derivitized amino acids upon absorption of low energy UV and visible photons [53]. These studies established that DNP-leucine and DNP-isoleucine could be differentiated based on their photodissociation products. Experiments by Gimon-Kinsel *et al*. using a two-stage

linear TOF examined 193-nm photodissociation of peptides and proteins [99,100]. Precursor ions were isolated and irradiated at the end of the first TOF mass analyzer, and the remaining precursors and resulting fragment ions were reaccelerated approximately one microsecond after photoactivation. Fragment ions and neutrals were thus separated from the precursor ions prior to detection. Although fragment ion masses could not be determined, a dissociation rate in excess of 10^6 s^{-1} demonstrated the viability of combining 193-nm photodissociation of biological molecules with tandem TOFMS.

A reflectron TOF mass spectrometer was later designed in our laboratory for the mass analysis of photofragment ions [101,102]. Using this instrument, MALDI-formed ions were separated after delayed extraction into a 0.52 m first stage TOF, followed by isolation of the ions of interest and 193-nm photoactivation. A 0.9 m field-free drift region between the ion activation plane and the entrance grid of the reflectron provided approximately 10 μs for unimolecular decay of the activated ions. PSD focusing [103] was used to collect photofragment ion spectra. Sequence informative photofragment ions as well as side chain cleavage products were recorded with high mass accuracy and resolution; however, the analytical utility of the instrument was limited by several distinct disadvantages. Metastable ions formed in the first field free region contributed to the tandem mass spectra acquired, as well as photofragment ions of the metastable ion precursors. Post source decay focusing requires that several (>10) mass spectra are acquired at different reflectron voltages, followed by truncation and splicing, to obtain a complete photofragment ion spectrum, resulting in a high instrument duty cycle.

Additionally, the long fragmentation timescale caused the observation of ions resulting from low energy, metastable decay.

The purpose of the research described here is to improve upon TOF instrumentation used for photodissociation of peptide ions. Specifically, the goals include: (1) increasing experimental throughput and (2) decreasing contributions from metastable decay products to the photofragment ion spectra. The new mass spectrometer utilizes the design of Barbacci *et al*. [101,102] with the addition of a decelerating/ accelerating photodissociation cell centered about the photoactivation plane. Briefly, the benefits include rejection of low mass metastable ions prior to photoactivation of the ions of interest, the observation of only those ions formed through relatively fast fragmentation channels (*i.e.* $k(E) > 10^6\ s^{-1}$), and acquisition of a complete photofragment ion spectrum for each desorption/ionization event. The advantages of this design, as well as the advantages of prompt 193-nm photodissociation, are discussed in subsequent chapters.

Chapter II describes the design of the photodissociation MALDI TOF-TOFMS and illustrates the analytical utility of this instrument for studies of peptide fragmentation chemistry using tryptic and non-tryptic peptides. Chapter III contains tandem mass spectra of the promptly formed 193-nm photofragment ions of bradykinin and nine bradykinin analogues containing three charge carriers, $[M + H]^+$, $[M + Na]^+$, and $[M + Cu]^+$. Comparisons are made between photofragment ion spectra and high energy CID TOF-TOF spectra of these peptide ions to further illustrate the analytical utility of 193-nm photodissociation of peptide ions and to determine differences in

fragmentation chemistry of similar ions with different internal energies. It is important to note that a spectrum from the CID TOF-TOFMS used for these experiments is a composite of fragment ions resulting from both metastable decay as well as high energy CID, whereas a spectrum obtained using the photodissociation TOF-TOFMS contains very little fragment ions resulting from metastable decay. To differentiate between these two very dissimilar TOF-TOF mass spectrometers, data obtained using the photodissociation instrument will henceforth be referred to as "prompt photofragment ion spectra". Tandem mass spectra obtained using the method described by Barbacci *et al*. are referred to as "PSD focusing photofragment ion spectra".

Chapter IV compares the prompt photofragment ion spectra and high energy CID TOF-TOF spectra of synthetic homologous peptides having the sequence XVGVAZG, where amino acid X varies between arginine, histidine, and lysine and amino acid Z varies between proline, serine, and glycine. These peptides were chosen owing to the presence of charge-localizing basic residues at the N-termini to further illustrate differences in fragmentation chemistry of similar peptide ions with different internal energies and fragmentation timescales. Chapter V contains a comparison of photofragment ion spectra acquired with two different fragmentation timescales and shows examples of the prompt 193-nm photodissociation of phosphorylated peptides. Chapter VI contains a summary, conclusions, and future directions for these experiments.

CHAPTER II

MALDI-TOF-TOFMS DESIGN FOR PROMPT FRAGMENTATION OF PEPTIDES BY 193-NM PHOTODISSOCIATION

Introduction

Matrix-assisted laser desorption/ionization (MALDI) [22,23] combined with TOFMS is a powerful technique for rapid analysis of biological molecules. The integration of a reflectron [15] and use of delayed extraction [104,105] permit high mass measurement accuracy (~10 ppm) and resolution (in excess of 14,000 (m/Δm)) for ions having m/z up to 2000 Da [14,28,106-108], which have led to widespread use of TOFMS for proteome analysis [109-111].

Proteins that contain post-translational modifications, or those not predicted by a recorded genome, must be identified using tandem mass spectrometry. Typically, peptide ions of interest are mass-selected by the first mass analyzer (MS^1), activated by collisions with a neutral buffer gas (collision-induced dissociation (CID)), and the resulting fragment ions are then mass analyzed by MS^2. The amino acid sequence is then determined by manual inspection of the data [30], or via database searching [109-111]. Although CID has several limitations, it is the most commonly employed method for tandem MS analysis [38,39]. For example, activation through single or multiple low energy collisions, such as performed in a quadrupole ion trap or Fourier transform ion cyclotron resonance mass spectrometer, results in fragmentation via the lowest energy dissociation pathways (e.g. b_i- and y_i-type ions) [32,33]. In some cases, relatively few ion signals are present in the CID spectra, because these dissociation channels have

significantly lower energy requirements [112]. An increase in collision energy or the numbers of collisions can result in a greater number of sequence informative fragment ions [58] (e.g. a_i-, c_i-, x_i-, d_{ia}-, and w_{ia}-type ions), but this also causes an increase in non-sequence informative ions. The presence of ions arising from small neutral loss from sequence informative ions and internal fragment ions in tandem mass spectra complicate *de novo* sequencing. Another important consequence of CID coupled to TOFMS is the kinetic energy loss [61] through momentum transfer to the neutral gas molecules and loss of ions through scattering processes [38]. Kinetic energy loss causes an increase in the distributions of velocities of isomass ions, resulting in decreased mass measurement accuracy and resolution.

A viable alternative to CID for tandem MS analysis of peptide ions is photodissociation. Photon absorption does not affect ion kinetic energy [113], and ultrahigh vacuum is maintained in the mass spectrometer. Previous experiments in our laboratory have shown the utility of UV photodissociation for peptide sequencing [102,114]. Gimon-Kinsel *et al*. [99] have demonstrated 193-nm photodissociation rates greater than 10^6 s^{-1} for high m/z peptide ions, owing to the fact that each amide bond along the peptide ion backbone and several amino acid side chains act as natural chromophores for 193-nm radiation [88,90,115]. An energy deposition of 6.43 eV/photon is sufficient to produce sequence informative ions of (a_i, b_i, x_i, and y_i) as well as side chain cleavage product ions (especially v_i, w_{ia}, and d_{ia}). Recent experiments by Thompson *et al*. [116,117] using 157-nm irradiation from an F_2 excimer laser also demonstrate the utility of this method.

Our previously reported photodissociation TOFMS experiments were performed using the PSD focusing method [103] for mass analysis of photofragment ions. A disadvantage of PSD focusing is the appearance of metastable decay products in the tandem mass spectrum, as well as the inclusion of photofragment ions of PSD products formed within the first field-free drift region of the mass spectrometer. Additionally, the PSD focusing method requires acquisition of many summed spectra at various reflectron voltage settings in order to observe all fragment ions, resulting in a high instrument duty cycle [103].

The instrument described herein makes use of post-source acceleration to separate ions of interest from their metastable decay products formed in the first drift region. Promptly-formed photofragment ions along with the ions of interest are reaccelerated into the second mass analyzer approximately 1 μs after photoactivation, eliminating both the need for spectral splicing and the appearance of metastable decay product ions formed in the second field-free region of the mass spectrometer.

Proteomic analysis typically involves enzymatic digestion of proteins using the site specific protease trypsin, which causes cleavage at the C-terminal side of each arginine and lysine amino acid residue. Resulting peptides thus have basic residues at the C-termini, with the exception of the peptide produced from the C-terminal end of the protein. Four synthetic peptides that fit this criterion were chosen to demonstrate the potential of 193-nm photodissociation mass spectrometry for the analysis of biological molecules. The utility of this method for additional analyte classes is demonstrated using a set of peptides with basic N-terminal amino acids.

Photodissociation MALDI-TOF-TOFMS

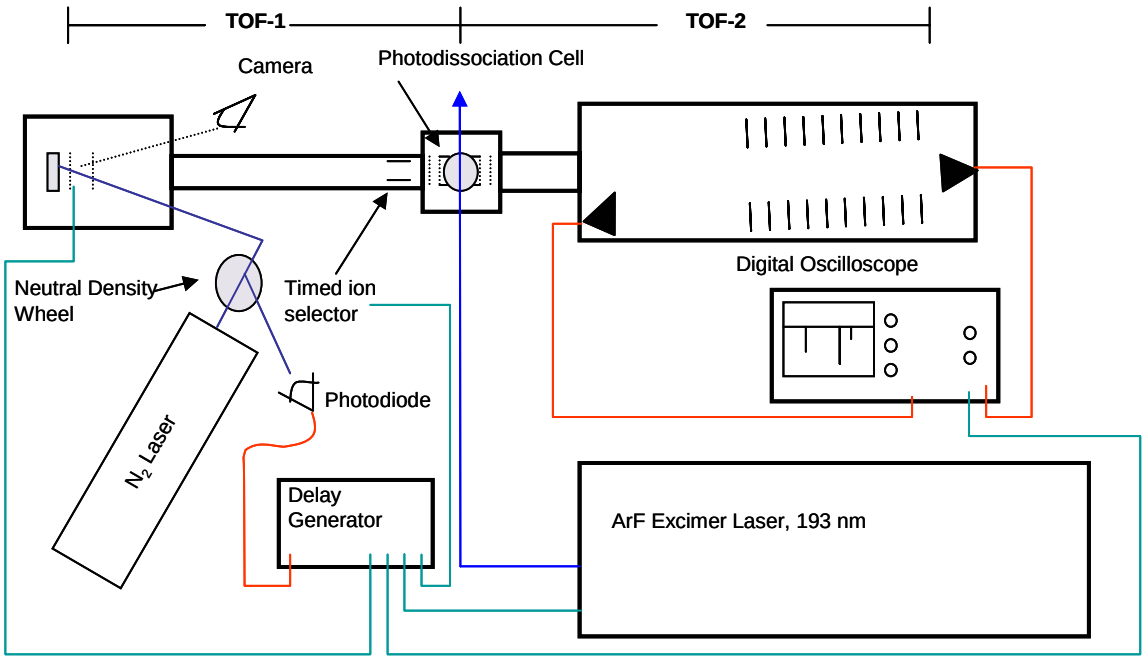

Figure 10. Schematic diagram of the photodissociation MALDI-TOF-TOFMS apparatus.

The instrument, shown schematically in Figure 10, is a homebuilt DE MALDI reflectron TOFMS contained in a stainless steel vacuum system (baseline pressure $1x10^{-8}$ Torr) maintained by two turbomolecular pumps [101]. Pumping speeds are 330 L/s for the ionization source pump (TPH 330, Pfeiffer Vacuum Technology, Inc., Nashua, NH) and 170 L/s for the analyzer pump (TPU 170, Pfeiffer). Backing pressure for the turbo pumps is maintained by two mechanical pumps (2004A, 2012A, Alcatel Vacuum Products, Hingham, MA).

The MALDI sample plate is introduced into the main vacuum chamber through a gated sample inlet system, and is held in place by an assembly consisting of two

precision steel translation stages (UMR8.51, Newport Corp., Irvine, CA) allowing 51 mm of motion in both x and y directions [101]. The sample plate is positioned by operation of two linear motion feedthroughs (BLM-133-2, MDC Corp., Hayward, CA). The DE source is composed of two 70 line per inch (l.p.i.) nickel mesh grids (MN17, Precision Eforming LLC, Cortland, NY) stretched over 19 mm apertures formed by ring electrodes. The spacing for the two source grids is 3 mm and 20 mm from the MALDI plate. A CCD camera (Watec WAT-502A, Edmund Scientific Co., Barrington, NJ) with variable zoom lens (Zoom 6000, Navitar, Inc., Rochester, NY) is used to view the sample stage through a window in the source vacuum chamber.

MALDI is performed using a nitrogen laser (VSL-337ND, Laser Science, Inc., Franklin, MA) directed at the sample spot at a 20° angle of incidence. Laser beam diameter is controlled by a mechanical iris, and photon density is attenuated by using a neutral density wheel (28660, Oriel Corp., Stratford, CT). Start time for the TOF experiment is defined by a signal from a photodiode (DET200, ThorLabs, Inc., Newton, NJ) that captures a reflection of the desorption laser beam from the neutral density wheel. This signal is used as T0 for a digital delay generator (9650, EG&G PARC, Princeton, NJ) which controls timing of output pulses for the high voltage switches for delayed extraction (Behlke HTS300, Eurotek, Inc., Morganville, NJ), the timed-ion-selector (TIS) (Behlke HTS 31, Eurotek, Inc., Morganville, NJ), and the output pulse that triggers the photodissociation laser (LPX-120i, Lambda Physik, Acton, MA). The timing of the digital delay generator output pulses are stable to within 2 ns and the

excimer laser has a jitter of less than one ns, both of which are critical features of this experiment [101].

The TIS and photodissociation window are located at distances of 0.52 m and 0.58 m from the ion source, respectively. The linear-field reflectron is 0.5 m in length and is set at 1.5° off-axis with respect to the ion beam. The distance from the exit of the photodissociation cell to the entrance of the reflectron is 0.9 m. The 25 mm microchannel plate detector (Advanced TOF, Burle Technologies, Inc., Sturbridge, MA) is located 0.5 m from the exit of the reflectron. The effective flight path length of the reflectron TOF-MS is 3.9 m.

Potentials are applied to the source repeller plate, extraction grid, and reflectron by three high voltage power supplies (RR30-1.5R/DDPM, Gamma High Voltage Corp., Ormond Beach, FL) capable of 30 kV, positive or negative. The detector and timed-ion selector are biased with 3 kV power supplies (RR3-15R/DDPM, Gamma High Voltage Corp., Ormond Beach, FL). Power supply output voltages are set by 16 bit digital-to-analog converters (DAC) which are controlled by a PC via a digital I/O card (PC DIO-96, National Instruments, Austin, TX) using software written in-house with LabWindows CVI (National Instruments, Austin, TX). Delay generator pulse times are set via GPIB from the PC.

A deceleration/acceleration photodissociation cell was designed using SIMION 7.0 (Scientific Instrument Services, Inc., Ringoes, NJ) (Appendix A). Drawings of parts for construction of the apparatus (Appendix B) were created using AutoCAD 2002 software (Autodesk, Inc., San Rafael, CA). The photodissociation cell (Figure 11)

consists of a central lens element and four 70 l.p.i. nickel mesh grids. Two grids held at the same potential as the central element are each held in place by a ring electrode that makes a press fit into the central element. Machinable ceramic (MACOR) is used to mount the central element, and six MACOR spacers are used to separate the electrodes. Grids mounted on two cylindrical electrodes define the potentials of the front and back ends of the photodissociation cell. These two electrodes are grounded to the vacuum system in the three-way cross where the photodissociation window is mounted. The photodissociation cell is held together by three threaded rods. Spacing between grids that define the two electric fields is 10 mm, and the complete cell is 100 mm in length. Potential is applied to the central element of the photodissociation cell using a 30 kV power supply (RR30-1.5R/DDMP, Gamma High Voltage Corp., Ormond Beach, FL).

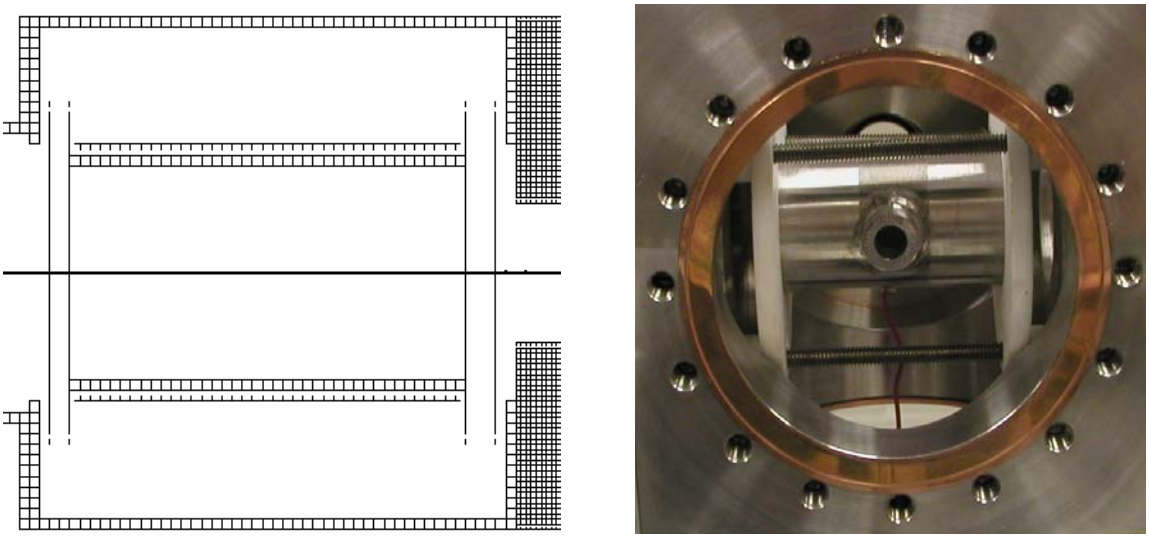

Figure 11. SIMION rendering and photograph of the photodissociation cell.

Photodissociation Tandem MS Experiment

MALDI-formed ions are accelerated by the ion source to 15 keV and m/z selected at the end of the first field-free drift region (TOF-1) by the TIS. Delay time and the first source grid potential are adjusted such that the ions of interest are temporally focused at the photodissociation window [14]. Selected ions are decelerated to 7 keV as they enter the photodissociation cell where they are irradiated by a pulse of 193-nm photons from the ArF excimer laser. The excimer laser is operated in constant energy mode, set to 70-100 mJ per pulse as measured at the laser aperture by an internal power meter. The laser beam is reflected by a mirror, passed through a mechanical iris, and focused with a plano-convex lens (30 cm focal length) prior to passing through the photodissociation window. The laser beam energy at the intersection with the ion beam is approximately 500 μJ as measured by a pyroelectric joule meter (Vector D200P, Scientech Inc., Boulder, CO). The laser beam dimensions at the intersection with the ion beam are 5 mm in height by 0.25 mm in width, resulting in an approximate irradiance of 2×10^6 /cm^2.

A fraction of photoactivated ions dissociate as they traverse the remaining field-free length of the central photodissociation cell element. An ion having m/z 1000 traverses this 4 cm in 1.0 μs, thus photodissociation must occur at a minimum rate of 1×10^6 s^{-1}. Upon exiting this region precursor ions and photofragment ions are accelerated into reflectron TOF-2 by an 8 kV electric field. For tandem MS experiments, the reflectron voltage is held at the same potential as the ion source such

that all ions having m/z up to and including the parent ion m/z are spatially focused at the detector, and maximum resolution is achieved for photofragment ions.

The signal output of the microchannel plate detector is acquired using a 1 GHz digital storage oscilloscope (LC574AM, LeCroy Corp., Chestnut Ridge, NY), and this data is transferred to a PC via GPIB interface. Data from the oscilloscope is converted to an ASCII X-Y data set using the Grams/32 spectral conversion tool (Galactic Industries Corp., Salem, NH) and imported into SigmaPlot (SPSS Inc., Chicago, IL).

Photofragment ions formed within the photodissociation cell have identical velocities to the selected ions of interest, and thus are variable in kinetic energy. The variation in kinetic energy is small relative to overall kinetic energy of the ions analyzed by TOF-2, but must be accounted for in the calibration. Since the kinetic energy of an ion of a given velocity is directly proportional to m/z, the kinetic energy of a fragment ion prior to exiting the photodissociation cell can be expressed as $KE_i = e(V_1 - V_0)(m_f/m_p)$, where V_1 and V_0 are the electric potentials applied to the central element of the photodissociation cell and the source plate, respectively, m_f is the m/z of the fragment ion, m_p is the m/z of the parent ion, and e is the charge of an electron. The kinetic energy of the fragment ion subsequent to exiting the photodissociation cell is $KE_f = e(V_1 - V_0)(m_f/m_p) + eV_1$. The term eV_1 corresponds to the kinetic energy added to the ion by the accelerating electric field. From the expression $KE = \frac{1}{2}mv^2$ we derive an expression for TOF, $t = d(m_f/2KE_f)^{1/2}$, where d is the effective flight path length of TOF-2. Substituting the above expression for KE_f results in a new expression for TOF, equation (6).

$$t = \frac{d}{\sqrt{2}}\left(\frac{m_f}{e(V_1 - V_0)(m_f / m_p) + eV_1}\right)^{\frac{1}{2}} \quad (6)$$

In general terms, $t = a(m_f/(bm_f + c))^{1/2} + t_0$. Parameters *a* and *c* are constant for given mass spectrometer dimensions and voltages for the source and photodissociation cell. Parameter *b* is inversely proportional to the m/z of the parent ion and the intercept (t_0) is directly proportional to the square root of the m/z of the parent ion. Regression analysis using SigmaPlot software is performed to determine parameter values using m/z versus measured TOF from a tandem mass spectrum of a precursor having known photofragment ions (Figure 12).

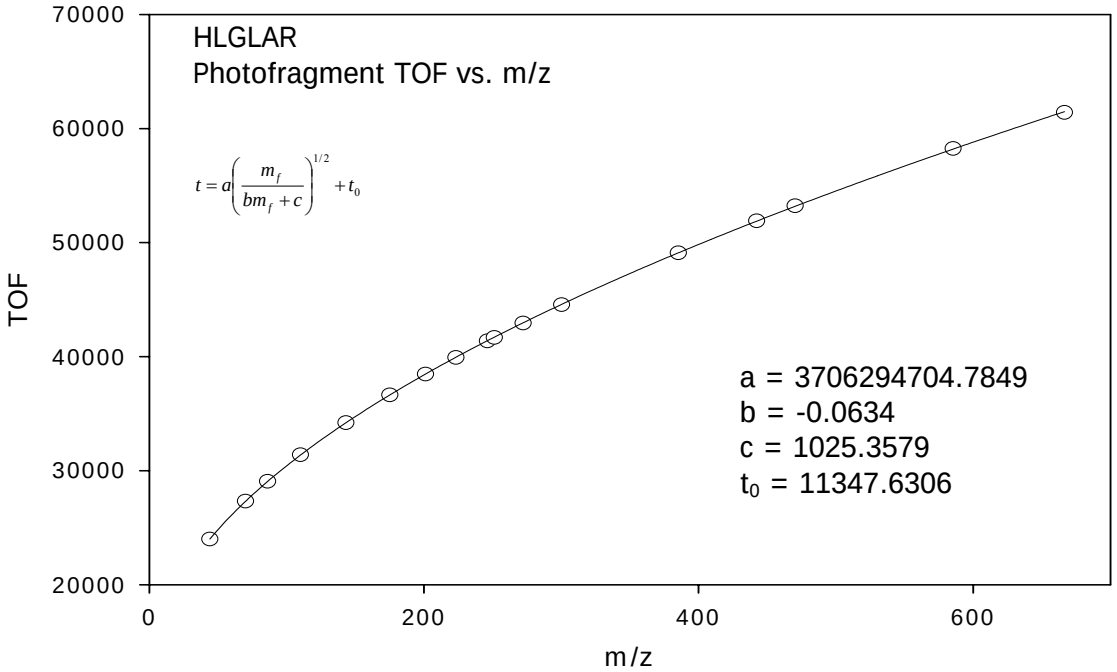

Figure 12. Regression analysis plot for photofragment ions of peptide HLGLAR.

Parameter *b* is plotted as a function of $1/m_p$, and t_0 is plotted as a function of $m_p^{½}$ for several photodissociation standards (Figure 13). Linear equations derived from these plots are used to determine parameter *b* and t_0 values for unknowns based on measured parent ion m/z.

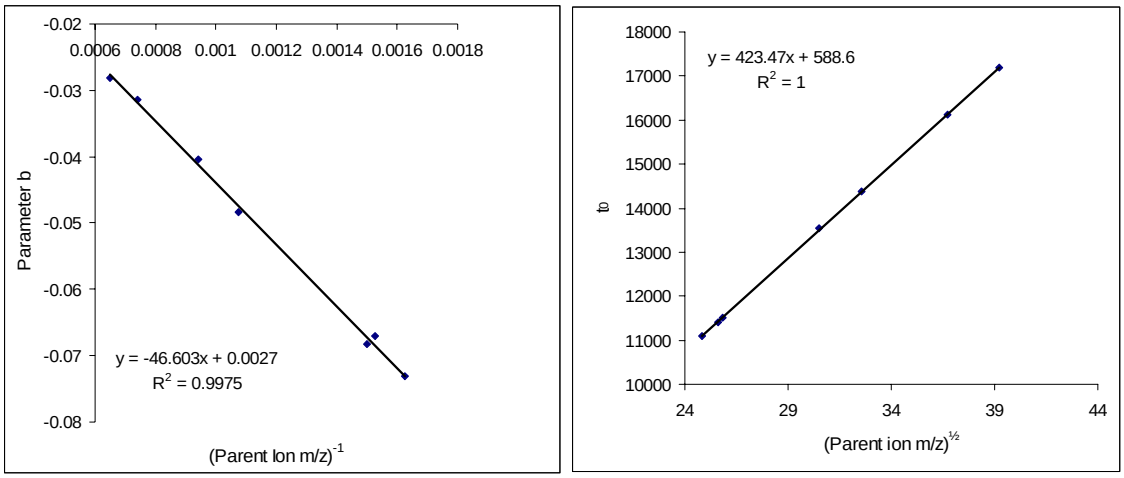

Figure 13. Calibration plots for photodissociation TOF-TOFMS.

Peptides [D-Ala^2, Leu^5, Arg^6] enkephalin (YAGFLR), dynorphin A fragment 1-6 (YGGFLR), VPDPR, VGVRVR, C-telopeptide (EKAHDGGR), [Tyr^5, D-Trp^{6,8,9}, Arg^{10}] neurokinin fragment 4-10 amide (DYWVWWR-NH_2), laminin fragment 925-933 (CDPGYIGSR), and [D-Tyr^{27,36}, D-Thr^{32}] neuropeptide Y fragment 27-36 amide (YINLITRQRY-NH_2) were obtained from American Peptide Company (Sunnyvale, CA). HLGLAR, angiotensin I (DRVYIHPFHL), angiotensin II (DRVYIHPF), angiotensin III (RVYIHPF), Val^4-angiotensin III (RVYVHPF), substance P amide (RPKPQQFFGLM-NH_2), and a-cyano-4-hydroxycinnamic acid (CHCA) were obtained from Sigma-Aldrich (St. Louis, MO). All peptide samples were dissolved in water at 0.1 mg/mL, diluted 1:20, then mixed 1:1 with 12 mg/mL CHCA. Droplets (0.5 μL) were

spotted onto a stainless steel MALDI plate and dried under atmosphere prior to introduction into the mass spectrometer. For comparison, high energy CID spectra were acquired on the Applied Biosystems 4700 Proteomics Analyzer. Sample preparation was identical to that used for the photodissociation experiments. A collision gas pressure of medium and 1 kV accelerating potential were used.

Results

In general, the most abundant fragment ions of prompt 193-nm photodissociation of peptides that carry charge at the C-termini are side chain cleavage products v_i and w_{ia}. For these peptides, other product ions observed included x_i-type sequence informative fragments with lesser contributions from y_i- and z_i-type ions. N-terminally charged peptide ions promptly photodissociate to yield predominantly a_i-type ions and less abundant side chain cleavage products, especially d_{ia}. Although photofragment ions resulting from proton migration are observed, the majority are indicative of the most basic site within the peptide. Furthermore, contributions from secondary fragmentation, such as small neutral losses from sequence informative fragments and internal cleavage products, are minimal.

The CID spectrum of enkephalin is shown in the top panel of Figure 14. Many fragment ion types are present having both N- and C-terminal charge retention. Several internal cleavage product ions are present, and side chain cleavage product ions appear in low relative abundances. The photofragment ion spectrum of enkephalin is shown in the bottom panel of Figure 14. This spectrum contains a complete series of x_i-type

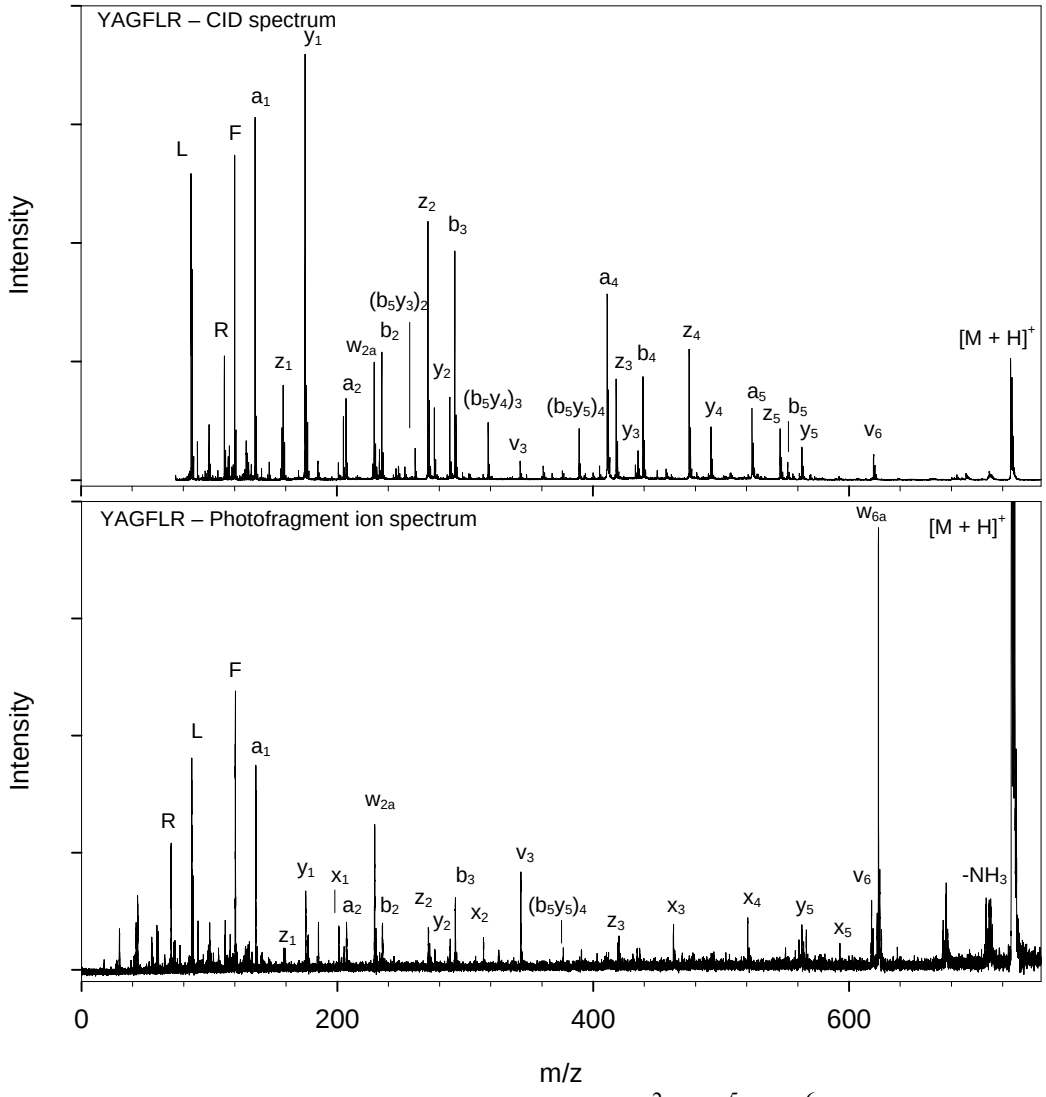

Figure 14. Tandem mass spectra of [D-Ala^2, Leu^5, Arg^6] enkephalin (YAGFLR).

ions, corresponding to cleavage of carbon-carbon bonds along the peptide backbone with charge retention by the C-terminal fragment. Abundant side chain cleavage product ions are also observed, arising from bond cleavage between the α- and β-carbons of the side chains of z_i-type ions (w_{ia}-type ions) and from bond cleavage between the peptide backbone and the α-carbons of the side chains of y_i-type ions (v_i-type ions). The w_{2a} ion confirms the presence of leucine, rather than isoleucine, at the fifth amino acid.

Sequence assignments made using backbone cleavage products are confirmed using v_i-type ions. The most abundant peak in this mass spectrum corresponds to a tyrosine side chain loss from the intact ion (w_{6a}), likely a result of the high extinction coefficient of tyrosine at 193-nm [118]. Note that relative abundances of internal fragment ions are minimal and small neutral loss ions from sequence-specific ions are absent from this spectrum. Aside from two b_i type ions and the a_1 ion, sequence informative ions retain charge at the C-terminal side of the dissociating bond. The low occurrence of secondary fragmentation and product ions resulting from proton migration simplifies *de novo* sequencing from photofragment ion spectra versus that of high energy CID spectra.

Figure 15 contains the tandem TOF mass spectrum of this peptide ion acquired on the photodissociation instrument using identical mass spectrometer operating conditions without photoactivation. Note that only two PSD fragment ions are present in low abundance as a result of small neutral losses.

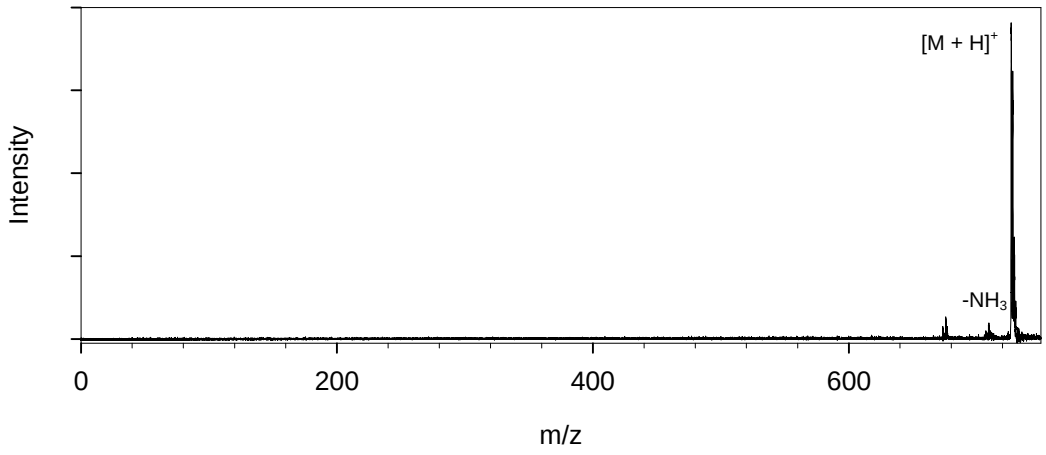

Figure 15. Tandem MS of enkephalin with laser turned off.

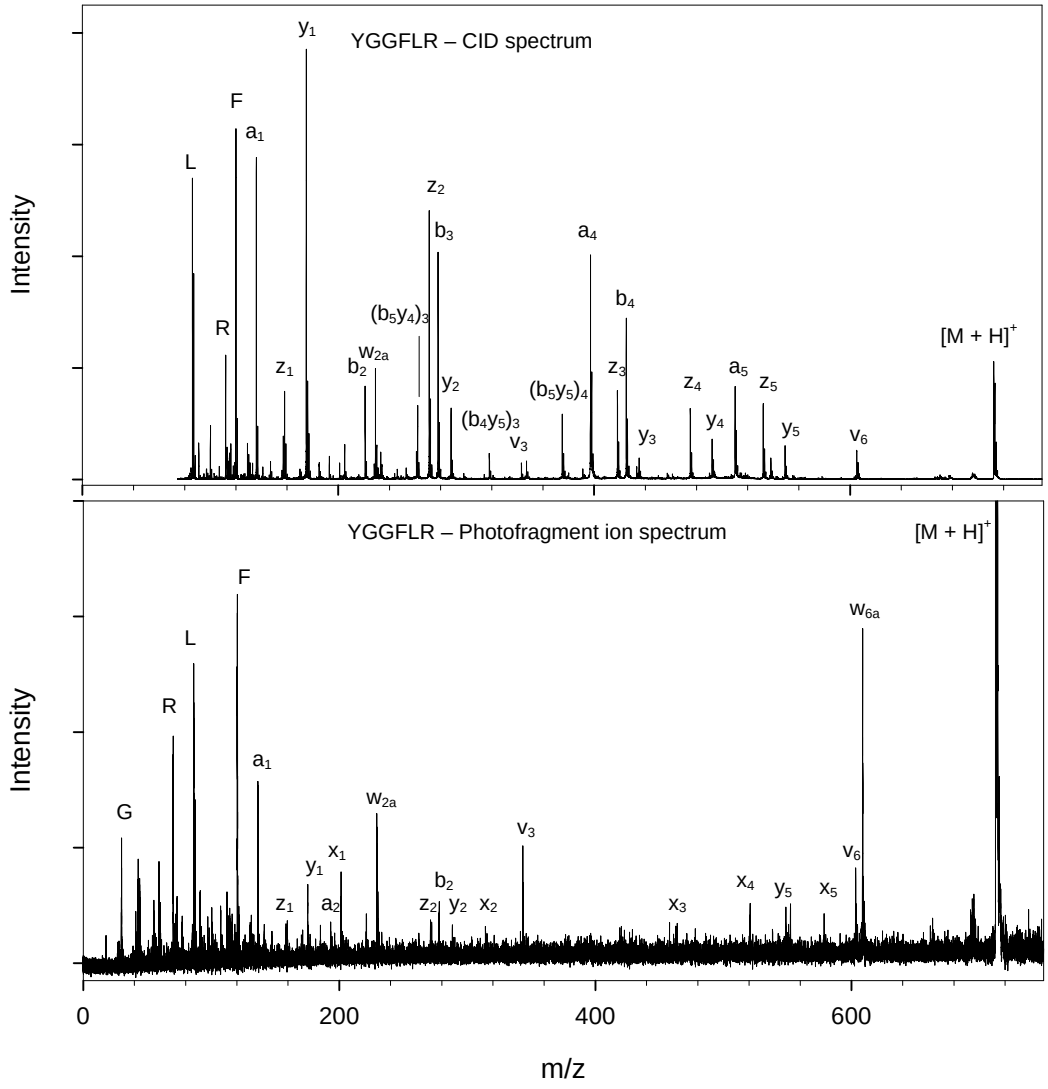

Figure 16. Tandem mass spectra of dynorphin A fragment 1-6 (YGGFLR).

The CID spectrum of a similar peptide, dynorphin A fragment 1-6 (YGGFLR) is shown in the top panel of Figure 16. Abundant a_i and b_i ions are also observed in this CID spectrum, owing to charge transfer during fragmentation. Again, ammonia loss occurs from y_i ions to yield a greater abundance of z_i ions. Three internal cleavage products are observed, as are lower abundances of side chain cleavage product ions. The bottom panel of Figure 16 contains the photofragment ion spectrum of this peptide ion.

Side chain cleavage at the tyrosine residue to yield the abundant w_{6a} ion is observed, accompanied by a second side chain loss of this amino acid to yield v_6. A complete x_i ion series is present, although in lower abundances than for enkephalin. Side chain cleavage products w_{2a} and v_3 are observed as strong photofragment ions.

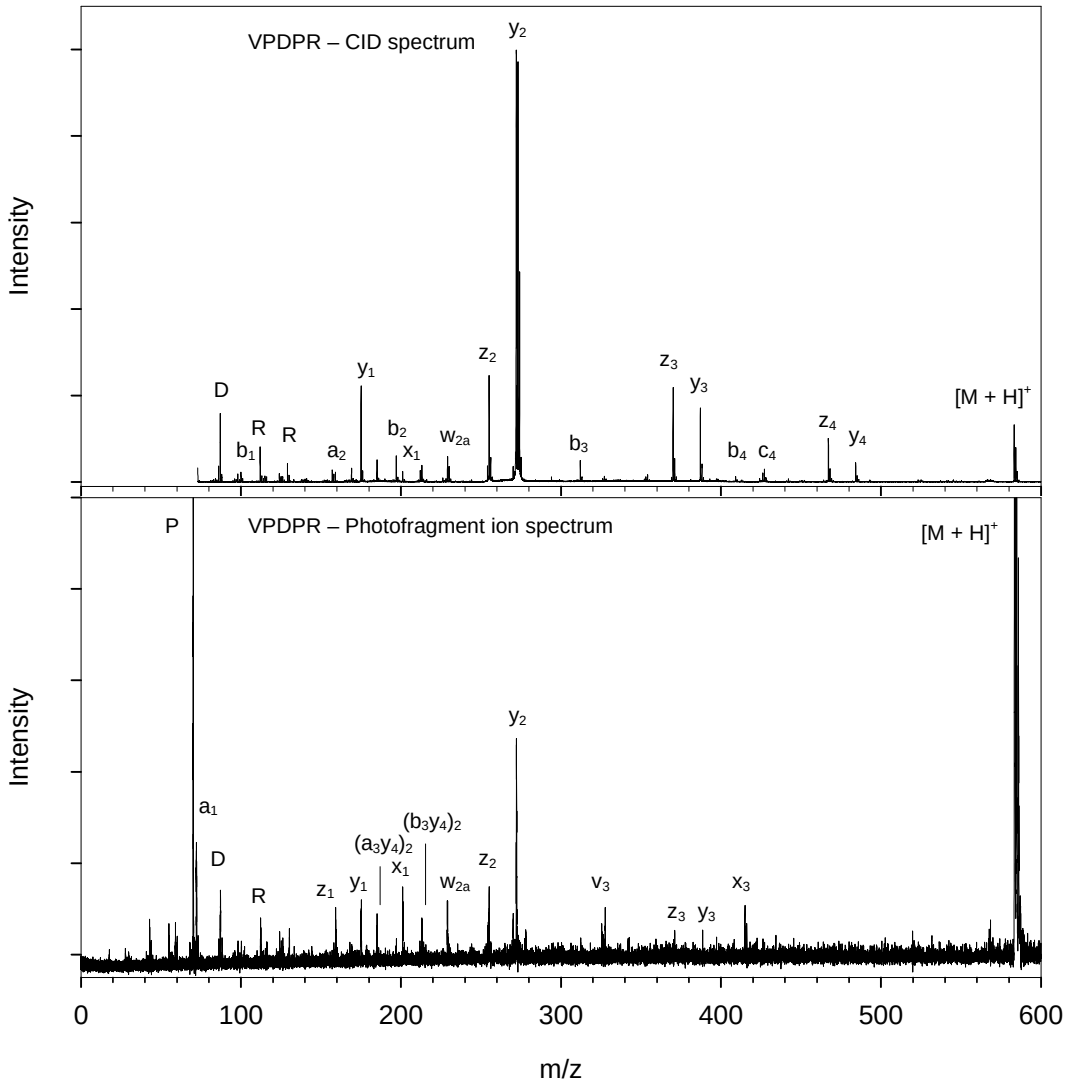

Figure 17. Tandem mass spectra of VPDPR.

The top panel of Figure 17 contains the CID spectrum of synthetic peptide VPDPR. The y_2 ion dominates the spectrum owing to the acidic nature of the aspartic acid residue. The majority of the y_i type ions lose ammonia to yield z_i type ions. The z_3 and z_4 ions appear in greater relative abundances than their y_i counterparts. Although they appear in low relative abundances, N-terminal charge carrying fragment ions are present in the CID spectrum.

The photofragment ion spectrum of VPDPR (Figure 17, bottom panel) also contains an abundant y_2 peak from cleavage after the aspartic acid residue with C-terminal charge retention. Aside from two internal cleavage products and immonium ions, the dominant photofragment ions present retain charge at the C-terminal arginine. Two side chain cleavage product ions (w_{2a} and v_3) are present to confirm sequence assignments deduced from x_i, y_i, and z_i-type ions. It is important to note, however, that the x_2 and x_4 ions are not observed. We attribute this to the occurrence of secondary fragmentation to yield the proline immonium ion, which appears in high relative abundance.

The most abundant peak in the CID spectrum of synthetic peptide VGVRVR (Figure 18, top panel) is the b_5+H_2O, the result of C-terminal amino acid loss. The total relative abundances of N-terminal charge carrying product ions is roughly the same as that of the C-terminally charged fragments. Several of the low abundance fragment ions do no correspond to mass-to-charge ratios expected for this peptide, and thus could not be identified. The bottom panel of Figure 18 contains the photofragment ion spectrum

of VGVRVR. This peptide was chosen owing to the additional basic amino acid and the C-terminal arginine, representing a missed cleavage in a tryptic digest. The b_5+H_2O ion

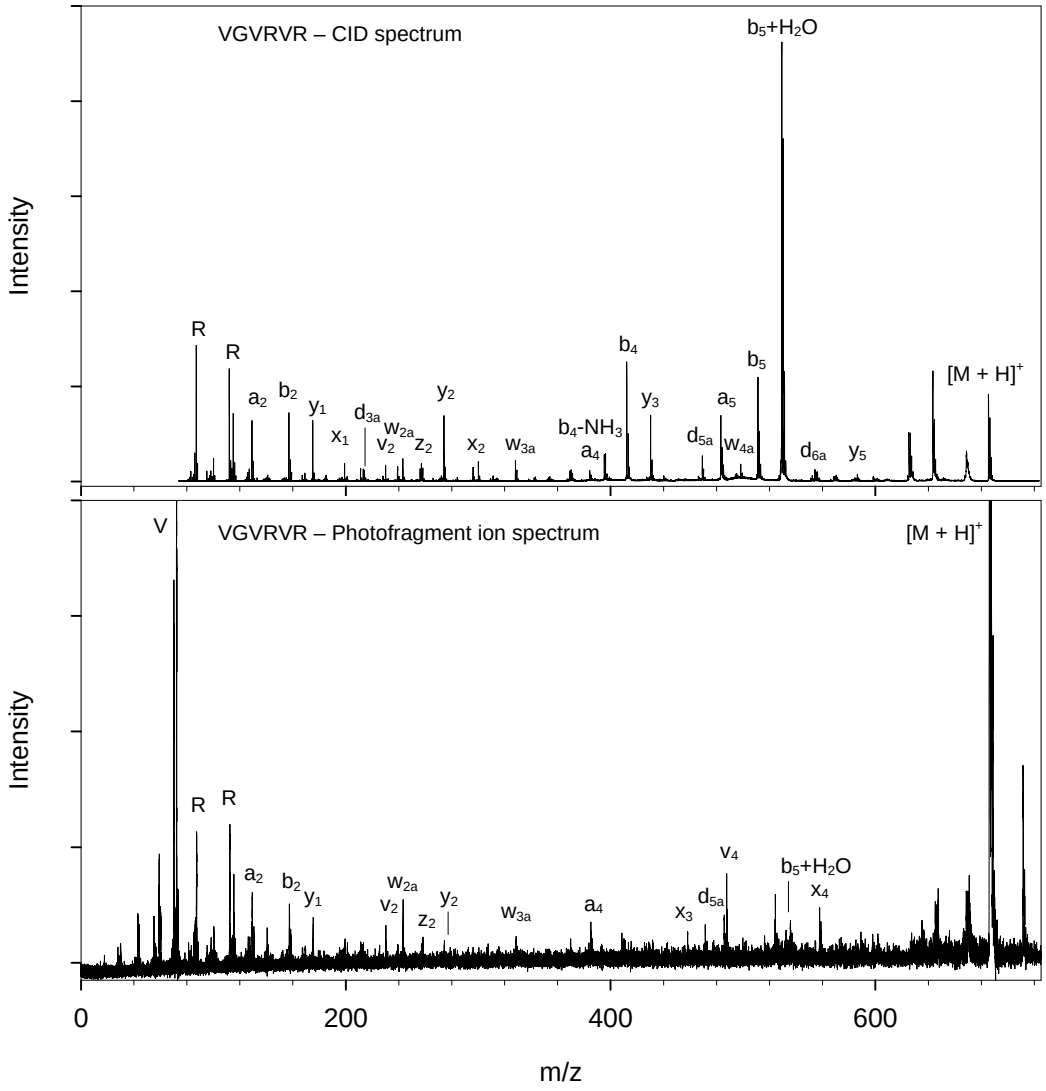

Figure 18. Tandem mass spectra of VGVRVR.

appears in much lower relative abundance in this tandem mass spectrum. Four side chain cleavage ions are present which correspond to valine residues. Three of these (v_2, w_{2a}, and v_4) have C-terminal charge retention. The d_{5a} ion is the result of side chain cleavage at valine with N-terminal charge retention. Three other photofragment ions

with N-terminal charge retention are present, which we attribute to proton binding either to the N-terminal amine (a_2 and a_4) or the arginine side chain at the fourth amino acid (d_{5a}).

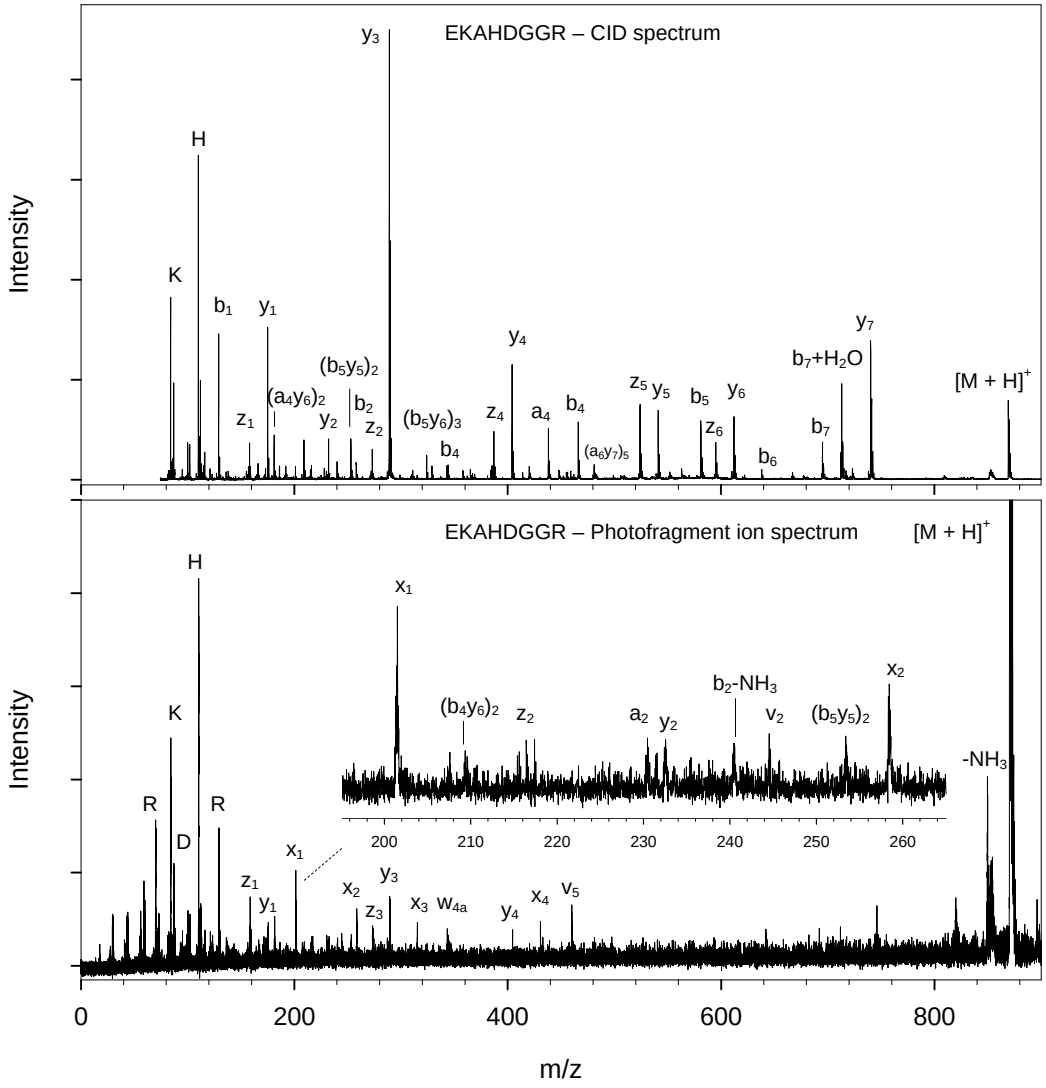

Figure 19. Tandem mass spectra of C-telopepetide (EKAHDGGR).

Tandem mass spectra of C-telopeptide are contained in Figure 19. The CID spectrum (top panel) is dominated by the y_3 ion, a result of amide bond cleavage on the

C-terminal side of the aspartic acid residue. Otherwise, relative abundances of a_i, b_i, y_i, and z_i ions are approximately the same. Several internal cleavage product ions are observed in lower relative abundances, and the b_7+H_2O ion is observed for the loss of the C-terminal arginine. This ion is not observed in the photofragment ion spectrum of this peptide (bottom panel). Only two internal cleavage product ions are present in very low abundance. The y_3 ion is observed in similar relative abundance to that of the other sequence informative ions. The most commonly observed ions are of type x_i, appearing for the four C-terminal amino acids in the peptide. A high molar extinction coefficient for the UV absorbance of histidine leads to a prominent v_5 ion peak. Two other side chain cleavage products are observed, w_{4a} resulting from side chain loss at aspartic acid and v_2, side chain loss at glycine. Two low abundance N-terminal charge carrying fragment ions are observed, a_2 and b_2-NH_3.

The CID spectrum of [Tyr^5, D-$Trp^{6,8,9}$, Arg^{10}] neurokinin fragment 4-10 amide (DYWVWWR-NH_2) (Figure 20, top panel) contains high relative abundances of b_i ions. The most abundant ion signal in this spectrum (y_6) is also the result of amide bond cleavage C-terminal to an aspartic acid residue. All other y_i ions in this spectrum are complemented by strong signals resulting from ammonia loss products (z_i ions). Side chain cleavage product ions (v_2, v_3, v_6, and w_{4a}) appear in low abundance in this spectrum. Three side chain cleavage product ions are observed, as are several low abundance ions that do not correspond to ions predicted by the nomenclature. The y_6 ion is also an abundant signal in the photofragment ion spectrum of this peptide (Figure 20, bottom panel). The most abundant signal is the tryptophan immonium ion, owing to

multiple appearances of this amino acid within the peptide and a high UV absorbance. Side chain cleavage product ions v_2, v_3, w_{4a}, and v_5 appear in similar relative abundances as sequence informative ions. The majority of the photofragment ions retain charge on the C-terminal side of the dissociating bond; however, the a_2, b_2, and b_3 ions are observed.

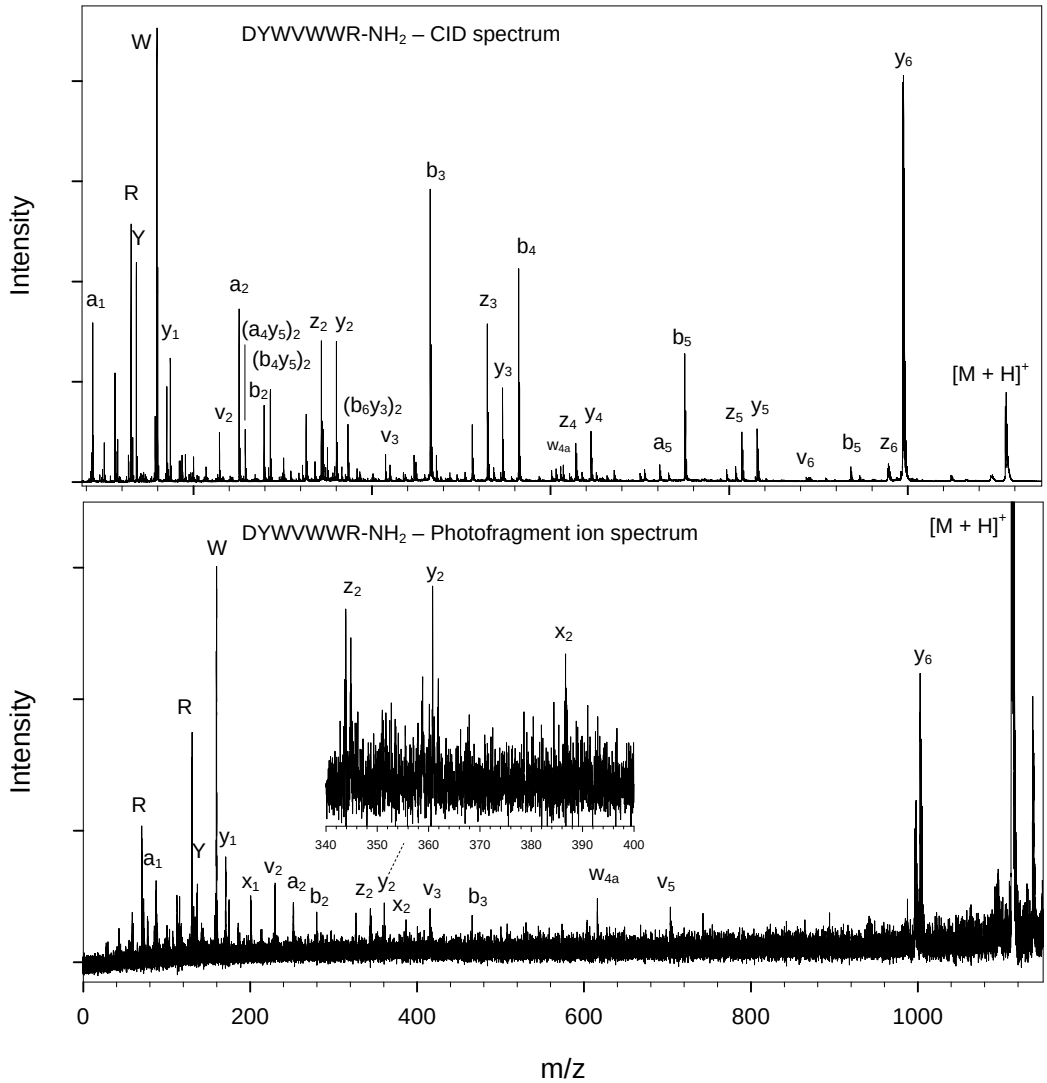

Figure 20. Tandem mass spectra of [Tyr^5, D-Trp^{6,8,9}, Arg^{10}] neurokinin fragment 4-10 amide (DYWVWWR-NH_2).

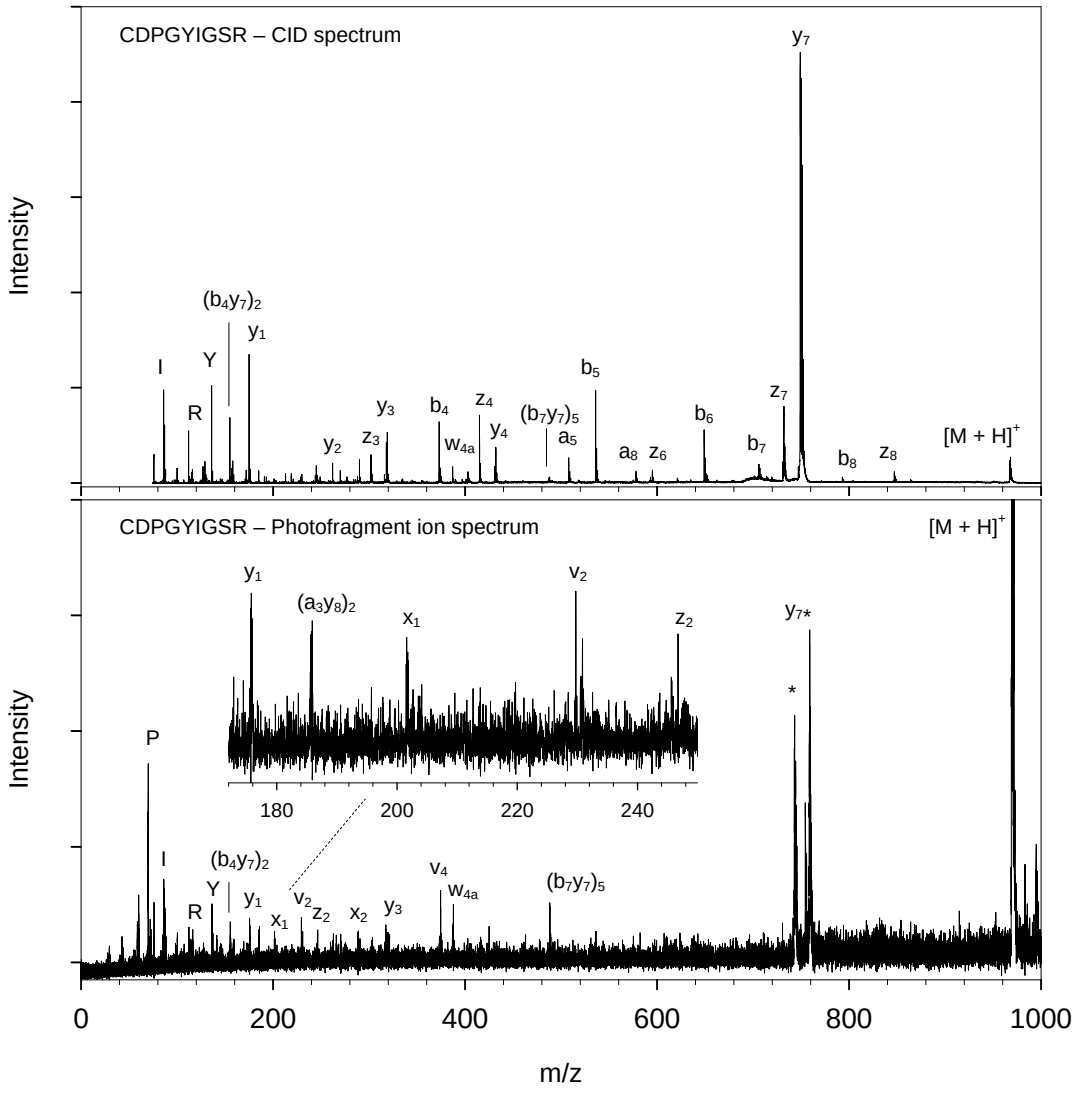

Figure 21. Tandem mass spectra of laminin fragment 925-933 (CDPGYIGSR).

The CID spectrum of laminin fragment 925-933 (CDPGYIGSR) is contained in the top panel of Figure 21. The strongest fragment ion signal (y_7) is again the result of amide bond cleavage following the aspartic acid residue. N-terminal sequence ions are observed mostly as b_i ions, while some a_i ions are present in low abundance. C-terminally charged fragment ions appear as y_i and z_i ions. The ammonia loss ions z_6 and

z_8 appear in low abundances, while y_i ions are absent at these amino acid positions. One side chain cleavage product ion (w_{4a}) is observed in low relative abundance. Two internal cleavage product ions are present, both of which are partly attributable to amide bond dissociation C-terminal to the aspartic acid residue. The same two internal cleavage product ions are observed in the photofragment ion spectrum (Figure 21, bottom panel). Cleavage of the amide bond C-terminal to aspartic acid occurs during flight through multiple locations within the mass spectrometer, causing this fragment ion (y_7) to arrive at the detector at three different arrival times (shifted signals are marked with an asterisk). Of the remaining ions, the strongest sequence informative ions are the v_4 and w_{4a} ions due to side chain cleavages. Side chain cleavage is also observed at the serine residue as the v_2 ion. Aside from immonium ions, all remaining ions detected retain charge on the C-terminal side of the dissociating bonds.

Many ions of various types appear in the CID spectrum of [D-Tyr^{27,36}, D-Thr^{32}] neuropeptide Y fragment 27-36 amide (YINLITRQRY-NH_2) (Figure 22, top panel). The most abundant signals arise from amide bond cleavage. Low abundance z_i ions appear along with y_i ions of the same amino acids, with the exception of the z_8 ion which appears in much higher relative abundance than the y_8 ion. Several low abundance side chain cleavage product ions are observed (w_{4a}, v_5, w_{6a}, w_{7a}, d_{8a}, and v_9). The photofragment ion spectrum of this peptide (bottom panel) contains very few sequence informative ions, and is dominated by immonium ions. This is likely due to the high UV absorbance of the tyrosine side chain, resulting in multiple photon absorption.

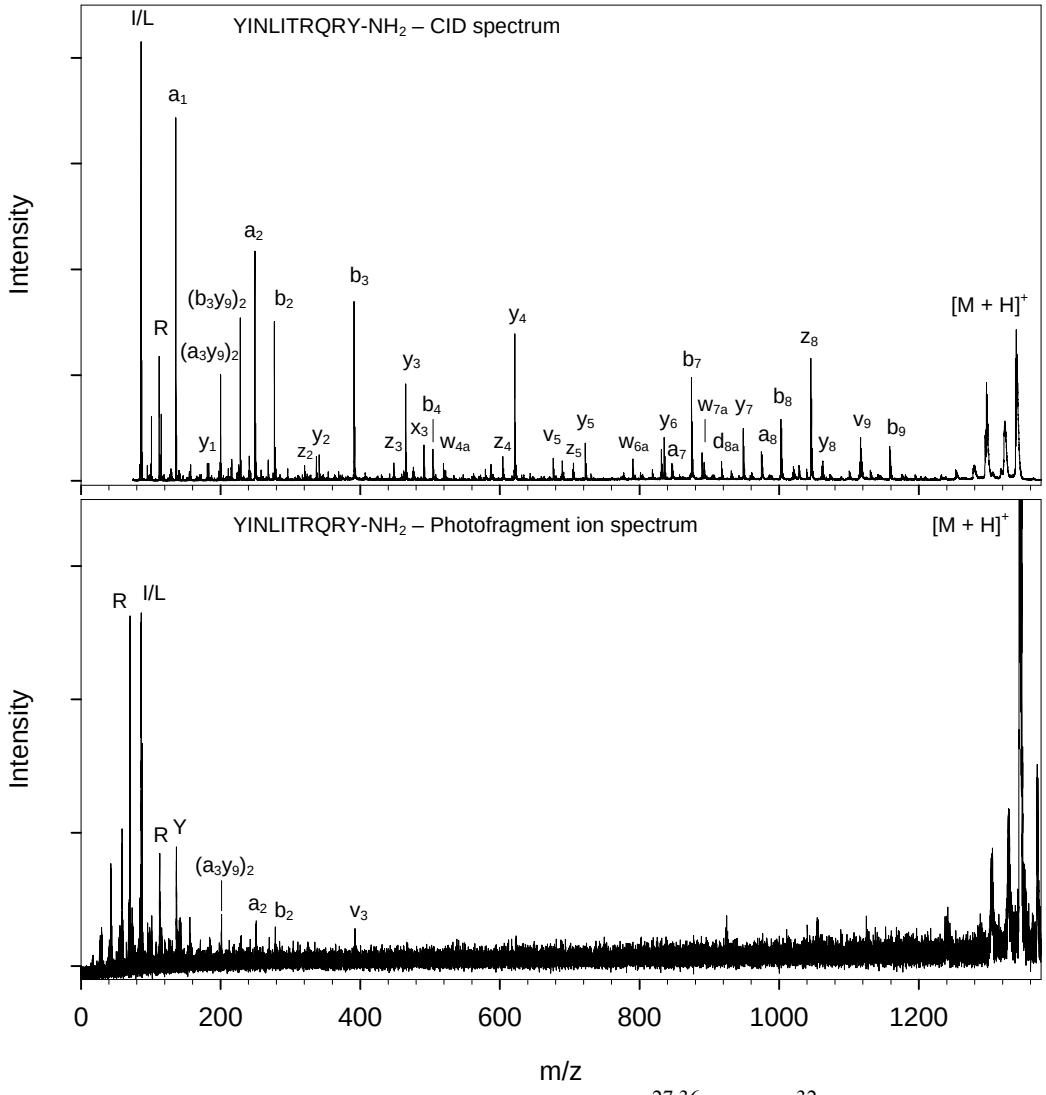

Figure 22. Tandem mass spectra of [D-Tyr^{27,36}, D-Thr^{32}] neuropeptide Y fragment 27-36 amide (YINLITRQRY-NH_2).

The CID spectrum of synthetic peptide HLGLAR is shown in the top panel of Figure 23. Complete series of b_i and y_i ions are present, along with the b_5+H_2O ion. The a_1 and a_2 ions are also present in high abundance. Low relative abundance ions include other a_i ions, z_i ions, and w_{ia} ions for leucine. Photodissociation of peptide HLGLAR (Figure 23, bottom panel) yields a complete series of x_i-type ions. The a_1, a_2,

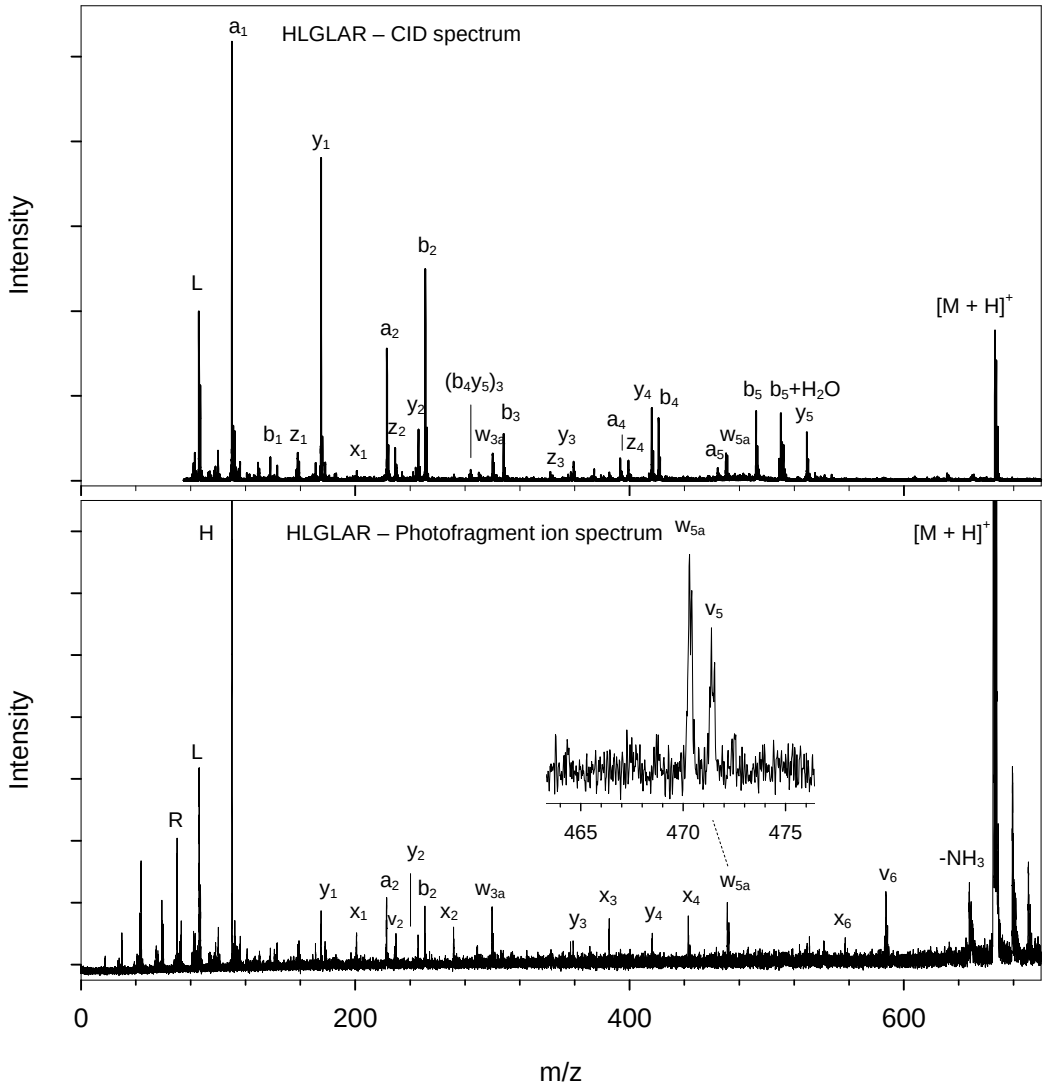

Figure 23. Tandem mass spectra of synthetic peptide HLGLAR. [56] (Reprinted with permission from Elsevier)

and b_2 ions are the only N-terminally charged fragment ions present, likely appearing due to proton binding at the basic histidine residue or the N-terminal amine [119]. Also present are w_{3a}, w_{5a}, and v_5 ions, allowing both confirmation of the amino acid sequence and the unambiguous determination of leucine. Side chain loss ions are observed for histidine and alanine as further confirmation of the correct sequence. The inset in this

spectrum of the w_{5a} ion illustrates mass accuracy within 100 ppm and resolution in excess of 2000 (m/Δm, fwhm) for photofragment ions. Only the all-^{12}C isotope of the ion of interest is irradiated with the photodissociation laser, thus the fragment ion at m/z 471 is identified as v_5 with confidence. Note that the side chain cleavage products are the most abundant fragment ions.

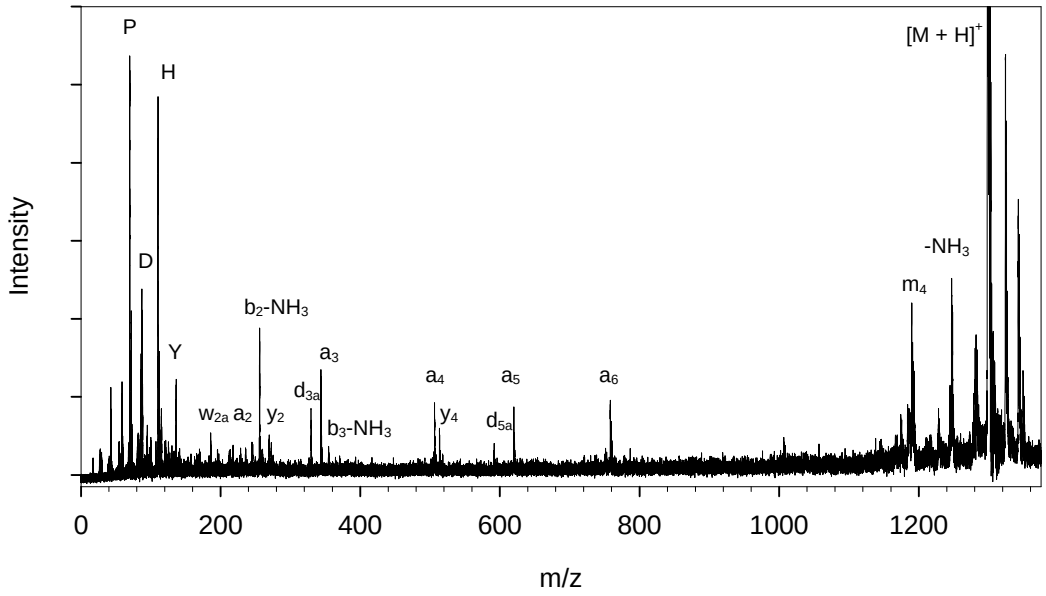

Figure 24. Photofragment ion spectrum of angiotensin I (DRVYIHPFHL).

Figure 24 contains the photofragment ion spectrum of angiotensin I (DRVYIHPFHL). For the first six amino acid residues, a_i-type ions are observed resulting from carbon-carbon bond cleavage along the peptide backbone with charge retention at the N-terminus. N-terminally charged side chain cleavage product ions are observed for valine (d_{3a}) and isoleucine (d_{5a}) which may be used to confirm sequence ion assignments and to unambiguously determine isoleucine versus leucine as the fifth amino acid residue. A few y_i-type ions and the w_{2a} ion appear in lower abundance,

attributable to a small fraction of $[M + H]^+$ ions that are initially formed with the C-terminal amino acid as the charge carrier. With the exception of the b_2-NH_3 ion, small neutral loss ions and internal cleavage product ions are formed in very low abundance compared to sequence informative ions.

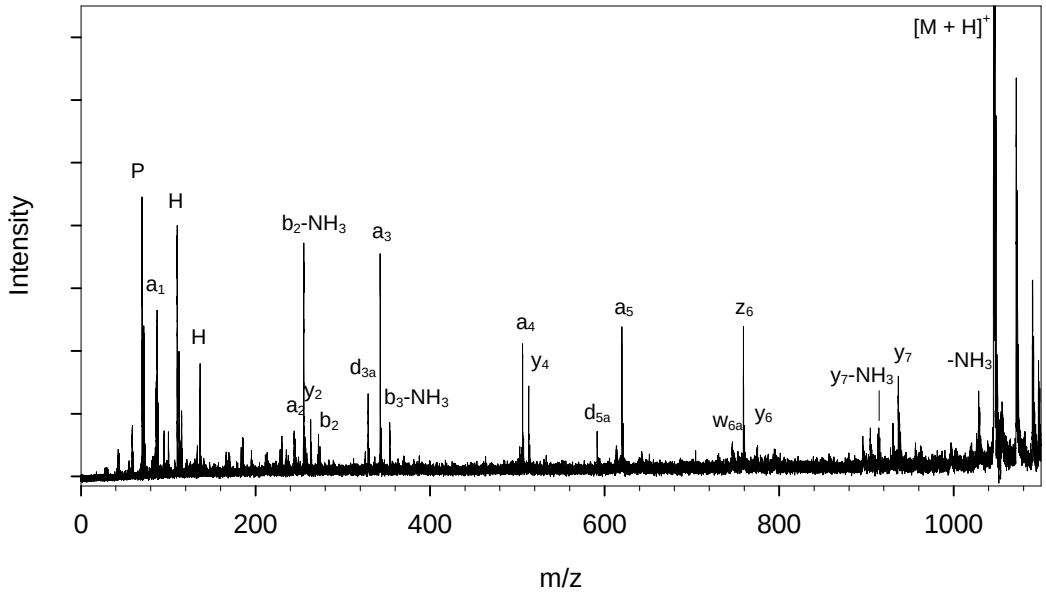

Figure 25. Photofragment ion spectrum of angiotensin II (DRVYIHPF). [56] (Reprinted with permission from Elsevier)

Angiotensin II (DRVYIHPF) has the same amino acid sequence as angiotensin I with the omission of two residues from the C-terminus. The photofragment ion spectrum of this peptide is contained in Figure 25. Photofragment ions and their relative abundances are similar to those of angiotensin I, except for the appearance of the z_6 ion and the disappearance of the a_6 ion. The y_7 ion appears as a result of amide bond cleavage following the aspartic acid residue with C-terminal charge retention. Mass accuracy and resolution for the photofragment ions of angiotensin II are shown in Table 2. The majority of photofragment ions appear within 0.5 Da of their predicted m/z's,

with an average absolute error of 0.28. Note that the mass measurement error for the y_7 ion is in excess of 1 Da, while mass resolution is greatest for this fragment.

Table 2. Mass measurement error and resolution for photofragment ions of angiotensin II.

Ion	Measured m/z	Calculated m/z	Error	Resolution (m/Δm, fwhm)
$[M+H]^+$	1046.07	1046.54	0.47	1969
y_7	930.28	931.52	1.24	3509
z_6	759.10	759.40	0.30	2665
a_5	619.94	619.36	-0.58	2689
d_{5a}	591.63	591.33	-0.30	2352
y_4	513.06	513.28	0.22	2900
a_4	505.98	506.27	0.29	2554
b_4-NH_3	353.90	354.18	0.28	1359
a_3	343.00	343.21	0.21	1125
d_{3a}	329.05	329.19	0.14	1014
b_2	272.26	272.14	-0.12	1598
y_2	263.21	263.14	-0.07	1538
b_2-NH_3	255.26	255.11	-0.15	862
a_2	244.32	244.14	-0.18	745
$(b_7y_3)_2$	235.38	235.12	-0.26	840
$(a_3y_7)_2$	228.45	228.18	-0.27	2810
y_1	166.32	166.09	-0.23	580
Y	136.41	136.08	-0.33	588
H	110.34	110.07	-0.27	366
R	87.25	87.09	-0.16	380
V	72.16	72.08	-0.08	323
P	70.13	70.07	-0.06	307
		Average:	**0.28**	**1503**
		Std. Deviation:	**0.25**	**1009**

We speculate that the y_7 ion is formed in the first mass analyzer as a product of metastable decay. Although this ion arrives at the photodissociation cell entrance at the same time as the parent ion and is transmitted to the detector, its position is shifted from that of the parent ion prior to photoactivation, and thus no photodissociation products of

the y_7 ion are detected. The reflectron voltage used in these tandem MS experiments is optimal for temporal focusing of PSD product ions having m/z approximately 90% of the m/z of the parent ion. Although resolution decreases with decreasing m/z, monoisotopic resolution is attained for all photofragment ions appearing in the tandem mass spectrum. The average resolution is approximately 1500.

The photofragment ion spectrum of angiotensin III (RVYIHPF) is contained in Figure 26. For this peptide, the photofragment ion a_2 is greater in abundance than b_2-NH_3. Also in contrast to angiotensin I and II, Y_3 appears due to amide bond cleavage between tyrosine and isoleucine rather than the y_i-type ion. This result may be either due to direct photolysis of the amide bond at this position, or due to H_2 elimination from the y_3 ion, which is not detected. A double bond is formed between the nitrogen atom at the cleavage point and the adjacent backbone carbon to make an imine in the Y_i ion, whereas the y_i ion contains a primary amine [33].

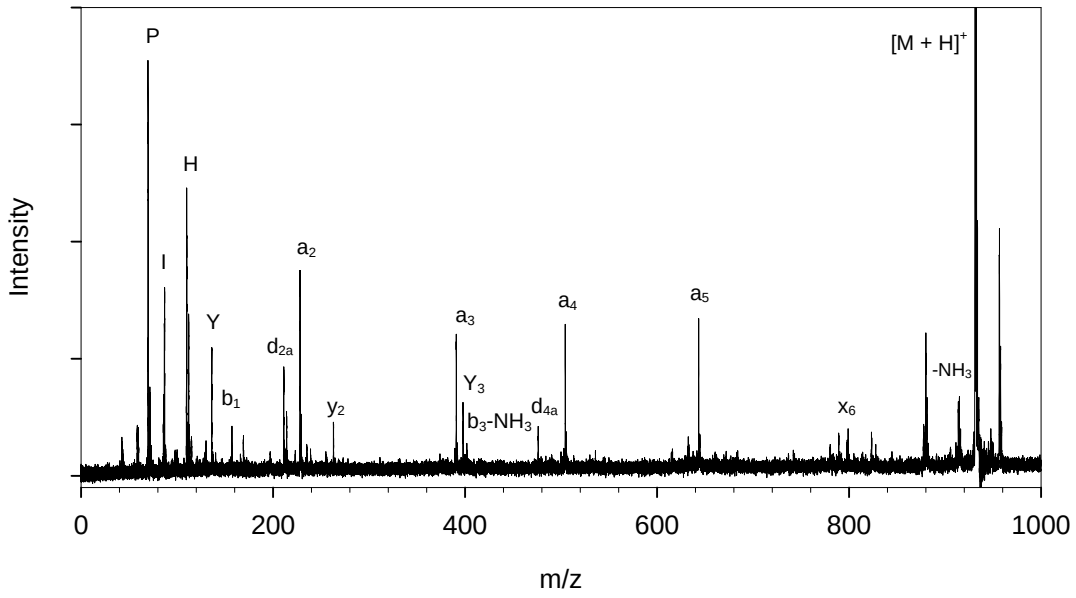

Figure 26. Photofragment ion spectrum of angiotensin III (RVYIHPF).

Similar results are observed in the photofragment ion spectrum of Val^4-angiotensin III (RVYVHPF) (Figure 27). Again, a_i ions are present for the first five amino acids in the peptide sequence. The y_3 ion is observed instead of a Y_3 ion, and a greater number of y_i ions appear. Likewise, two z_i ions are present resulting from ammonia loss from the y_i ion. In contrast to the other angiotensin analogues presented, the $b_{n-1} + H_2O$ ion appears in high relative abundance. N-terminal side chain cleavage products are observed for both valine residues (d_{2a} and d_{4a}) and a C-terminal side chain cleavage product is observed for the arginine residue (w_{7a}). One internal cleavage product is observed ($(a_3y_6)_2$) resulting from carbon-carbon bond dissociation between tyrosine and valine and amide bond cleavage between arginine and valine.

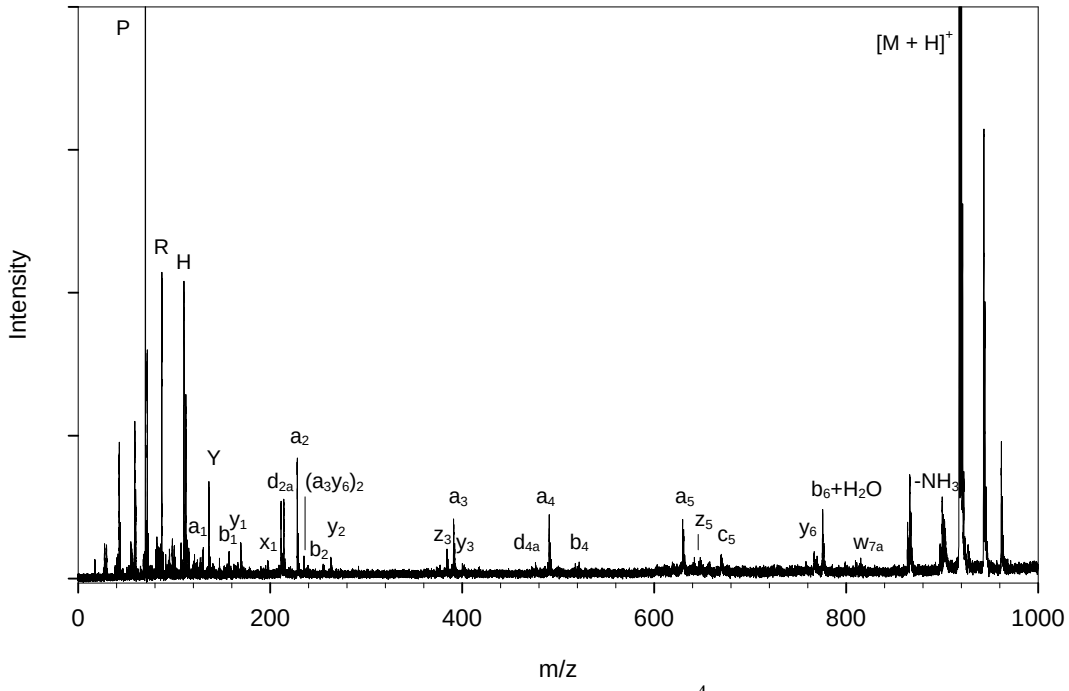

Figure 27. Photofragment ion spectrum of Val^4-angiotensin III (RVYVHPF).

Figure 28 contains the photofragment ion spectrum of substance P amide (RPKPQQFFGLM-NH_2). Bond cleavage occurs between backbone carbon atoms to yield a_i ions for the first eight amino acids. Fragment ions resulting from side chain cleavage at lysine (d_{3a}) and glutamine (d_{5a} and d_{6a}) are among the most abundant peaks in this tandem mass spectrum. Only one fragment ion appears resulting from secondary fragmentation. Note that there are no fragment ions observed resulting from migration of the proton from the N-terminal arginine. A previously reported 193-nm photofragment ion spectrum acquired using the PSD focusing method contained a large number of ions resulting from small neutral loss and several fragments resulting from amide bond cleavage (b_i ions) [102].

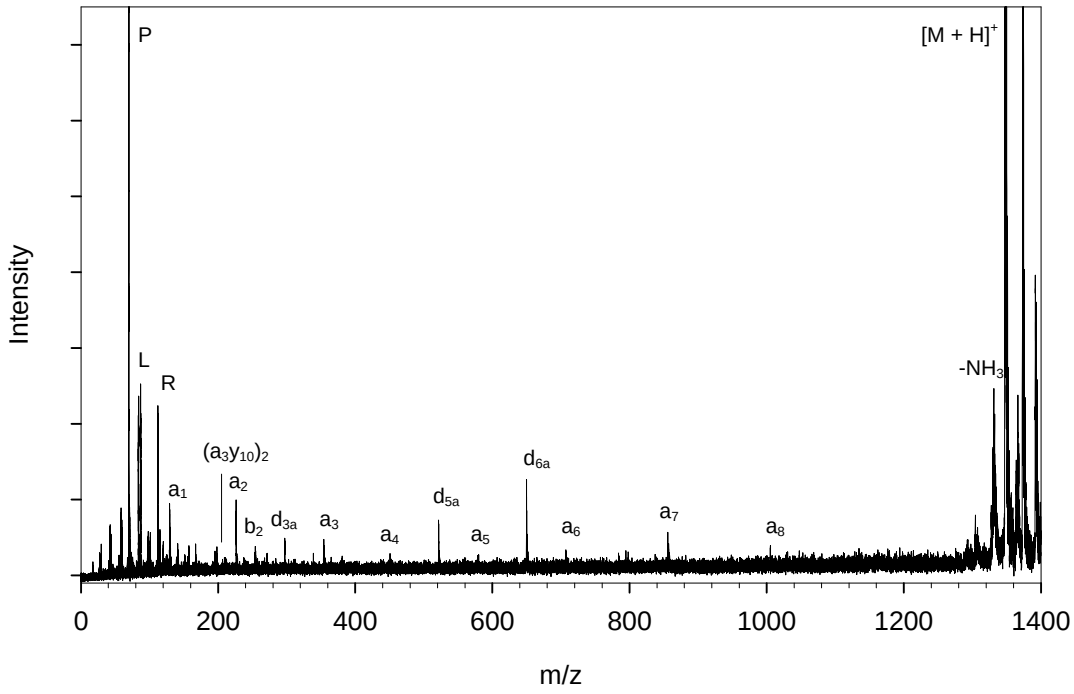

Figure 28. Photofragment ion spectrum of substance P amide (RPKPQQFFGLM-NH_2).

Discussion

Photoactivation has several advantages over activation through collisions for tandem TOFMS analysis. High resolution mass-selection optics is a requirement of tandem MS using CID, as any ion that traverses the collision chamber is subject to activation. When analyte ions are present which are similar in m/z to the ions of interest, fragment ions originating from unwanted precursors complicate data interpretation. The 17 ns excimer laser pulse used in these photodissociation experiments is sufficiently short to irradiate only the ions of interest, either a single isotope or all isotopes of a given precursor. Monoisotopic selection allows differentiation between two fragment ions that differ by a single m/z unit. Although the mass resolution of the TIS gate is too low to remove $[M + Na]^+$ from a tandem mass spectrum of $[M + H]^+$, no fragment ions are observed that contain sodium.

The internal energy of an ion is increased by 6.43 eV upon absorption of a single 193-nm photon. Variations in the internal energies of photoactivated ions are consequently the same as the variation of initial internal energies of MALDI generated ions. While the average internal energies of collisionally activated ions are considerably lower than for the 193-nm photoactivated ions, the distribution of internal energies is much greater since only a small fraction of collisions occur at the center of mass. In addition, photon absorption results in an electronic excitation at the chromophore, while activation through collision causes excitations of many vibrational modes, some of which give rise to undesirable small neutral losses.

Use of the decelerating/accelerating photodissociation cell has benefits as well. Metastable ions formed within the first field free region are separated from the intact ions of interest upon entering the photodissociation cell. Contrary to photodissociation TOFMS performed using the PSD focusing method, no metastable ions are activated. The timescale over which observable photofragment ions are produced is governed by the distance from the photodissociation window to the exit of the photodissociation cell and the voltages applied to the source and cell. Using this instrument geometry, only promptly-formed photofragment ions are observable, decreasing contributions from metastable ions to the photofragment ion spectra. As an added advantage, a complete photofragment ion spectrum is collected at a single reflectron voltage. Instrument duty cycle is decreased by an order of magnitude, and parent ion signal may be monitored during the experiment.

As demonstrated by the spectra exhibited in this chapter, 193-nm photodissociation consistently causes prompt fragmentation of carbon-carbon backbone bonds to produce x_i-type ions from C-terminally charged peptide ions and a_i-type ions from N-terminally charged peptide ions. Side chain cleavage products are formed for several amino acids, providing confirmation of sequence assignments and the unambiguous determination of the isomeric amino acids leucine and isoleucine.

The kinetics of fragmentation may be used to explain the preference for production of a_i and x_i ions in the prompt 193-nm photodissociation experiment. The Wahrhaftig diagram in Figure 29 illustrates this point. At low ion internal energy, fragmentations that have the lowest enthalpy are dominant. These are typically

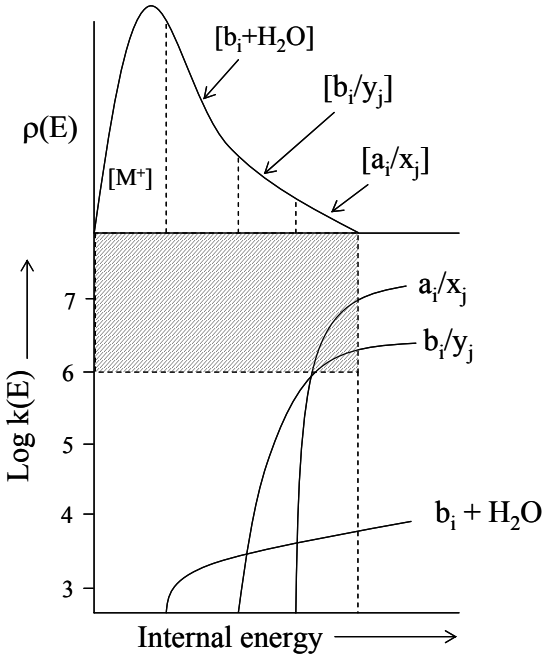

Figure 29. Wahrhaftig diagram illustrating the kinetics of peptide fragmentation.

rearrangement reactions such as those that yield $b_i + H_2O$ for peptide ions. Rearrangement reactions occur via a highly coordinated, or "tight", transition state and the maximum rate at which these fragmentations may occur is limited by entropy [1]. At higher internal energies different fragmentation pathways are accessed. Fragment ions such as b_i and y_i occur after the formation of an oxazolone or a diketopiperazine [120]. These are tight transition states, and thus fragmentation rate for these reactions is also limited by entropic factors. At very high internal energies fragmentations via "loose" transition states, such as simple bond cleavage to form a_i and x_i ions, become kinetically favored [1]. The abundance ratios of a_i to b_i, and x_i to y_i, in photofragment ion spectra become greater when only the fastest reactions are observed. These arguments also apply to the observation of high energy side chain cleavage product ions.

CHAPTER III

PROMPT FRAGMENTATION OF 193-NM PHOTOACTIVATED BRADYKININ ANALOGUES BY MALDI-TOF-TOFMS

Introduction

Matrix-assisted laser desorption/ionization (MALDI) [22,23] and electrospray ionization (ESI) [21] have had revolutionized the analysis of biomolecules by mass spectrometry (MS) techniques. Identification of proteins by using "bottom-up MS" techniques, *i.e.* enzymatic digestion of proteins or protein mixtures followed by peptide mass fingerprinting and database searching [121,122], is now routine, and *de novo* sequencing [30] and determination of post-translational modification using tandem mass spectrometry techniques is now commonly practiced in proteomic laboratories. The primary factor that complicates peptide structure determination is that the types of fragment ions observed in a tandem mass spectrum are related to the intrinsic properties of the gas-phase peptide ion [123], the activation method utilized, and the timeframe for probing unimolecular dissociation products [73,124]. For example, utilizing only the internal energy acquired during the desorption/ionization event and a relatively long fragmentation timescale (approximately 10 μs, as in post-source decay (PSD) experiments) favors product ions formed via the lowest energy channels [125], *i.e.* b_i and y_i type fragments [32,33]. As we showed previously, the observed fragment ions and their relative abundances change significantly if the timescale of the experiment is altered [53].

Collisional activation of gas-phase peptide ions with a neutral gas (eV to several keV collision energies) increases the internal energy of the ions; however, the resulting spectra contain a large number of non-sequence informative fragment ions, such as internal cleavage products and small neutral loss ions, which complicates primary structure elucidation and reduces sensitivity in sequence informative fragmentation channels. For a discussion of the salient issues see the recent review by Gabelica *et al*. [126]. Increasing collision energy leads to a greater abundance of sequence informative ions [58] (*e.g.* a_i-, c_i-, x_i-, w_{ia}-, d_{ia}-type ions) by permitting faster unimolecular decomposition channels to be accessed [1], but an increase in collision energy does not eliminate contributions from secondary cleavage processes. Additionally, kinetic energy loss [61] occurs due to inelastic processes involved in conversion of kinetic energy into internal energy modes, resulting in impaired mass resolution and mass measurement accuracy for time-of-flight (TOF) measurements.

In spite of rapid advances made in tandem MS techniques and increased understanding of peptide ion fragmentation chemistry, there remains substantial interest in developing methods to increase the efficiency and information content of MS-MS spectra. For the past several years we have focused our efforts on two general approaches: (1) 193-nm photodissociation and (2) varying the charge site of peptide ions by using a cationizing reagent with high affinity for specific amino acids. Peptide ions are intrinsic natural chromophores for vacuum ultraviolet radiation (*e.g.*, 157-nm and 193-nm), absorbing photons at the amide bonds and the aromatic amino acid side chains [90,118,127]. In contrast to activation of rotational and vibrational internal energy

modes via collision, photon absorption results in an electronically activated ion. Furthermore, ion kinetic energy is not affected by photoactivation. As demonstrated by our previous experiments [101,102,114,128], 193-nm ArF excimer laser irradiation provides sufficient energy (6.43 eV per photon) to cause prompt (*i.e.* lifetime of the dissociating ion is less than 1.0 μs), charge-remote fragmentation, resulting in sequence ions of type a_i and side-chain specific fragment ions d_{ia}, v_i, and w_{ia}. Recent papers by Reilly and coworkers [116,129] reported very interesting fragmentation products from peptide ions photodissociated using a 157-nm F_2 excimer laser. Complete sequence coverage was observed in the form of x_i-type ions for peptides containing a single, C-terminal arginine and a_i-type ions for peptides containing an N-terminal arginine as well as side chain cleavage product ions.

In this chapter, we also compare the effect of charge carrier on the types of fragment ions observed. Evidence for charge immobilization in $[M + Na]^+$ peptide ion was shown by Tomer *et al*. [130], where an increase in fragment ions resulting from charge-remote fragmentation and a decrease in production of internal fragment ions upon CID was observed. Experiments by Cerda *et al*. [131] and Teesch *et al*. [132] demonstrated that the sodium ion most strongly interacts with carbonyl oxygen atoms along the peptide backbone to produce primarily N-terminal fragment ions. Bluhm *et al*. [133] suggested that Cu^+ binds most strongly to the side chain of arginine and the charge is non-mobile. Previous experiments in our laboratory [134] have shown that the analytical utility of tandem mass spectrometry data for peptides is enhanced for $[M + Cu]^+$ versus $[M + H]^+$ peptide ions. Wysocki suggested that when the charge on a

peptide ion is immobilized the energy required for fragmentation increases [123]. In cases where sufficient energy is deposited to induce charge-remote fragmentation [58], relative abundances of resulting fragment ions are governed by the relative gas-phase basicities of all possible charge-bearing sites. Peptide *de novo* sequencing is best facilitated when one or more complete ion series (*e.g.* y_i, b_i, etc.) is present and few other ions are observed. A complete ion series only occurs when the terminal amino acid of a peptide ion acts as a charge-bearing site. For positive ions, when the terminal charge-bearing site of a peptide is sufficiently more basic than all others, or more strongly binds the charge carrier, a majority of the ions in the tandem mass spectrum will be sequence ions derived from that terminus [63,134]. In these experiments we investigate the utility of prompt 193-nm photodissociation of peptide ions bearing mobile and fixed charge carriers.

Our previous photodissociation experiments were performed on a homebuilt reflectron-TOF instrument [101] using the PSD focusing method [103] to analyze photofragment ions. Several disadvantages are inherent in the PSD focusing technique. First, metastable ions formed in the first field free drift region are activated causing secondary fragmentation products to appear [99]. Also, the PSD focusing method is an inherently low throughput experiment. These two issues were addressed in Chapter II. Finally, previously reported photofragment ion spectra also contain a large proportion of metastable decay products (b_i- and y_i-type ions along with small neutral loss ions) as described by RRKM [125] theory as a result of allowing 10 μs for fragmentation prior to

mass analysis of product ions. A new instrumental design was implemented to overcome these challenges.

Experimental

The photodissociation mass spectrometer (Figure 10) consists of a delayed extraction MALDI reflectron TOF instrument described previously [102] with the addition of a four-grid decelerating/accelerating photodissociation cell, 10 cm in length, centered about the photodissociation window following the timed-ion selector (TIS). These experiments were performed with a 15 kV source acceleration potential and 8 kV potential applied to the photodissociation cell. Field-free drift regions of TOF-1 and TOF-2 remain at common ground. During tandem operation, the reflectron potential is set to mirror the temporal focal point of the instrument source at the photodissociation window for maximum resolution of photofragment ion signal.

Mass-selected ions are decelerated to 7 keV of translational energy as they pass the first two grids of the photodissociation cell. Ions are then irradiated at the center of the cell with a 17 ns pulse from the 193-nm ArF excimer laser (Lambda Physik, LPX120i). A fraction of activated ions fragment prior to entering the accelerating electric field created by the third and fourth photodissociation cell grids. The timescale of in-cell fragmentation, which we define as "prompt" photodissociation, is approximately 1 μs for an ion of mass-to-charge (m/z) 1000, which corresponds to a unimolecular dissociation constant of $k(E) = 10^6\ s^{-1}$. Ions are mass analyzed in reflectron TOF-2 and detected with a dual microchannel plate detector (Burle, Advanced

TOF, Sturbridge, MA). Mass spectra are recorded and summed using a digital storage oscilloscope (LeCroy, LC574AM, Chestnut Ridge, NY).

Prior to acceleration into TOF-2, parent and corresponding fragment ions travel with the same velocities. Since kinetic energy is directly proportional to m/z, the kinetic energy of a fragment ion within the cell is equal to the kinetic energy of the parent ion multiplied by the ratio of fragment ion m/z to parent ion m/z. Kinetic energy for a fragment ion after acceleration into TOF-2 is obtained through kinematic analysis and is used to derive an expression for time-of-flight (Equation 7).

$$TOF = a\left(\frac{m_f}{bm_f + c}\right)^{\frac{1}{2}} + t_0 \tag{7}$$

Parameters (a) and (c) are constant for given source, cell, and reflectron voltages. Parameter (b) is inversely proportional to the parent ion m/z, and the intercept (t_0) is directly proportional to the square root of the parent ion m/z. Photofragment ion TOF data is downloaded from the oscilloscope and converted to an x-y list format using Galactic Grams/386 Spectral Conversion tool. Calibration is applied prior to plotting volts of signal versus m/z using SigmaPlot software (SPSS Inc., Chicago, IL).

Collision-induced dissociation mass spectra were acquired using the Applied Biosystems 4700 Proteomics Analyzer. Gas pressure for CID was set at medium, and 1 keV collision energy was used for all peptides analyzed. Collision-induced dissociation data were exported in ASCII x-y format using the Applied Biosystems Data Explorer software then plotted in SigmaPlot. Both CID and photofragment ion spectra were rendered in graphical software for the purpose of labeling.

It is important to note that a TOF-TOF mass spectrum is a composite of fragment ions resulting from post-source decay (PSD) as well as fragment ions arising from dissociation of precursors that are activated through collision or photon absorption [135]. Measures may be implemented to reduce contributions from PSD in a MALDI-TOF-TOFMS experiment. For example, we previously reported photodissociation experiments that utilized a binary matrix of CHCA and fructose to lower the internal energy of MALDI-formed ions [114]; however, the addition of fructose causes a reduction in parent ion signal. Both TOF-TOFMS experiments described herein were performed using a single component matrix and an ionization laser power slightly above the MALDI threshold. Use of the biased activation cell in the photodissociation experiments greatly reduces contributions from PSD fragment ions. As shown in a Chapter II, very few PSD fragment ions appear in tandem MS operating mode when no laser activation is used. Further examples of a reduced PSD background are apparent in the spectra shown here. The resolution of the TIS gate on the photodissociation instrument is not sufficiently high to eliminate $[M - H + 2Na]^+$ when examining $[M + Na]^+$, however no metastable fragment ions are observed that contain two sodium atoms.

Ten bradykinin analogs (Table 3) and cupric sulfate were obtained from Sigma-Aldrich (St. Louis, MO), sodium carbonate was obtained from EM Science (Gibbstown, NJ), and α-cyano-4-hydroxycinnamic acid (CHCA) was obtained from Aldrich Chemical (Milwaukee, WI). All peptides and reagents were used without further purification.

Table 3. Bradykinin analogues examined and m/z for various charge carriers.

		Theoretical Monoisotopic m/z		
Peptide	**Sequence**	**$[M + H]^+$**	**$[M + Na]^+$**	**$[M + Cu]^+$**
Bradykinin Fragment 1-5	RPPGF	573.3	595.3	635.2
Bradykinin Fragment 1-6	RPPGFS	660.3	682.3	722.3
Bradykinin Fragment 1-7	RPPGFSP	757.4	779.4	819.3
Bradykinin Fragment 2-7	PPGFSP	601.3	623.3	663.2
des-Pro^2-Bradykinin	RPGFSPFR	963.5	985.5	1025.4
D-Phe^7-Bradykinin	RPPGFSFFR	1110.6	1132.6	1172.6
des-Arg^1-Bradykinin	PPGFSPFR	904.5	926.5	966.4
des-Arg^9-Bradykinin	RPPGFSPF	904.5	926.5	966.4
Lys^1-Bradykinin	KPPGFSPFR	1032.6	1054.5	1094.5
Bradykinin	RPPGFSPFR	1060.6	1082.5	1122.5

Stock solutions of all bradykinin analogues were prepared at a concentration of 50 mg/mL in distilled deionized water. For analysis of protonated peptides, stock solution was mixed 1:1 with 12 mg/mL CHCA in methanol, and then spotted in 1 μL droplets on a stainless steel MALDI plate. Cuprated peptide ions for photodissociation analysis were formed by using the same dried droplet sample preparation on a copper MALDI plate [136]. Cationization with sodium for both experimental techniques and copper for analysis on the Applied Biosystems 4700 instrument were performed by mixing the diluted peptide solution 1:1 with 20 mM sodium carbonate or copper sulfate salt and incubating at room temperature for one hour prior to introduction of two parts of the matrix solution.

Results and Discussion

Bradykinin fragments 1-5, 1-6, 1-7, 1-8, 2-9, bradykinin, des-Pro^2-bradykinnin, D-Phe^7-bradykinin, Lys^1-bradykinin, and bradykinin fragment 2-7 are shown as examples of peptide fragmentation by photodissociation and CID. The bradykinin

system was chosen for these experiments owing to the variation in probable location of the charge within the peptide ion and because we have an extensive library of structural information based on previous ion mobility mass spectrometry (IM-MS) and molecular dynamics studies [137]. Fragmentation of bradykinin fragment 1-5 as it relates to previously determined secondary structure is discussed. A subset of fragment ion data is presented to compare the analytical utilities of photodissociation and CID for *de novo* peptide sequencing.

We interpret the appearance of C-terminal charge retention products in the photofragment ion spectra of bradykinin fragment 1-5 (RPPGF) $[M + H]^+$ and $[M + Na]^+$ (Figure 30) as evidence that these ions have multiple charge-bearing sites. Both N- and C-terminal fragment ions also appear in the CID spectrum of RPPGF $[M + H]^+$ (Figure 31). Note that in contrast to the photofragment ion spectrum of this peptide, b_i- and y_i-type ions appear in greater relative abundances than a_i-type ions. The photofragment ion spectrum of RPPGF $[M + Na]^+$ is similar to that of $[M + H]^+$. In general, immonium ions are formed in much lower relative abundance and photodissociation to yield Na^+ is observed for all bradykinin analogue photofragment ion spectra. The minimum observable fragment m/z for tandem operation on the Applied Biosystems 4700 is set at 69.0 by the proprietary software; consequently sodium ion detachment could not be investigated in the CID experiments.

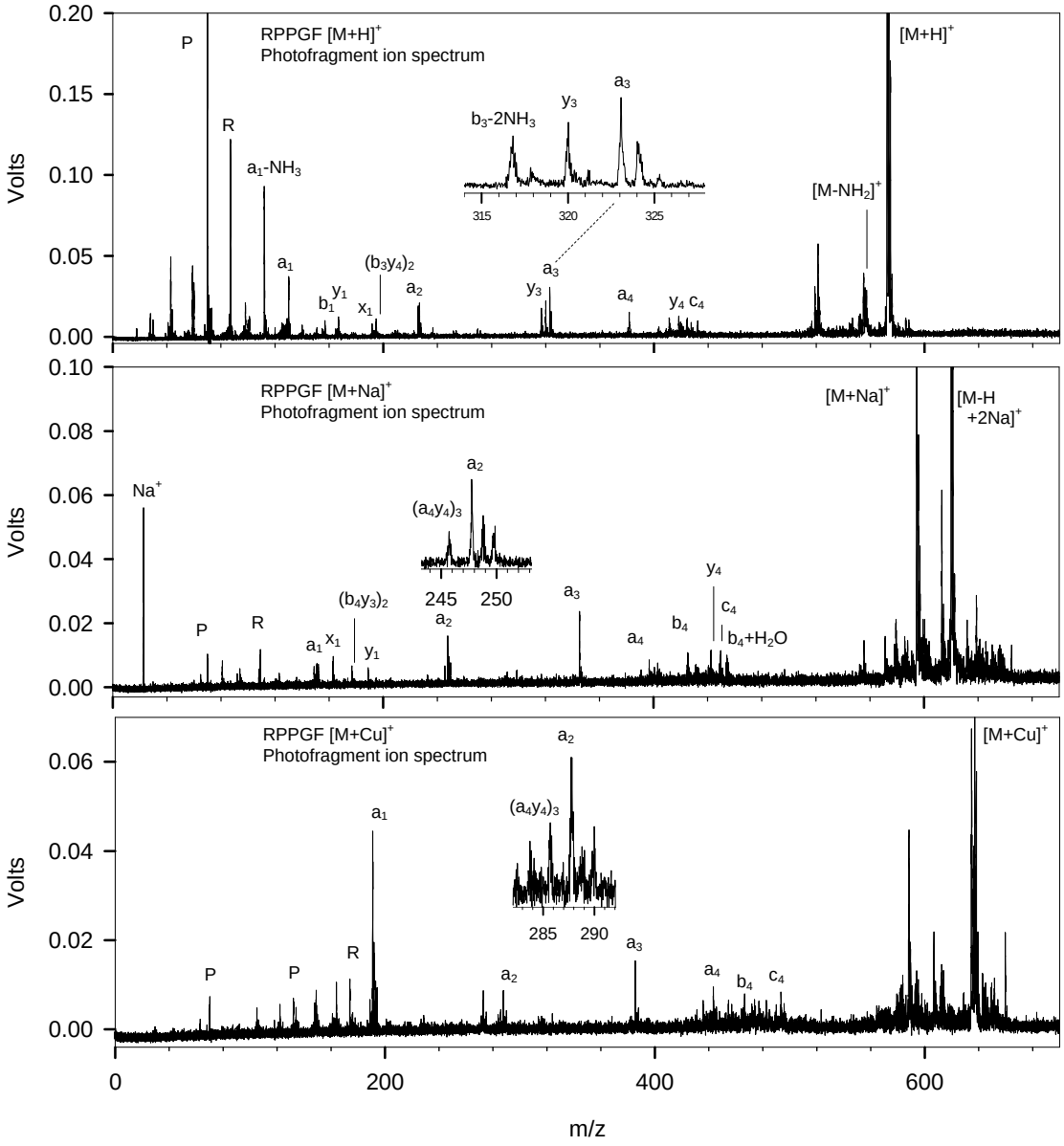

Figure 30. Photofragment ion spectra of bradykinin fragment 1-5 (RPPGF).

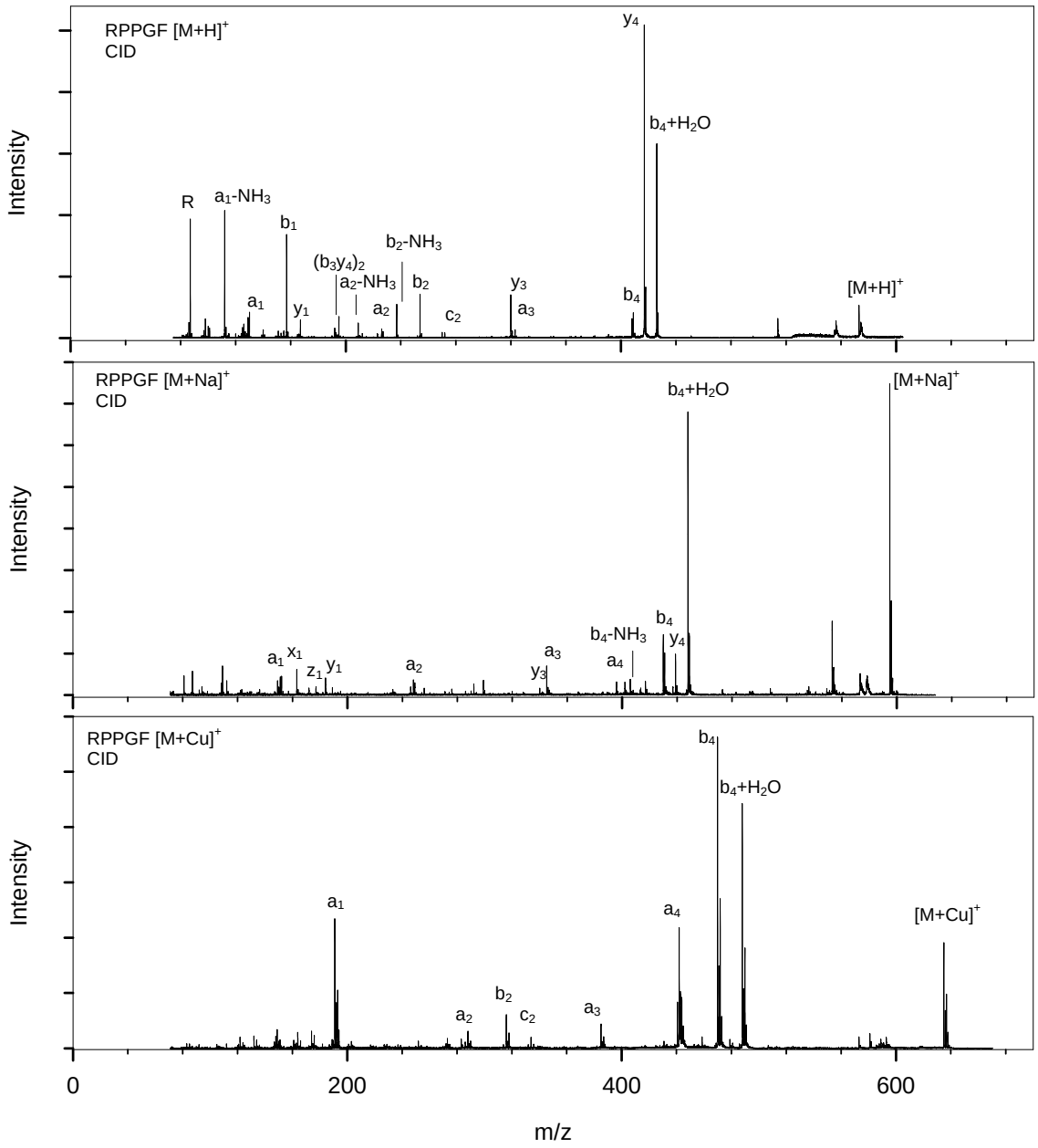

Figure 31. CID spectra of bradykinin fragment 1-5 (RPPGF).

The CID spectrum of RPPGF $[M + Na]^+$ contains few ions corresponding to ammonia loss, in contrast to the $[M + H]^+$ counterpart. Furthermore, a decrease in immonium ion relative abundance for $[M + Na]^+$ versus $[M + H]^+$ is observed. C-terminal amino acid loss [138-142] to form $b_4 + H_2O$ occurs to a high degree during the

CID TOF-TOFMS experiment; however this product appears in low abundance in the photofragment ion spectrum.

The photofragment ion spectrum of RPPGF $[M + Cu]^+$ contains a_4, b_4, and c_4 ions, revealing less bond selectivity along the peptide backbone between glycine and phenylalanine, which supports N-terminal residue charge-site interaction with the phenylalanine side chain likely via salt-bridging intramolecular solvation [137]. The reduced abundance of the a_2 ion relative to that for a_1 and a_3 ions further confirms the bond stabilization that occurs between the two proline residues via β-turn interaction (in agreement with solution-phase measurements using NMR and circular dichroism [143]). All photodissociation and CID product ions of RPPGF $[M + Cu]^+$ correspond to N-terminal charge retention. With the exception of the a_1 ion, which is lower in abundance for the $[M + H]^+$ and $[M + Na]^+$ ions, relative abundances of N-terminal sequence ions are similar for all three photofragment ion spectra, which we attribute to similar secondary structure regardless of charge carrier [137,144]. Cleavage between glycine and phenylalanine, yielding a_4, b_4, $b_4 - NH_3$, and $b_4 + H_2O$, occurs to a much greater degree in the CID spectra, possibly due to a combination of greater time allotted for fragmentation, lower energy requirements for bond cleavage, and the effects of charge-solvation involving the phenylalanine side chain and the charge carrying group of arginine. For example, our previous IM-MS studies of peptides containing an N-terminal arginine residue showed that the charge-bearing guanidino group either interacts with backbone carbonyl oxygen atoms of the first four amino acids or the phenylalanine side chain, depending upon the hydrophobicity of the solvent present

during pre-formation of ions in the MALDI spot. Both of these conformations are among MALDI-formed ions when both organic and aqueous solvents are used in sample preparation [137,144].

Photofragment ion spectra of bradykinin fragment 1-6 (RPPGFS, Figure 32) contain similar a_i-type fragment ions to those of RPPGF. Fewer C-terminal fragment ions are present, appearing as x_i-type ions rather than y_i. The CID spectra (Figure 33) of $[M + H]^+$ and $[M + Na]^+$ also contain higher relative abundances of b_i- and y_i-type ions than their corresponding photofragment ion spectra, as well as a much greater number of small neutral loss ions and internal cleavage products. Note that various fragment ions resulting from charge-directed cleavage at the serine residue (*i.e.* a_5, b_5, $b_5 + H_2O$, and d_{6a}) appear in high abundance in the CID spectrum of $[M + Na]^+$ which are absent from the photofragment ion spectrum. This result is likely due to a greater effect of the mobile charge within the vibrationally activated ion over a longer timescale of observable fragmentation. Dissociation of $[M + Cu]^+$ results in higher abundances of a_i- and b_i-type ions for both methods while greatly reducing contributions from multiple cleavage products.

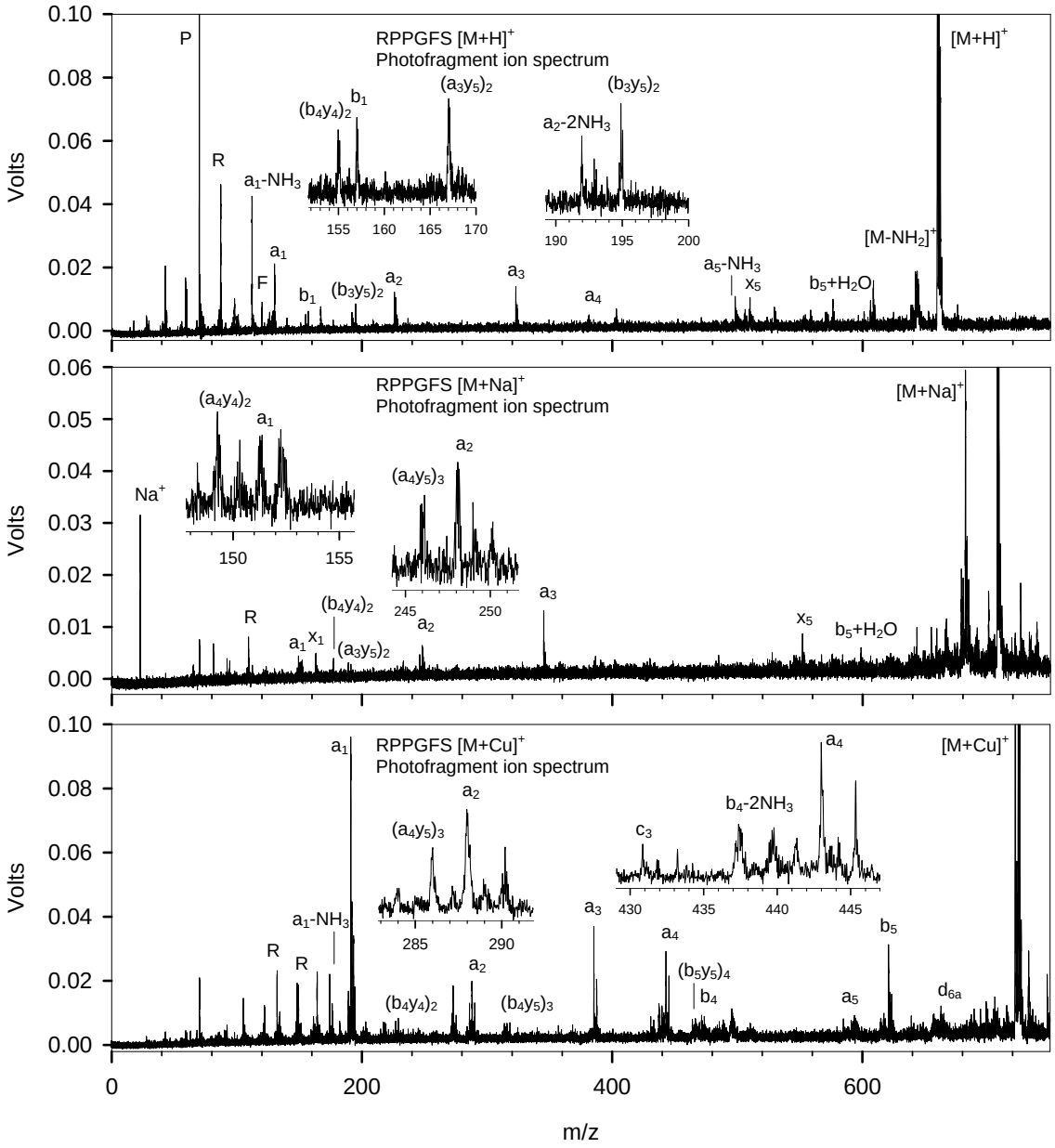

Figure 32. Photofragment ion spectra of bradykinin fragment 1-6 (RRPGFS).

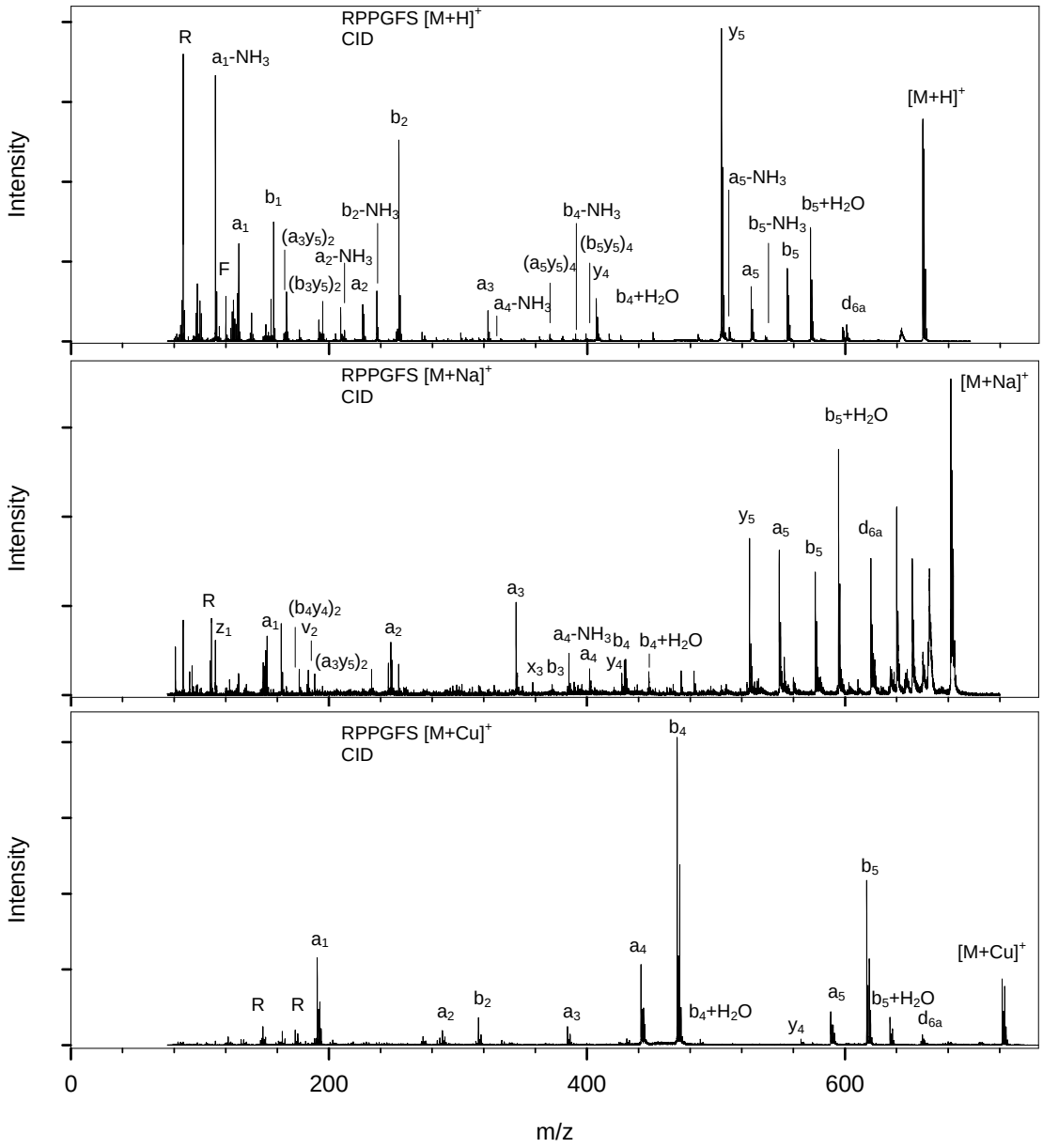

Figure 33. CID spectra of bradykinin fragment 1-6 (RRPGFS).

Photofragmentation of bradykinin fragment 1-7 (RPPGFSP) $[M + H]^+$ (Figure 34) yields a complete series of a_i ions and low abundance of internal fragments and small neutral losses from fragment ions. Complete sequence information is also obtained from the CID spectrum of this peptide (Figure 35) by examining both N- and

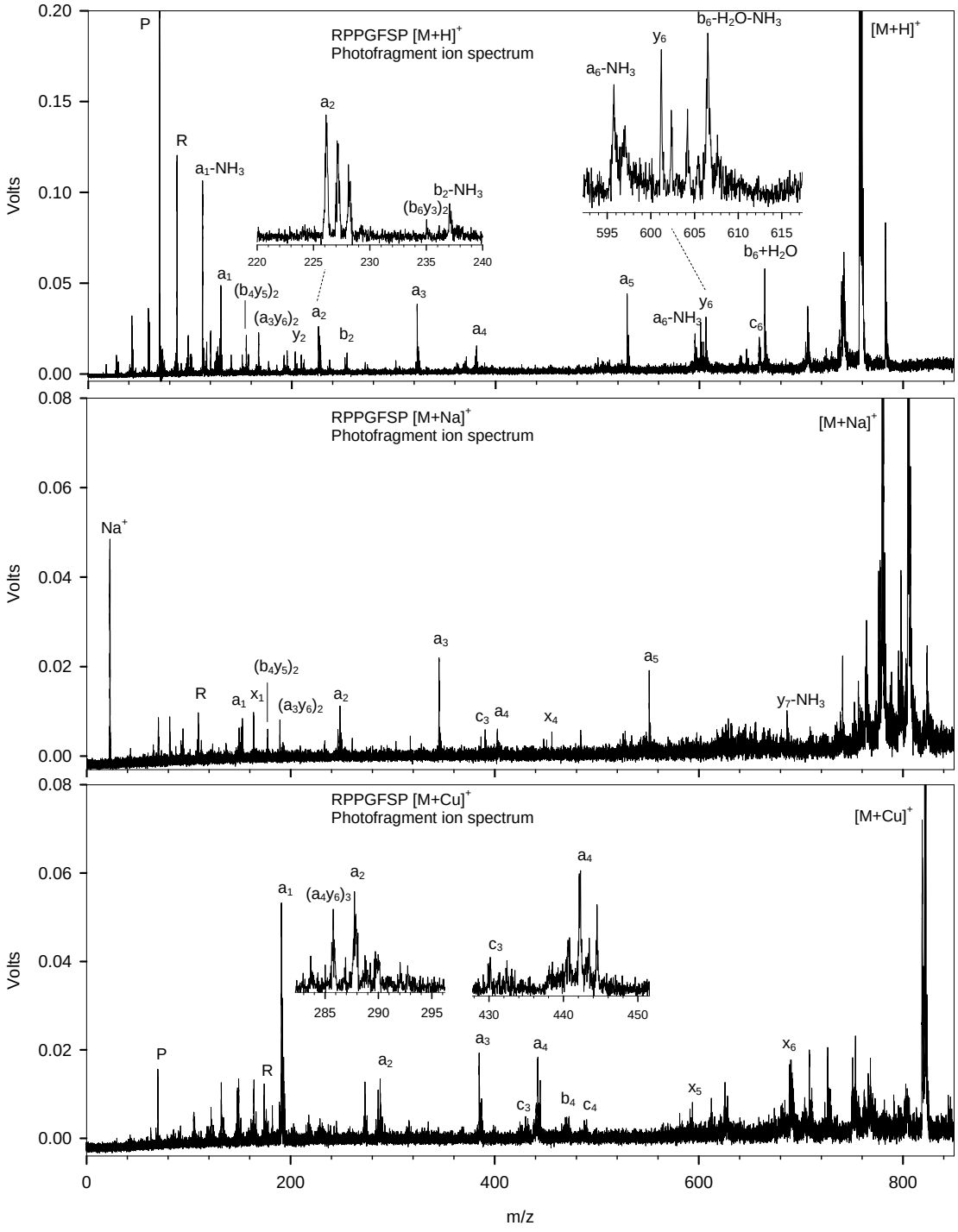

Figure 34. Photofragment ion spectra of bradykinin fragment 1-7 (RPPGFSP).

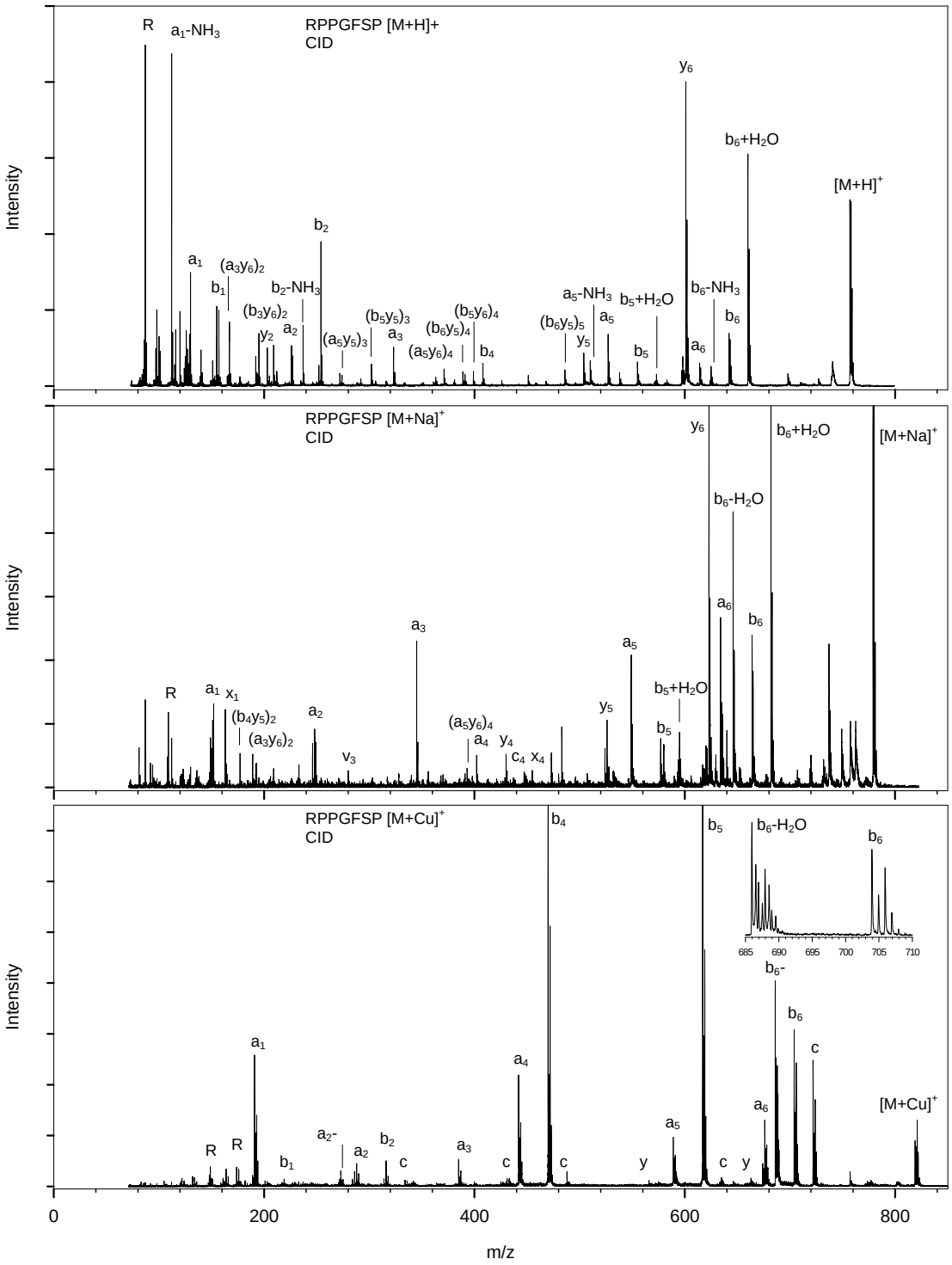

Figure 35. CID spectra of bradykinin fragment 1-7 (RPPGFSP).

C-terminal ions; however, this CID spectrum is congested by secondary fragmentation products. Many ions are identified in the CID spectrum of RPPGFSP $[M + Na]^+$ arising from fragmentation at the serine residue (such as a_6, b_6, $b_6 - H_2O$, and $b_6 + H_2O$), whereas sequence ions are observed in the photofragment ion spectrum for the first five amino acid residues only. Fragmentation of $[M + Cu]^+$ by CID results in increased signal from b_i-type ions, while the photofragment ion spectrum is composed primarily of a_i-type ions. Both RPPGFSP $[M + Cu]^+$ mass spectra contain a majority of N-terminal sequence informative ions.

Photodissociation of bradykinin fragment 1-8 (RPPGFSPF) $[M + H]^+$ (Figure 36) yields predominantly a_i-type ions. The $b_7 + H_2O$ is observed in low abundance, and is absent from the photofragment ion spectra of $[M + Na]^+$ and $[M + Cu]^+$. The $[M + Cu]^+$ ion photodissociates in a qualitatively similar manner to its $[M + H]^+$ counterpart. The most abundant sequence ions in the CID spectrum of RPPGFSPF $[M + H]^+$ (Figure 37) are y_7 and $b_7 + H_2O$. The remaining fragments consist of mainly a_i- and b_i-type ions with their corresponding ammonia loss ions. The CID of RPPGFSPF $[M + Na]^+$ results in a greater abundance of a_3 and a_5 ions as well as a much greater abundance of y_7 ion, again revealing that Na^+ preferentially binds to the backbone carbonyl oxygen atoms at phenylalanine and proline residues. Fragmentation of RPPGFSPF $[M + Cu]^+$ by this method results in exclusively N-terminal charge carrying ions, strong evidence that the copper ion is permanently bound to the N-terminal arginine. In contrast to the $[M + H]^+$ and $[M + Na]^+$ ions by CID and all three by photodissociation, b_i-type ions are in much higher abundance than a_i-type ions. As demonstrated by Dongré *et al*. [63], a peptide

ion having a highly localized charge requires greater activation energy for fragmentation. Due to increased activation energy for dissociation of $[M + Cu]^+$, lower energy fragmentation products [120] are observed in greater relative abundance under the same MS operating conditions.

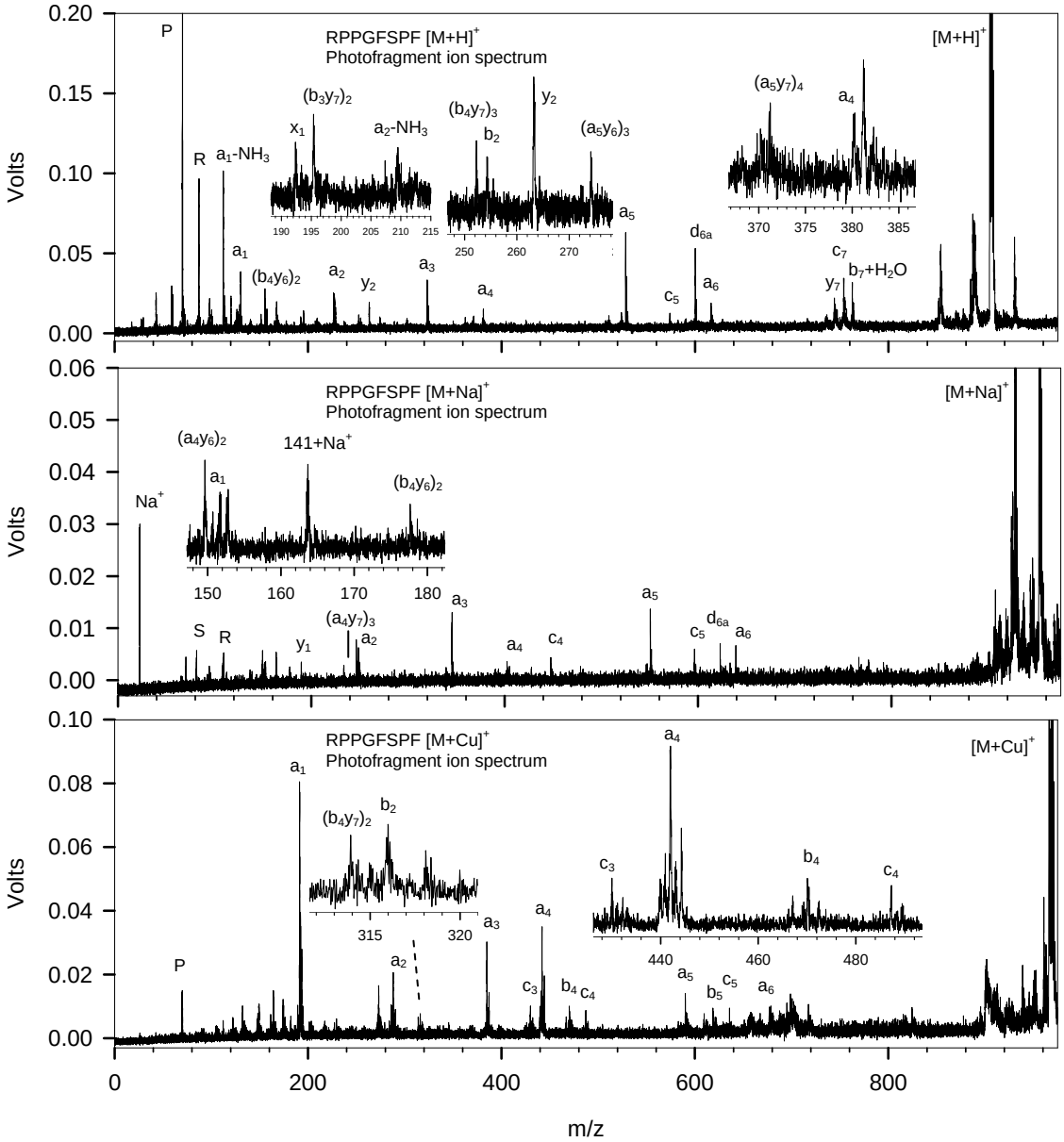

Figure 36. Photofragment ion spectra of bradykinin fragment 1-8 (RPPGFSPF). [56] (Reprinted with permission from Elsevier)

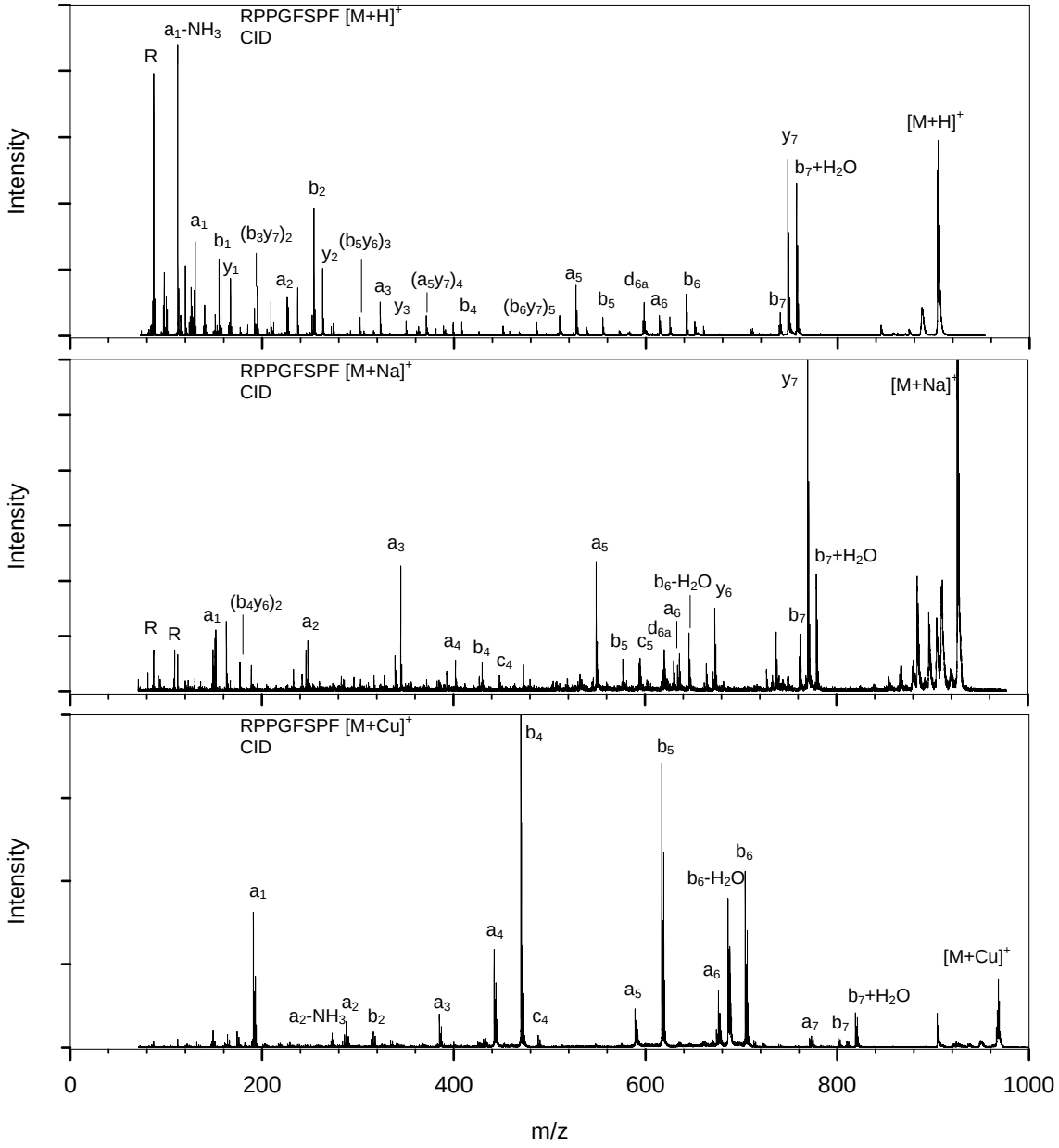

Figure 37. CID spectra of bradykinin fragment 1-8 (RPPGFSPF).

The photofragment ion spectrum of bradykinin fragment 2-9 (PPGFSPFR) $[M + H]^+$ ions contains both N-terminal and C-terminal fragment ions (Figure 38). The C-terminal fragment ions are primarily x_i-type ions, the result of cleavage of a carbon-

carbon bond along the peptide backbone. Other ions observed having C-terminal charge retention include those arising from bond cleavage between a side-chain α-carbon and the backbone of a y_i-type ion (v_i-type ions) and from cleavage between α- and β-carbons of the side-chains of z_i-type ions (w_{ia}-type ions). Similar to the photofragment ion spectrum, a greater abundance of C-terminal fragment ions is observed in the CID spectrum of PPGFSPFR (Figure 39) relative to that of the N-terminal arginine containing peptides. Note the appearance of a strong peak for $b_7 + H_2O$ in the CID spectrum that is absent in the photodissociation spectrum. Conversely, this product is the most abundant fragment ion in the photodissociation of PPGFSPFR $[M + Na]^+$. The remaining photofragment ions of $[M + Na]^+$ are limited to N-terminal charge carriers and sodium ion. Similar amplification of the $b_7 + H_2O$ ion occurs in the CID spectrum of PPGFSPFR $[M + Na]^+$. Similar to the photofragment ion spectrum, N-terminal sequence ions are detected.

The $b_7 + H_2O$ ion is not present among the photodissociation products of PPGFSPFR $[M + Cu]^+$ and is also absent from the CID spectrum of this peptide. This result is best explained using the mechanism for C-terminal amino acid loss proposed by Renner and Spiteller [145]. When the Cu^+ ion is bound to the guanidino group of the arginine side chain, the C-terminal amino acid fragment retains the positive charge, leaving $b_7 + OH$ as a neutral (Figure 40). This mechanism explains the appearance of m/z 191, isomass with the a_1 ion of the N-terminal arginine containing $[M + Cu]^+$ peptide ions, in both tandem mass spectra of PPGFSPFR $[M + Cu]^+$. The decreased relative

abundance of N-terminal versus C-terminal fragment ions confirms prior results that copper binding energy is higher for arginine side chain than the N-terminal amine [133].

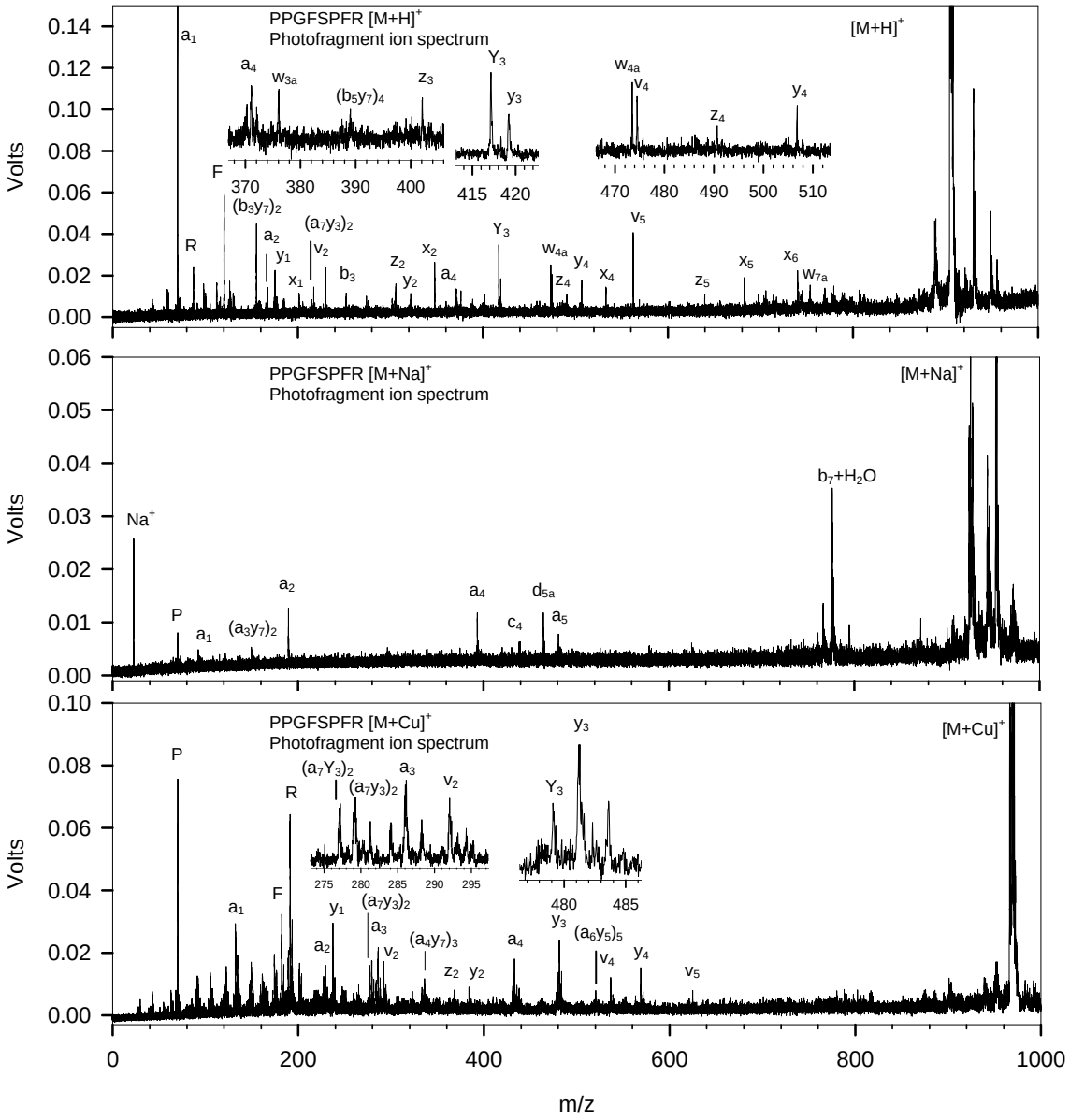

Figure 38. Photofragment ion spectra of bradykinin fragment 2-9 (PPGFSPFR).

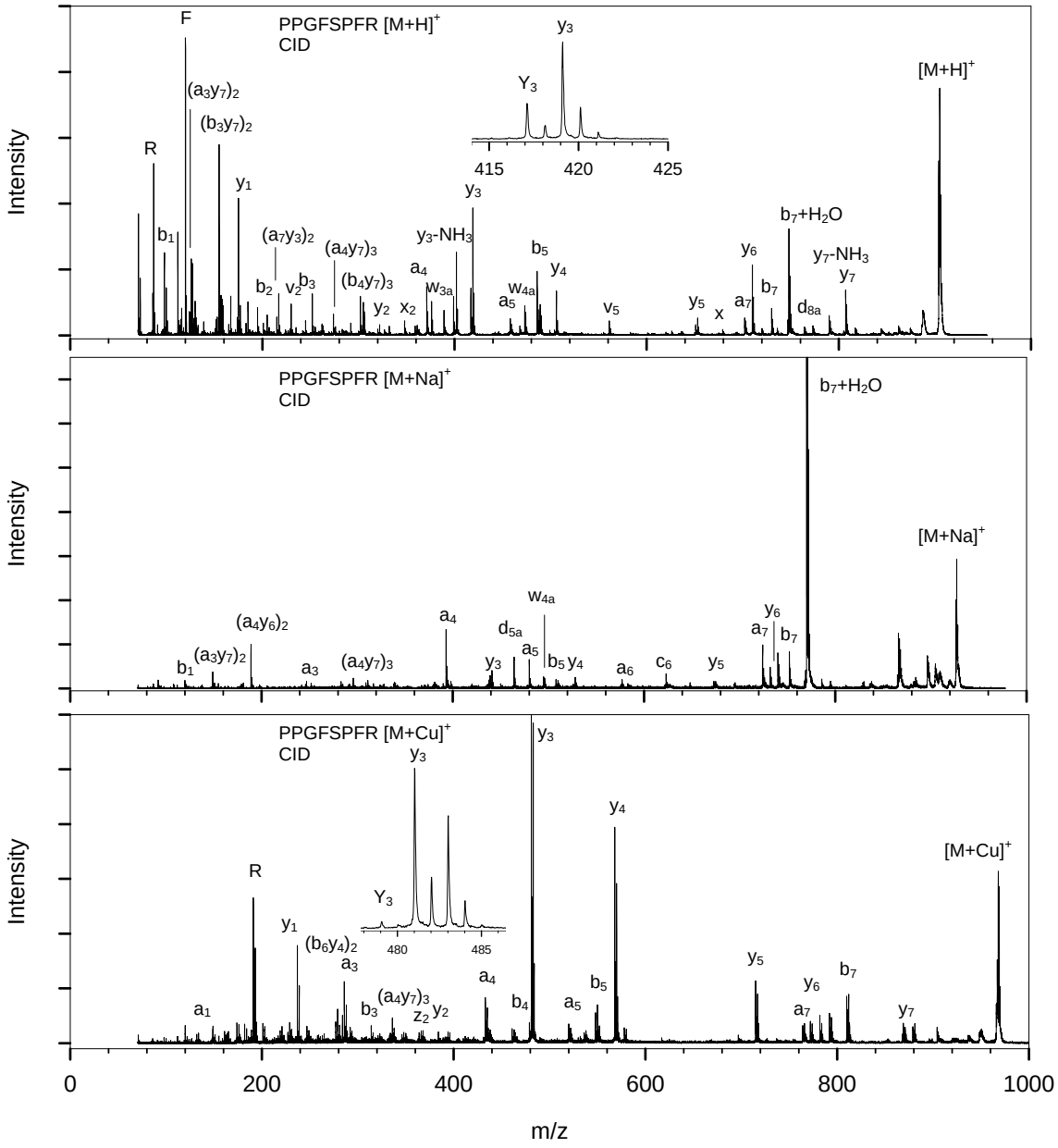

Figure 39. CID spectra of bradykinin fragment 2-9 (PPGFSPFR).

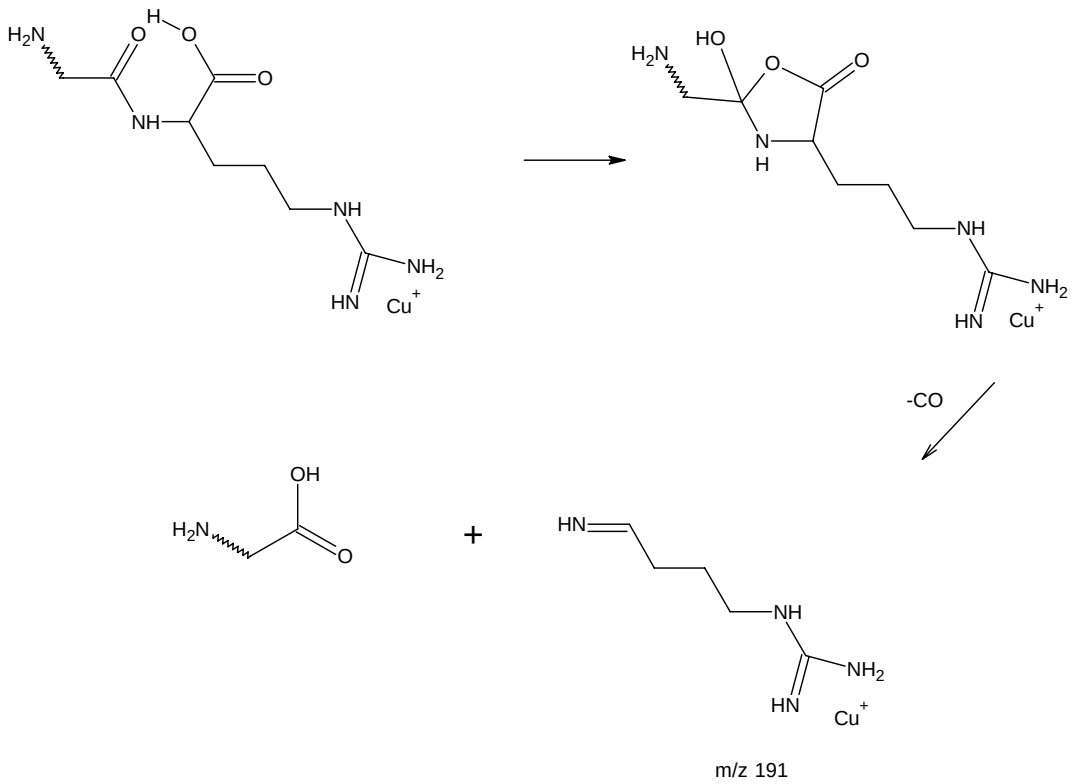

Figure 40. Fragmentation scheme for C-terminal amino acid loss with copper ion immobilized on the arginine side chain.

The photofragment ion spectrum of bradykinin (RPPGFSPFR) $[M + H]^+$ (Figure 41) contains a_i-type ion signals for the first six amino acids in the sequence. The d_{6a} ion representing side-chain loss from serine is observed along with the a_6 ion. The most abundant photofragment ion is proline immonium ion, and two proline-containing internal fragments are present. We speculate that the proline residues provide basic sites for charge-directed fragmentation [63]. The appearance of the a_1 ion is consistent with the high basicity of the arginine side chain and/or the N-terminal amine. Note also the major peak $b_8 + H_2O$ corresponding to a rearrangement with loss of the C-terminal arginine. The CID spectrum of RPPGFSPFR $[M + H]^+$ (Figure 42) contains both N-

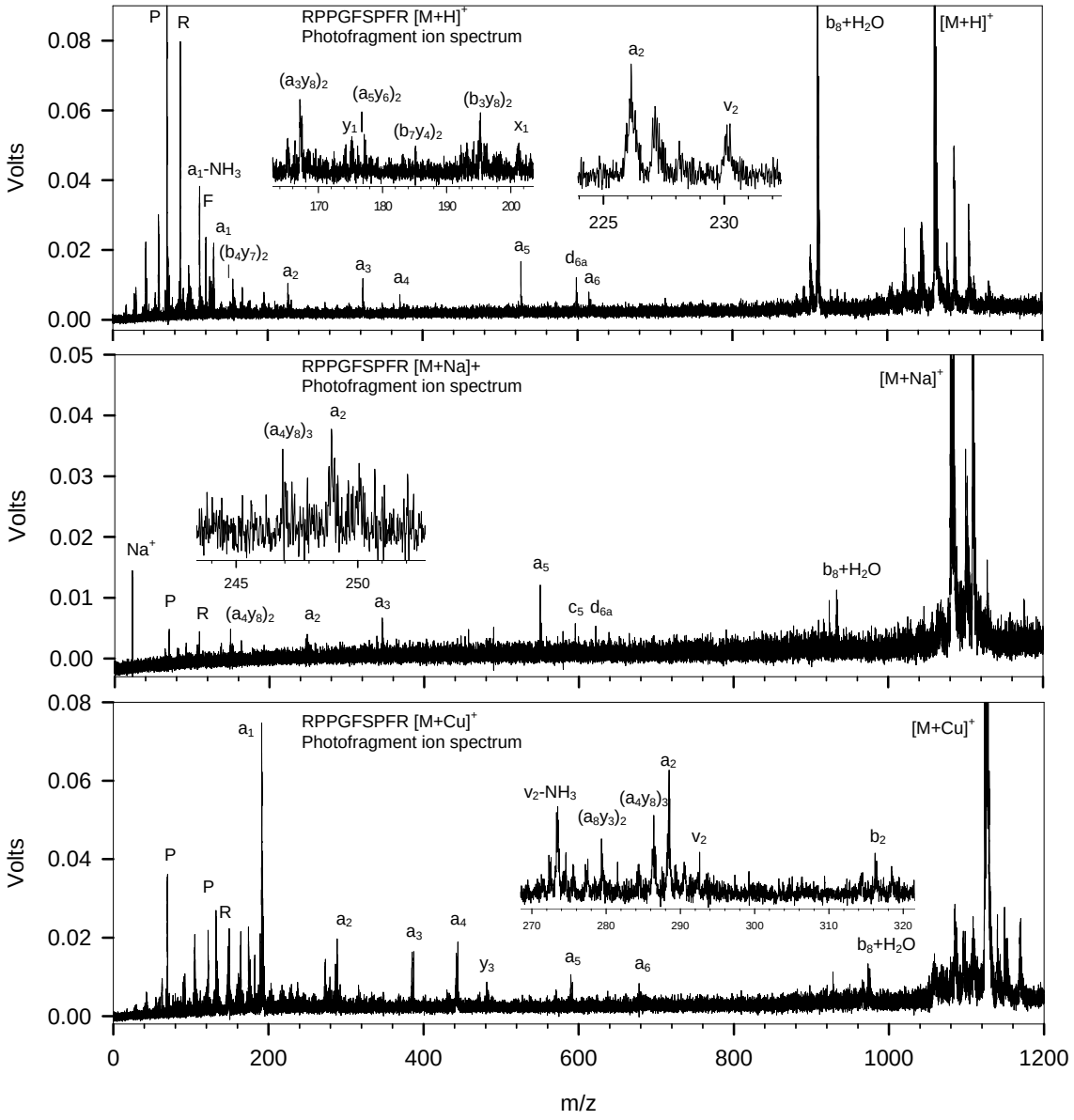

Figure 41. Photofragment ion spectra of bradykinin (RPPGFSPFR). [56] (Reprinted with permission from Elsevier)

and C-terminal charge carrying fragment ions and exhibits less bond selectivity along the peptide backbone. In addition, there are abundant signals for internal fragmentation products and ions resulting from small neutral loss from internal fragments.

Comparisons between the RPPGFSPFR $[M + Na]^+$ mass spectra are very similar to those of the peptides shown above.

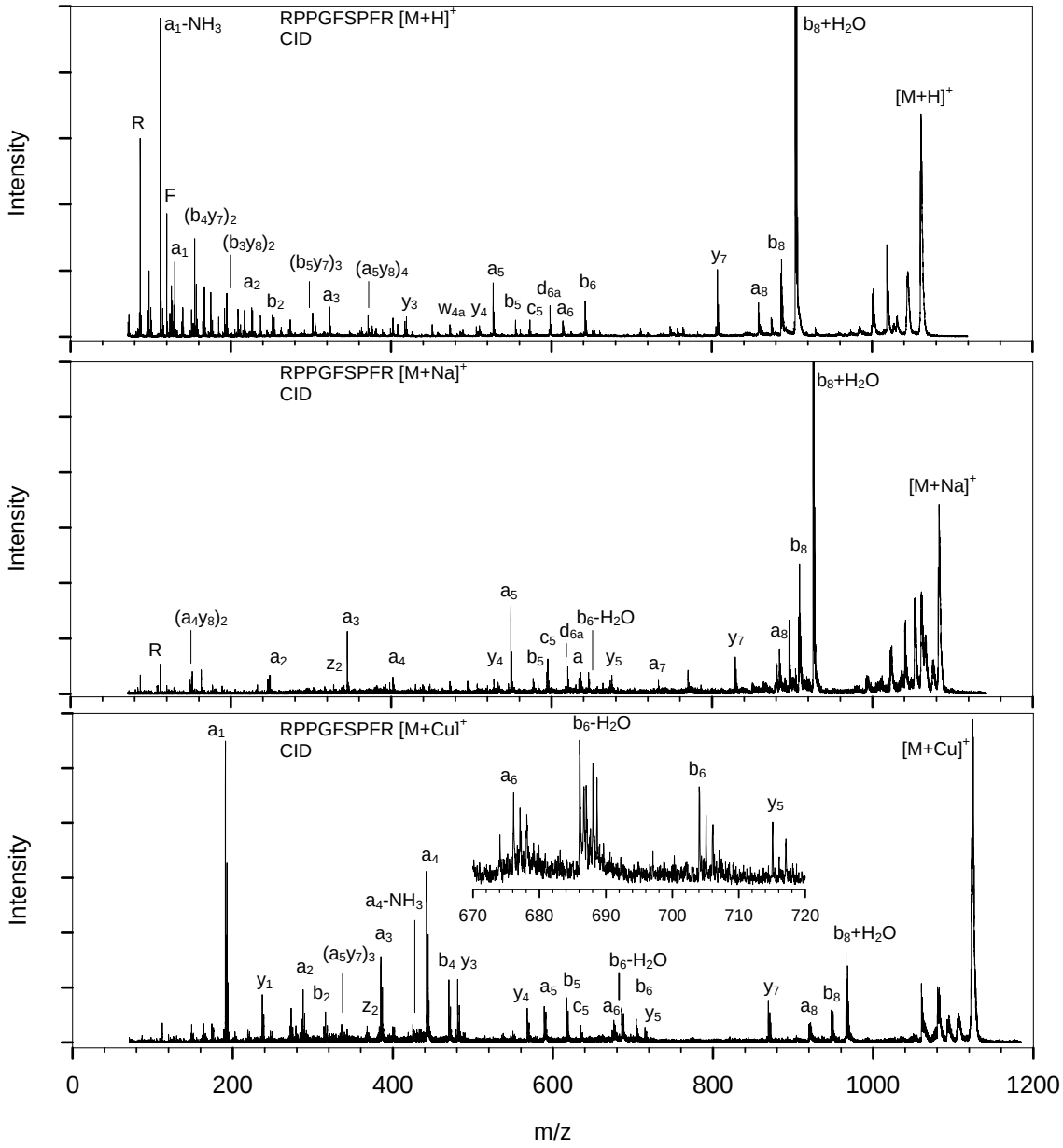

Figure 42. CID spectra of bradykinin (RPPGFSPFR).

Photodissociation of RPPGFSPFR $[M + Cu]^+$ also yields a_i-type ions for the first six amino acid residues. Similar to the photodissociation products of RPPGFSPFR $[M + H]^+$ and $[M + Na]^+$, the charge is predominantly retained on the N-terminal side of the dissociating bond. The appearance of the y_3 ion demonstrates that Cu^+ may also bind to the C-terminal arginine. Proline immonium ion appears in the spectrum twice, carrying the charge as both Cu^+ and H^+. Note that photodetachment of Cu^+ is not observed for any of the peptide $[M + Cu]^+$ ions examined. Similar a_i-type ion abundances are observed in the CID spectrum of RPPGFSPFR $[M + Cu]^+$ along with b_i-, c_i-, and y_i-type ions. Upon comparison of these two spectra we speculate that the copper ion is more strongly bound to the N-terminal arginine of bradykinin than the C-terminal arginine, as suggested by Bluhm *et al*. [133].

Photodissociation and CID product ions of des-Pro^2-bradykinin (RPGFSPFR, Figure 43-44) and D-Phe^7-bradykinin (RPPGFSFFR, Figure 45-46) are similar in identity and relative abundances to those of bradykinin. Differences include a small abundance of C-terminally charged fragment ions appearing in photofragment ion spectrum of RPGFSPFR $[M + H]^+$ and the appearance of the a_7 ion in the photofragment ion spectrum of RPPGFSFFR $[M + H]^+$. The latter result is likely due to the increased UV absorption of phenylalanine over that of proline.

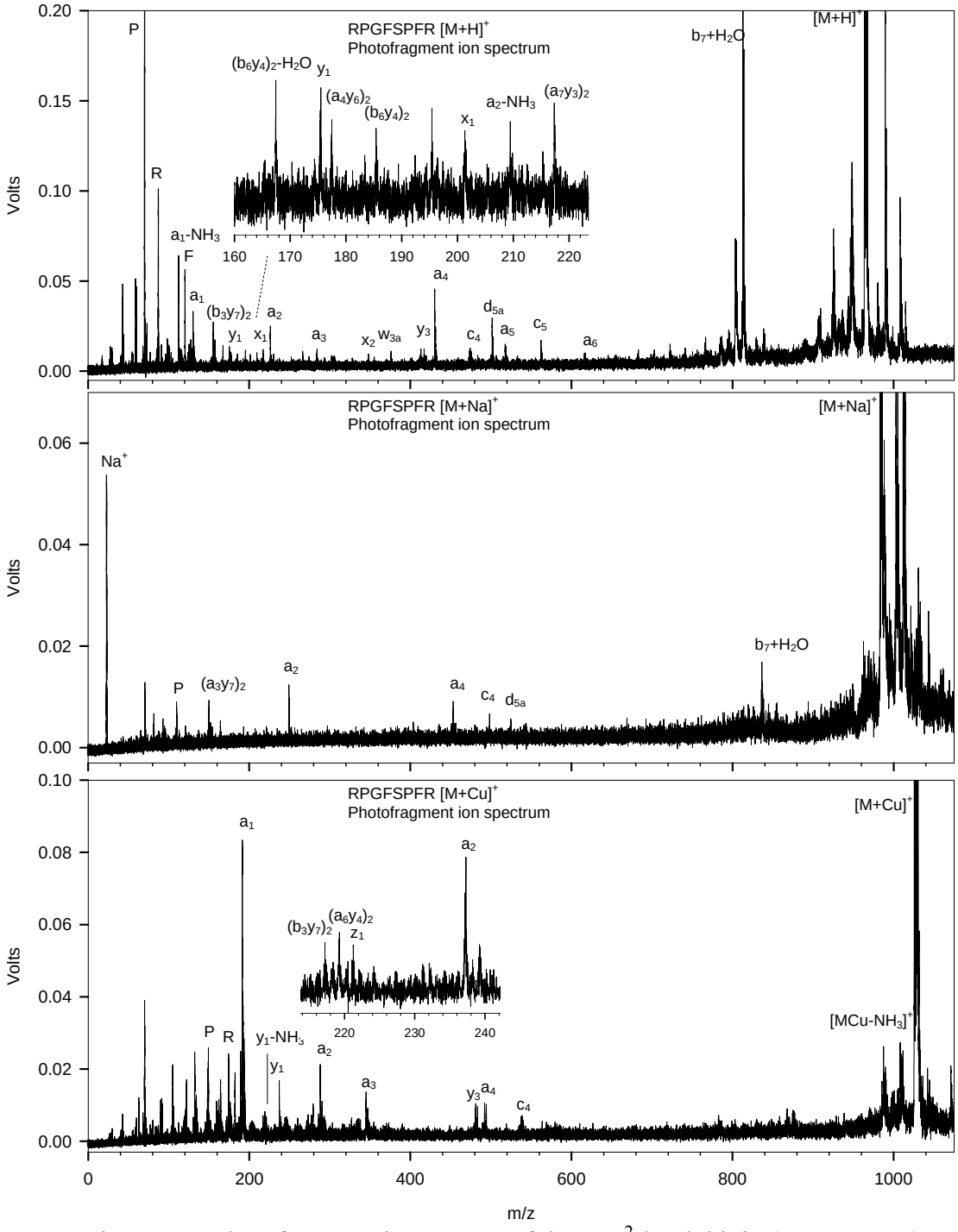

Figure 43. Photofragment ion spectra of des-Pro^2-bradykinin (RPGFSPFR).

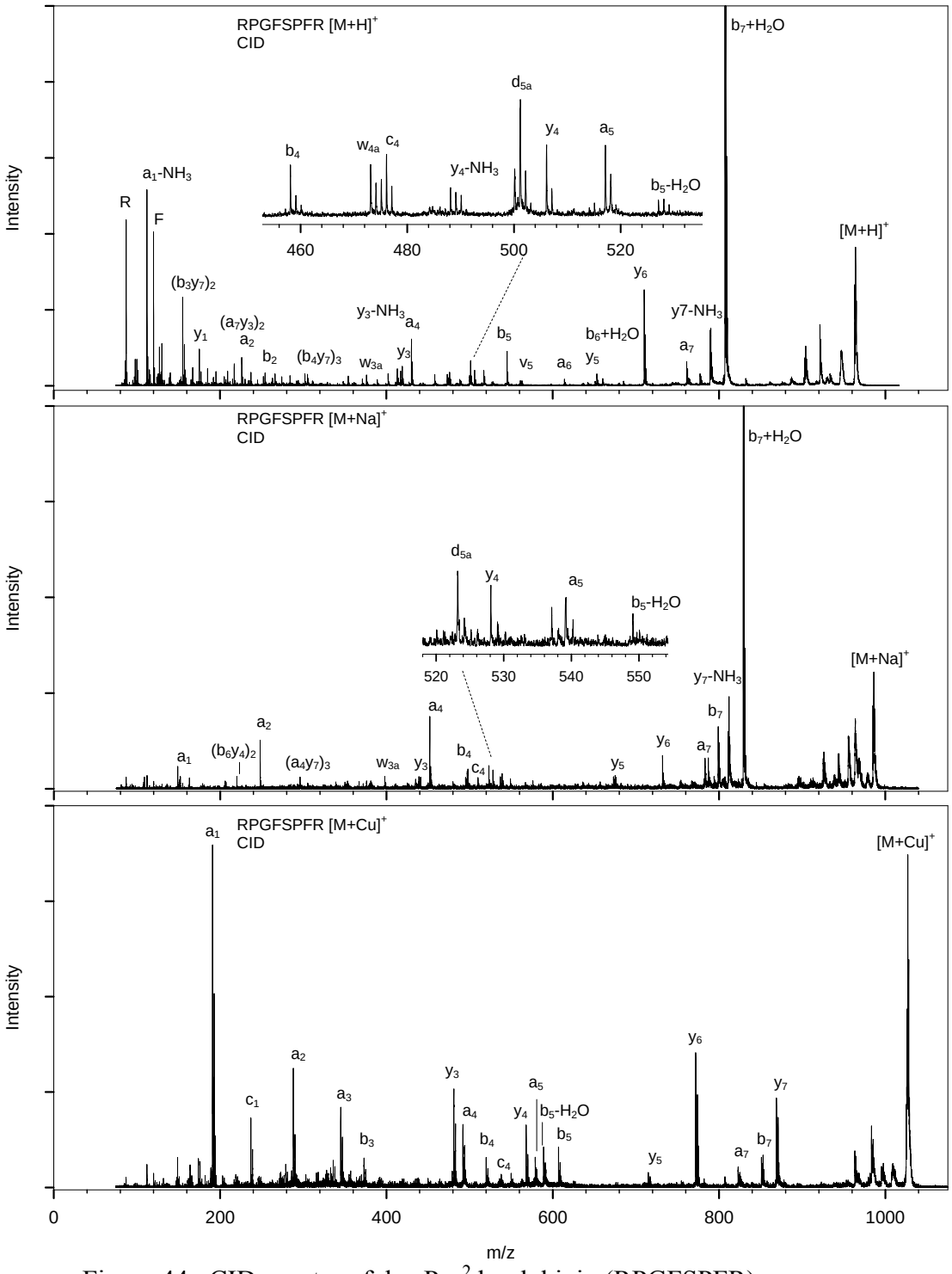

Figure 44. CID spectra of des-Pro^2 bradykinin (RPGFSPFR).

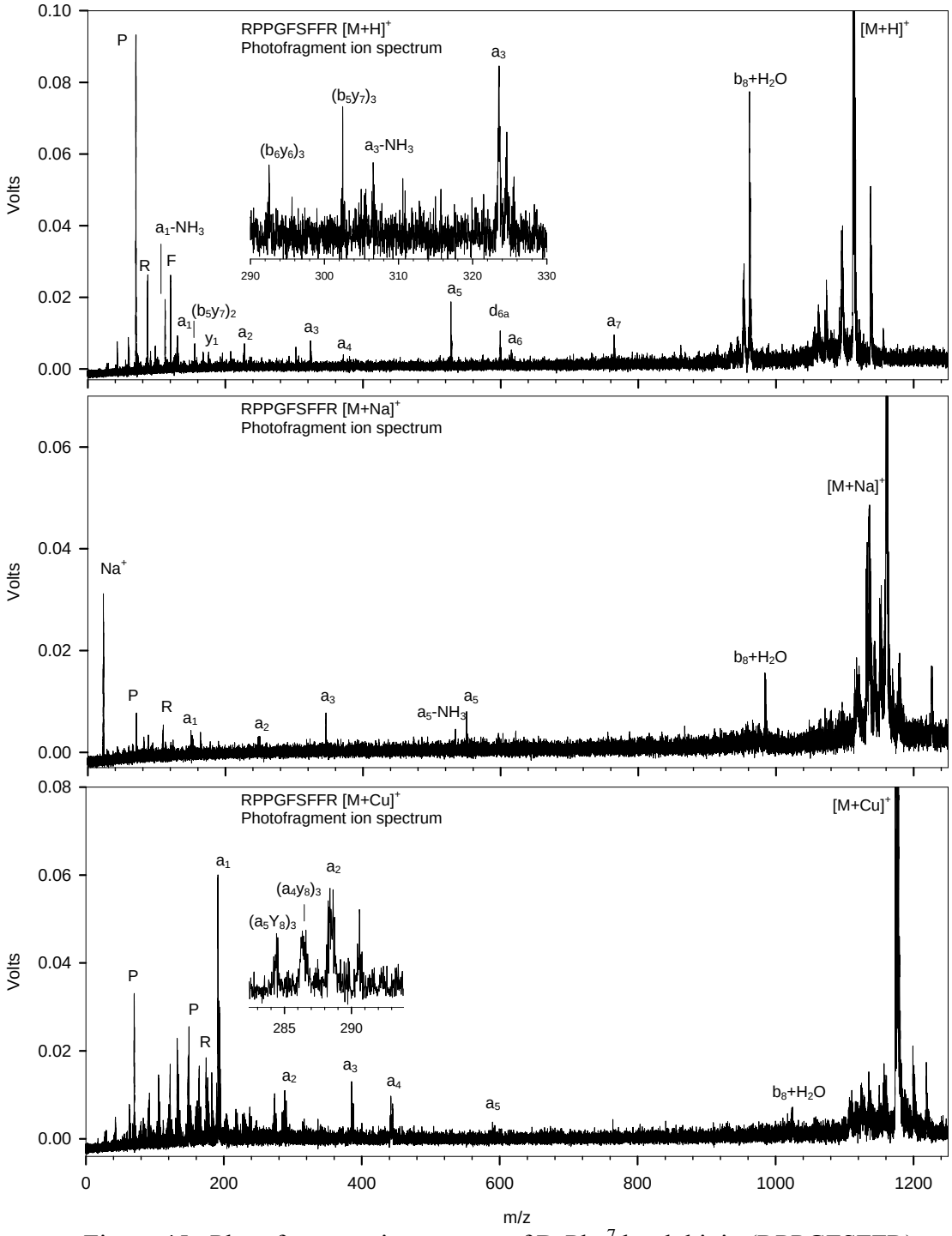

Figure 45. Photofragment ion spectra of D-Phe[7] bradykinin (RPPGFSFFR).

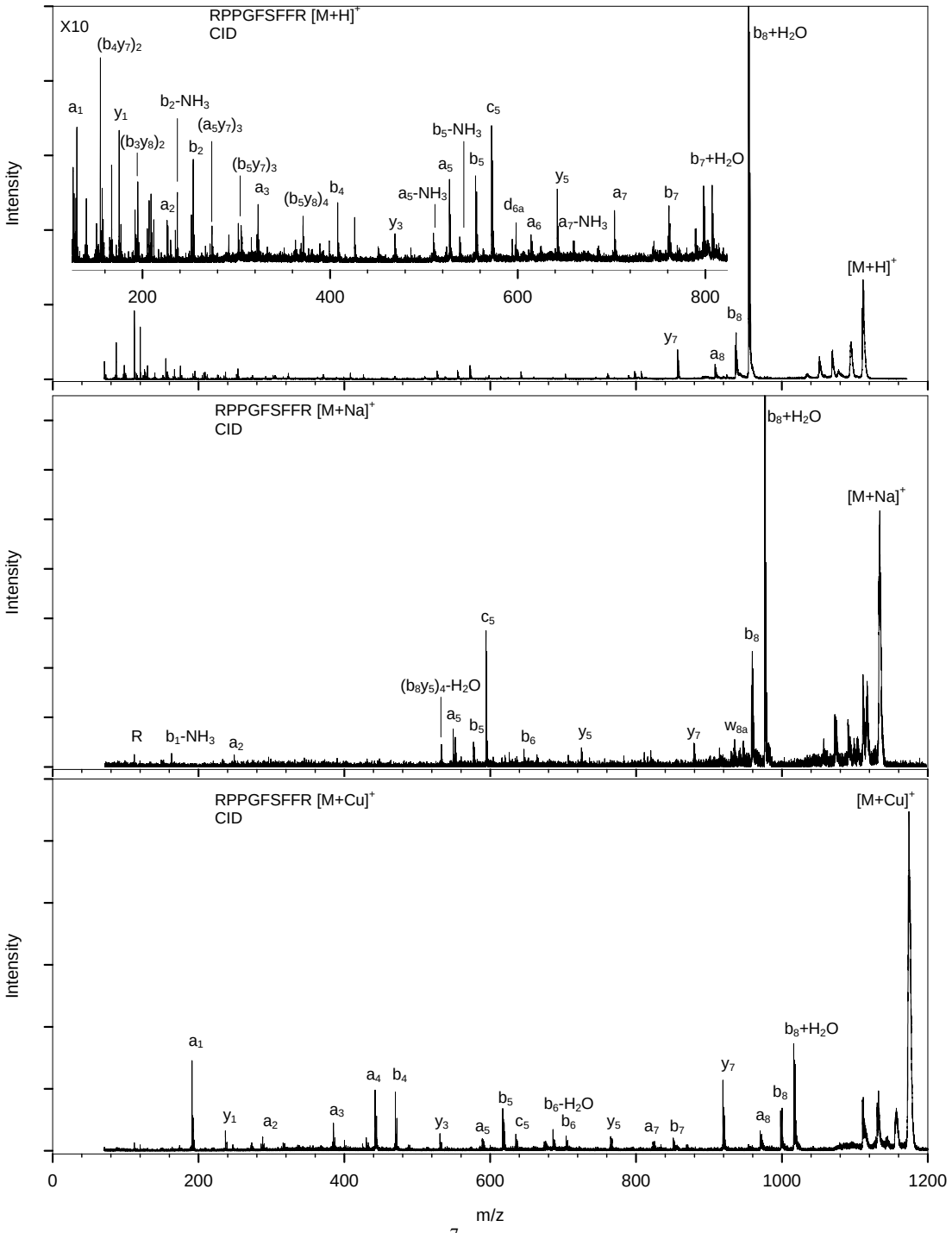

Figure 46. CID spectra of D-Phe^7 bradykinin (RPPGFSFFR).

In contrast to RPPGFSPFR $[M + H]^+$, photodissociation of Lys^1-bradykinin (KPPGFSPFR) $[M + H]^+$ (Figure 47) produces predominantly C-terminal sequence ions of types x_i, y_i, and z_i with significant abundances of side chain cleavage products of type v_i and w_{ia}. In this case, the C-terminal arginine has a higher proton affinity than the N-terminal lysine. Two Y_i-type ions are observed in this photofragment ion spectrum in similar abundance to their corresponding y_i-type ions. These products may be the result of direct cleavage of the amide bonds without oxazolone ring formation and proton transfer as described by Paizs and Suhai [120], or through H_2 elimination from the y_i-type ion. The abundances of the Y_i-type ions are greatly reduced in the photofragment ion spectrum of $[M + Cu]^+$. The same effect is observed in the CID spectra of these precursors (Figure 48), although relative abundances of the Y_i-type ions are always less than the y_i-type ions at the same position. The photofragment ion spectrum of KPPGFSPFR $[M + Na]^+$ is dominated by sodium ion and b_8+H_2O, while the CID spectrum contains many fragment ions. It may be that the charge carrier is not a product ion of CID, although this possibility could not be investigated. The photofragment ion spectrum of KPPGFSPFR $[M + Cu]^+$ contains nearly equal abundances of N-terminal and C-terminal fragment ions, a result of similar copper ion affinities for N-terminal lysine and C-terminal arginine (120.4 kcal/mol and 136.1 kcal/mol, respectively) [133]. An analogous result is also observed in the CID spectrum of $[M + Cu]^+$.

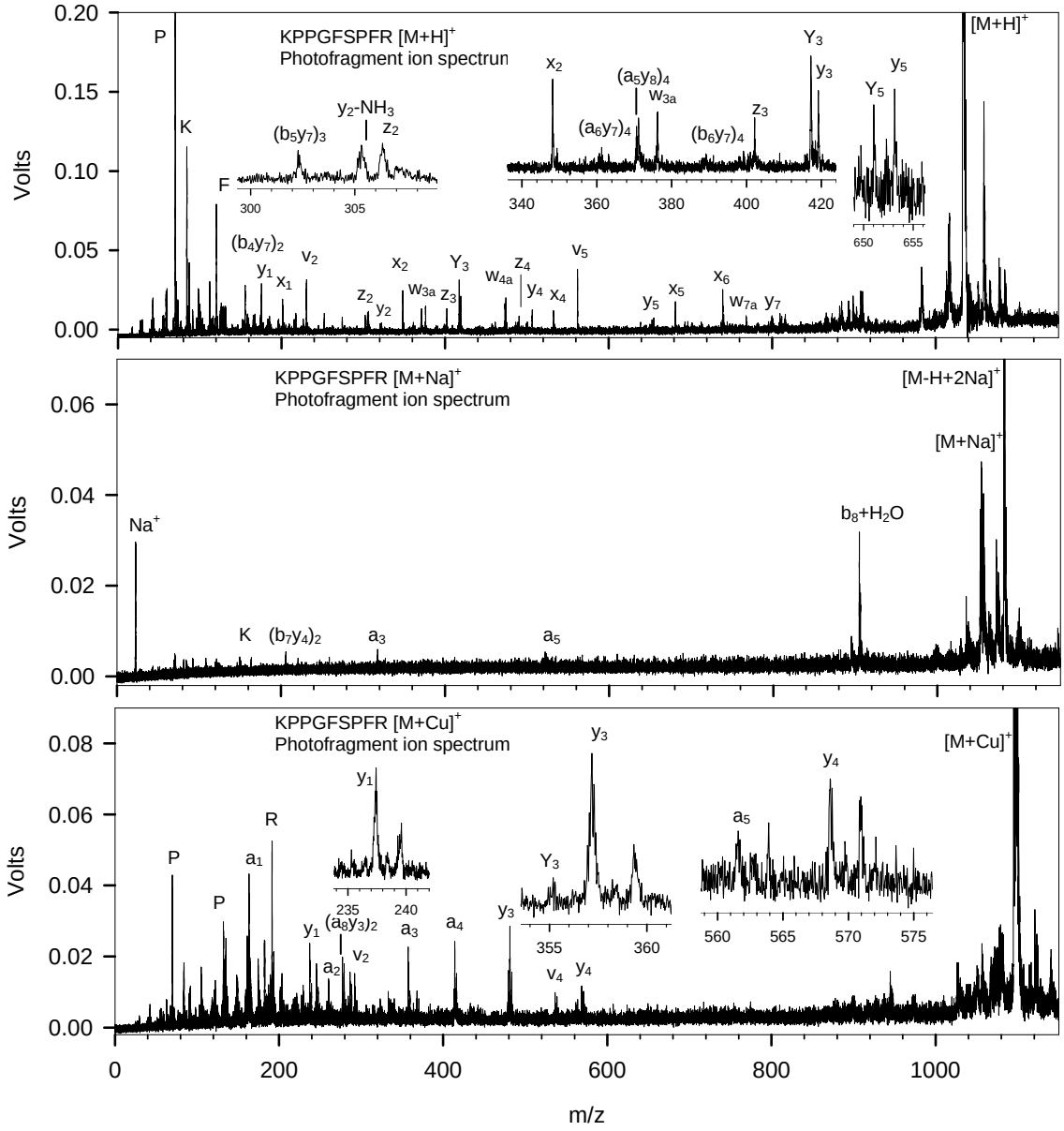

Figure 47. Photofragment ion spectra of Lys[1]-bradykinin (KPPGFSPFR).

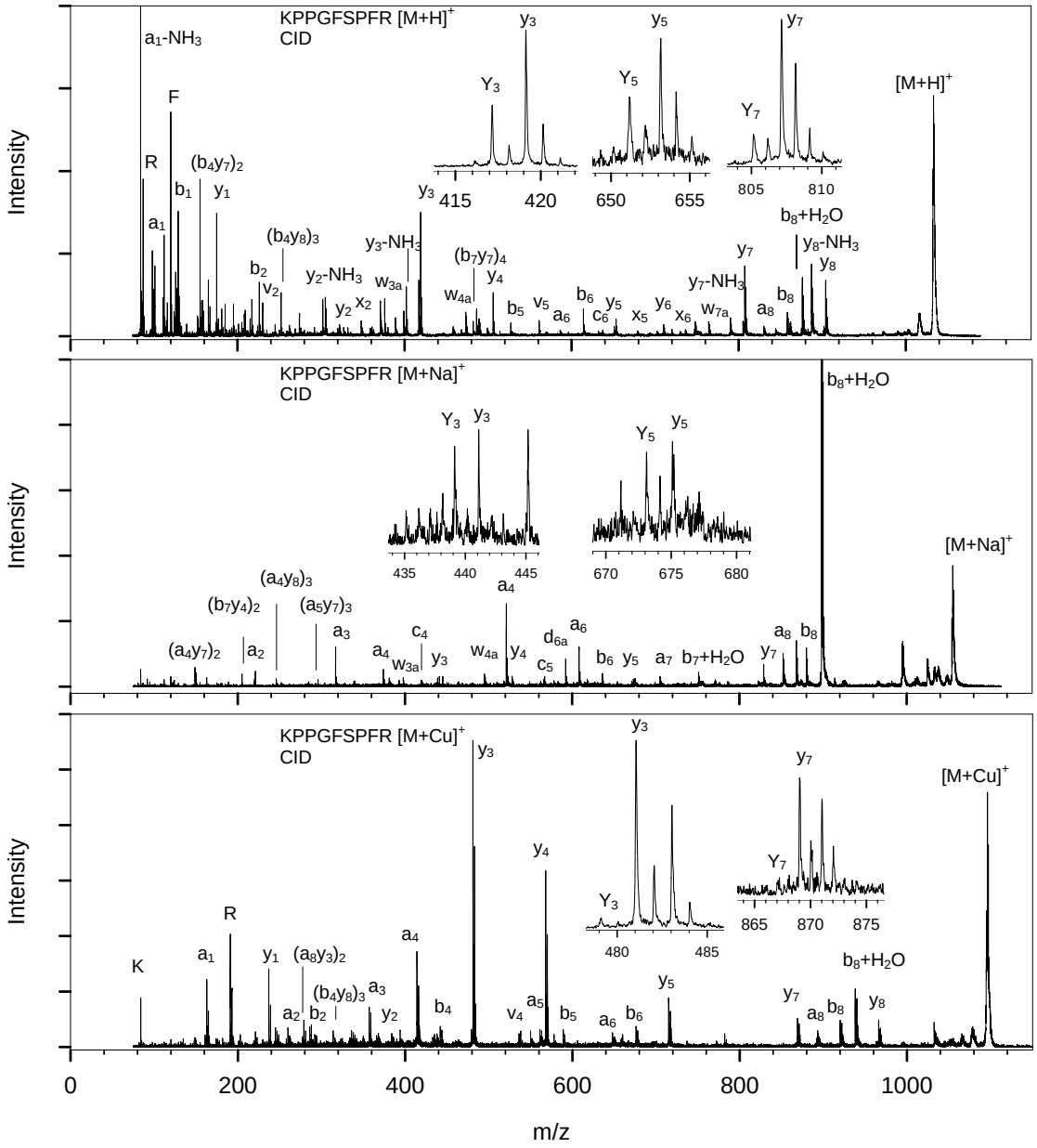

Figure 48. CID spectra of Lys[1]-bradykinin (KPPGFSPFR).

Photofragment ion spectra of bradykinin fragment 2-7 (PPGFSP) $[M + H]^+$ and $[M + Na]^+$ (Figure 49) contain a variety of sequence ion types, with both N- and C-terminal charge carriers, including internal fragment ions. Conversely the photofragment ion spectrum of PPGFSP $[M + Cu]^+$ is almost exclusively composed of

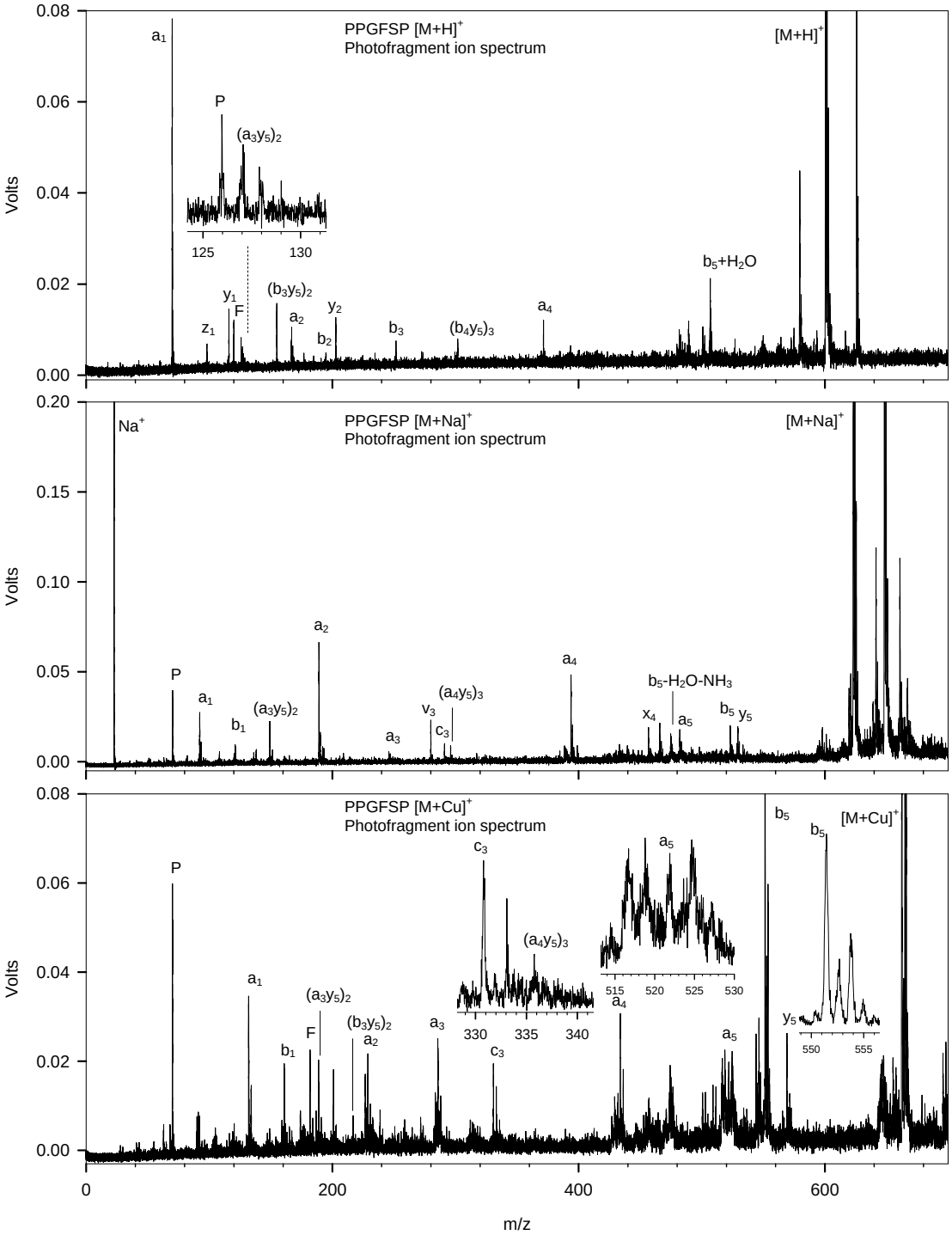

Figure 49. Photofragment ion spectra of bradykinin fragment 2-7 (PPGFSP).

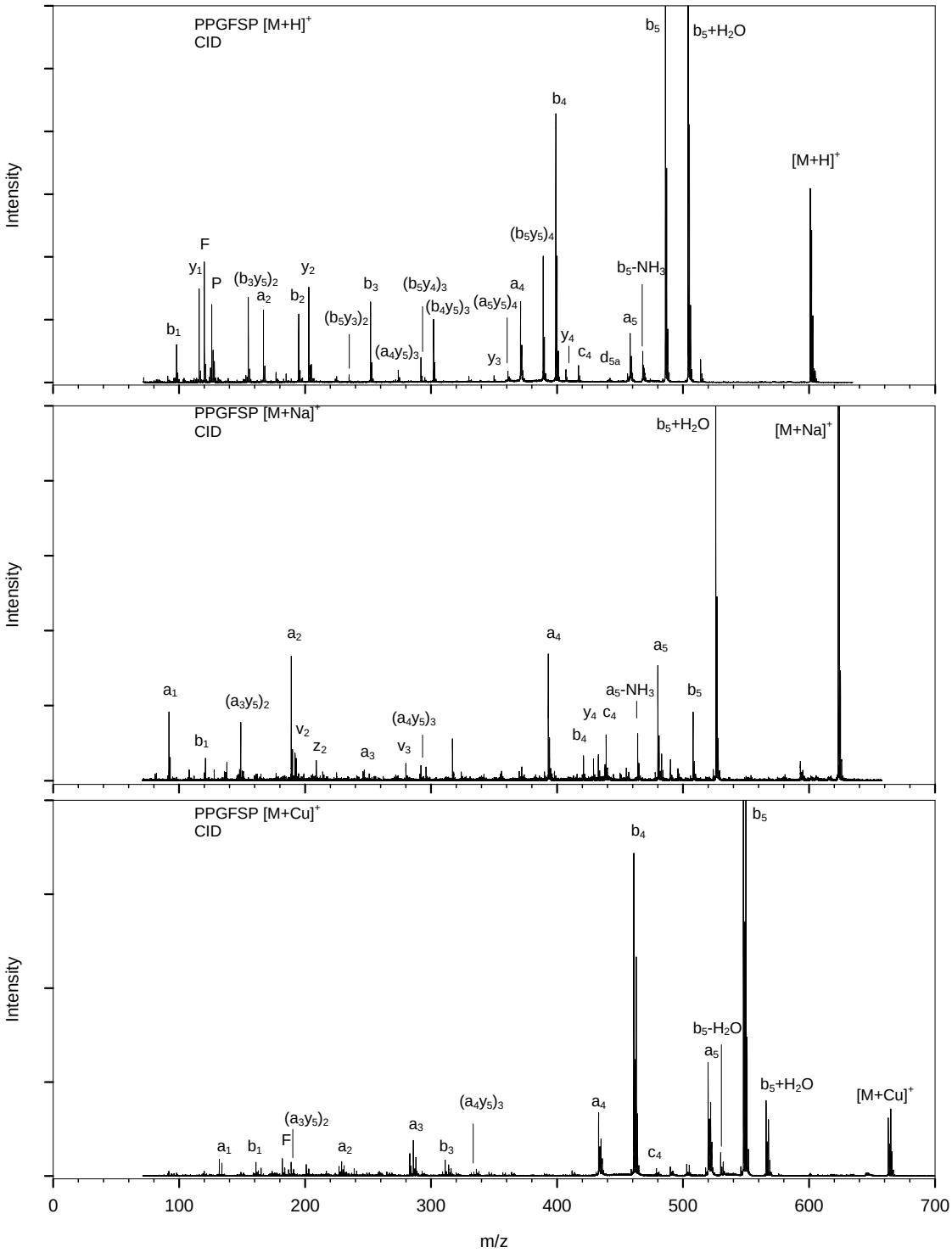

Figure 50. CID spectra of bradykinin fragment 2-7 (PPGFSP).

N-terminal ions, a consequence of copper binding to the N-terminal amine in the absence of arginine. Results of the CID of PPGFSP (Figure 50) are similar to those of bradykinin fragment 1-8. Fragmentation to a_i-type ions is enhanced when sodium is the charge carrier, and b_i-type ions form in greater abundance when copper is the charge carrier. The most abundant fragment of $[M + H]^+$ and $[M + Na]^+$ is $b_5 + H_2O$, which appears in low abundance in the CID spectrum of $[M + Cu]^+$.

A subset of the data is summarized in Table 4. The value "#NSI" refers to the total number of ion signals in the mass spectrum that correspond to internal fragments, small neutral loss ions, and ions that do not otherwise correspond to a predicted peptide fragment. The greater this value is with respect to the number of sequence informative ions in the spectrum, the more complicated *de novo* sequencing becomes. The projected utility for *de novo* sequencing for these methods is represented in the last column of Table 4 as a percentage of peaks in the spectrum that are sequence informative. The number of sequence informative ions observed relative to the total number of observed ions is 17% higher for the photodissociation spectra on average. Fragmentation of peptide $[M + Cu]^+$ results in a 5% increase in relative abundance of sequence informative ions versus $[M + H]^+$ in the photodissociation spectra, and a 26% increase for the CID spectra.

Table 4. Fragment ions of selected bradykinin analogues.

Peptide	Method	a_i	b_i	c_i	x_i	y_i	z_i	$b_{n-1}+H_2O$	# NSI*	%SI†
RPPGF $[M+H]^+$	193-nm	1-4	1	4	1	1,3-4		Y	5	70%
	CID	1-4	1-4	2,3	1	1-4		Y	16	50%
RPPGF $[M+Na]^+$	193-nm	1-4	4	4	1	1,4		Y	3	75%
	CID	1-4	2,4		2	3,4	1	Y	14	40%
RPPGF $[M+Cu]^+$	193-nm	1-5	4	4				N	3	70%
	CID	1-5	1-2,4	1-3	1		1	Y	8	60%
RPPGFS $[M+H]^+$	193-nm	1-4	1		5			Y	6	50%
	CID	1-5	1-2,5	2,4		4-5		Y	22	35%
RPPGFS $[M+Na]^+$	193-nm	1-3			1,5			Y	2	70%
	CID	1-5	3-5	3	5	4-5		Y	15	45%
RPPGFS $[M+Cu]^+$	193-nm	1-5	2,4-5					N	3	75%
	CID	1-5	2,4-5	3-4				Y	6	65%
RPGFSPFR $[M+H]^+$	193-nm	1-6		4-5	1-2	1,3		Y	8	60%
	CID	1-7	1-5,7	4-5	2	1,3-6		Y	33	40%
RPGFSPFR $[M+Na]^+$	193-nm	2,4		4				Y	3	50%
	CID	1-2,4-5,7	4,7	3,4		3-6		Y	15	45%
RPGFSPFR $[M+Cu]^+$	193-nm	1-4	2	4		1,3		N	2	80%
	CID	1-6,7	1-5,7			3-7		N	6	75%
RPPGFSFFR $[M+H]^+$	193-nm	1-7				1		Y	5	60%
	CID	1-8	1-4,6-8	4-6		1,3-5,7		Y	31	45%
RPPGFSFFR $[M+Na]^+$	193-nm	2-3,5						Y	2	60%
	CID	2,5	5-8	5		5,7		Y	12	45%
RPPGFSFFR $[M+Cu]^+$	193-nm	1-5						N	4	55%
	CID	1-8	2,4-8	3-5		1,3-5,7		Y	9	70%
KPPGFSPFR $[M+H]^+$	193-nm	5	3		1,2,4-6	1-5,7	2-4	Y	6	75%
	CID	1,5-6,8	1-2,5-6,8		1-2,5-6	1-8	1-2,7-8	Y	34	40%
KPPGFSPFR $[M+Na]^+$	193-nm	3,5						Y	2	50%
	CID	2-8	5-6,8	4-5		3-5,7		Y	16	50%
KPPGFSPFR $[M+Cu]^+$	193-nm	1-4				1,3-4		Y	3	70%
	CID	1-6,8	1-6,8			1,3-5,7-8		Y	9	70%

* #NSI - Number of non-sequence informative peaks present between the a_1 ion and $[M+H]^+$

† %SI - Percentage of peaks that are sequence informative.

Conclusions

Through comparison of the fragmentation spectra of these bradykinin analogues, we have demonstrated the utility of prompt ultraviolet photodissociation for determination of peptide primary structure. Use of a short fragmentation timescale reduces contributions from ions that are non-sequence informative, such as small neutral loss ions and internal cleavage products. The most commonly observed promptly-formed fragment ions of peptides activated with 193-nm light include a_i- and x_i-type

ions, the result of backbone carbon-carbon bond cleavage. For high energy activation methods such as keV energy CID and photodissociation, cationization with the non-mobile charge carrier Cu^+ enhances the value of information with respect to *de novo* peptide sequencing obtained from tandem mass spectrometry data.

Manual de novo sequencing from photofragment ion spectra is possible in many cases, especially based on the knowledge that a_i or x_i ions are likely to be present along with side chain cleavage products. Currently available automated de novo sequencing software is ill-equipped to determine peptide primary structure from photodissociation data, as these algorithms primarily utilize low energy fragments (b_i and y_i ions) rather than products of carbon-carbon bond cleavages. A limitation of the photodissociation experiment is decreased signal-to-noise for fragment ions relative to that of the CID experiment. Precursor ion signal may only be photodepleted by up to about 25%, above which multiple photon absorption occurs and immonium ion abundance is increased at the expense of backbone cleavage product ions. This limitation becomes more apparent for $[M + Na]^+$ and $[M + Cu]^+$ precursor ions that have lower ionization efficiencies. Increasing precursor ion signal through improvements in the MALDI source and ion optics may enhance the utility of prompt 193-nm photodissociation of peptides. Sampling of product ions formed over a relatively short timescale decreases the total abundance of fragment ions, but the analytical utility of the data is enhanced by a decrease in spectral congestion.

CHAPTER IV

ANALYSIS OF PROMPT FRAGMENTATION OF ANALOGOUS SYNTHETIC PEPTIDES BY 193-NM PHOTODISSOCIATION MALDI-TOF-TOFMS

Peptides were synthesized in our laboratory using Fmoc solid phase peptide synthesis [146] having amino acid sequence XVGVAZG, where the amino acids at positions X and Z were varied. The amino acid at position X was arginine, lysine, or histidine, and at position Z was proline, serine, or glycine. The variable amino acids at these positions were selected owing to differences in gas phase basicity [119], size, and conformational effects [143,147]. The photofragment ion spectra of these peptides are compared to high energy CID spectra acquired on the Applied Biosystems 4700 Proteomics Analyzer to attain greater understanding of prompt photodissociation using 193-nm laser irradiation.

Figure 51 (top panel) contains the CID spectrum of RVGVAPG $[M + H]^+$. In this tandem mass spectrum, b_i- and y_i-type ions appear in greater abundance than a_i-type ions. Ions resulting from ammonia loss are present along with N-terminal sequence ions for all positions except the sixth, and in most cases are in higher relative abundances than the sequence informative ions. For a peptide of unknown primary structure, *de novo* sequence determination is complicated by the appearance of these ions. The presence of an ammonia loss ion does not provide any information as to whether the ion 17 Da higher in mass is an a_i- or b_i-type fragment. Ions that differ in m/z by 17 Da may also be y_i- and z_i-type fragments. The CID spectrum of RVGVAPG $[M + H]^+$ also contains two internal cleavage product ions.

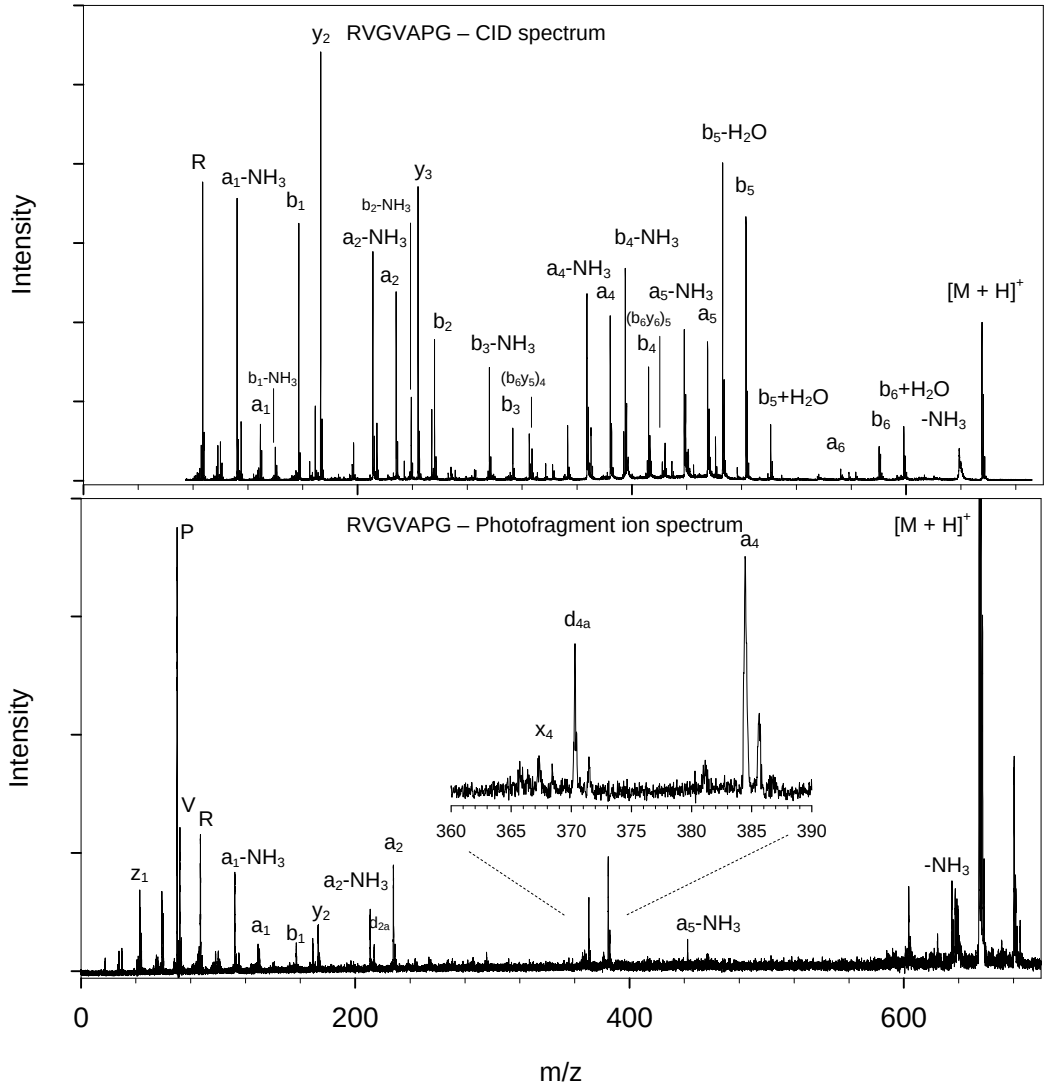

Figure 50. Tandem mass spectra of synthetic peptide RVGVAPG.

The photofragment ion spectrum of RVGVAPG $[M + H]^+$ is contained in Figure 51 (bottom panel). The strongest sequence informative ion signals present in this mass spectrum are the a_2 and a_4 ions resulting from carbon-carbon bond dissociation along the peptide backbone with charge retention at the N-terminal side of the dissociating bond. Side chain cleavage products d_{2a} and d_{4a} are also present, confirming the presence of valine at the second and fourth amino acid residues. Ammonia losses from the

guanidine group of arginine or from the N-terminus occur for a_i-type ions at positions 1, 2, and 5, and from a b_i-type ion at position 3. C-terminal charge retention products appear in low abundance with the exception of the y_2 ion for cleavage between alanine and proline. No internal cleavage products are observed in this photofragment ion spectrum, likely due to ammonia loss as an energetically favored secondary fragmentation over backbone bond cleavage. Through comparison of these two tandem mass spectra, we speculate that 193-nm photoactivation results in the prompt cleavage of certain bonds while peptide ions are more likely to form an oxazolone ring prior to fragmentation via CID, yielding product ions of amide bond cleavage [120].

The CID spectrum of RVGVASG $[M + H]^+$ (Figure 52, top panel) has lower relative abundances of y_i-type ions than the CID spectrum of RVGVAPG $[M + H]^+$, as the charge carrier is preferentially retained on the N-terminal side of the dissociating bonds. Ammonia loss ions occur in high relative abundances similar to the CID spectrum of the proline containing peptide. C-terminal amino acid loss to form b_6+H_2O and subsequent water transfer from the serine residue to form b_5+H_2O occurs to a greater degree in the CID experiment than in the photodissociation experiment. This result may be an effect of a longer fragmentation timescale or an effect of vibrational activation versus electronic activation, making charge directed fragmentation mechanisms more likely. Side chain loss at the first valine with C-terminal charge retention is observed in this CID spectrum as the v_6 ion.

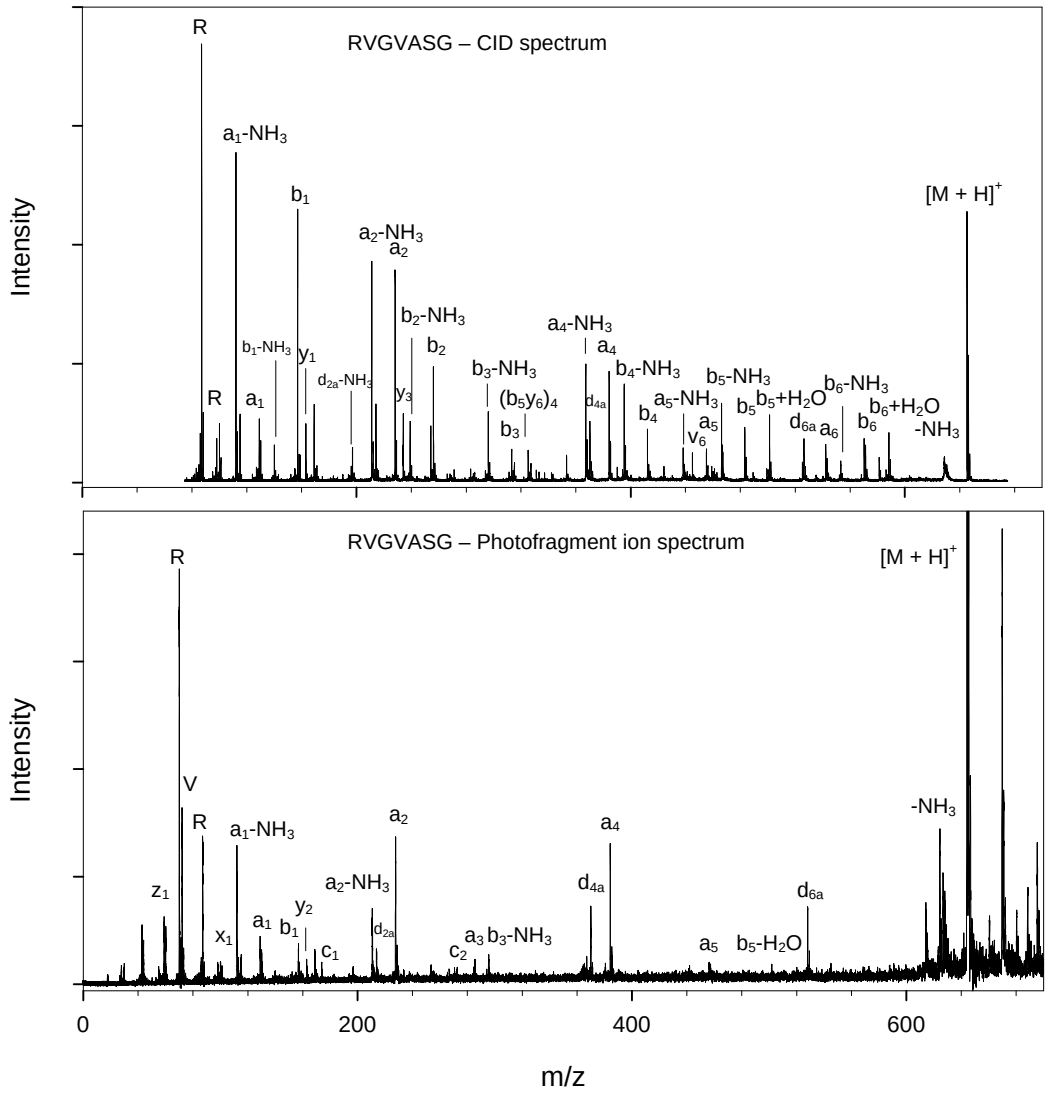

Figure 52. Tandem mass spectra of synthetic peptide RVGVASG.

The photofragment ion spectrum of RVGVASG $[M + H]^+$ (Figure 52, bottom panel) contains similar a_i- and d_{ia}-type ions and ammonia loss ions to the photofragment ion spectrum of RVGVAPG $[M + H]^+$ in similar relative abundances. The d_{6a} ion appears in this spectrum as a result of side chain cleavage at the serine residue from the a_6 ion, although the a_6 ion is not observed. The w_{2a} ion also appears for side chain cleavage at the serine residue with C-terminal charge retention. Photofragment ions c_1

and c_3 appear in low abundance as a result of cleavage between the amide nitrogen and backbone carbon containing the side chain.

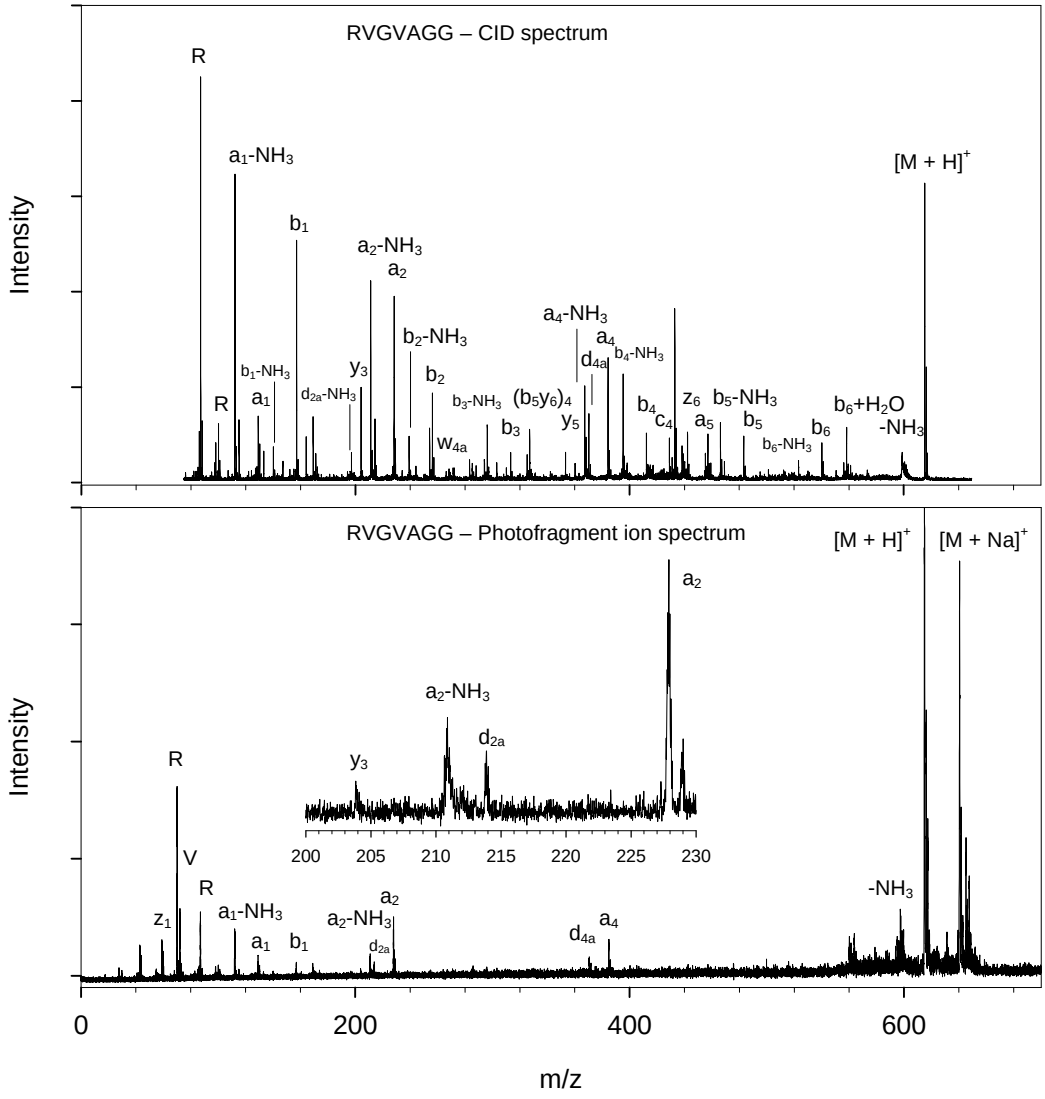

Figure 53. Tandem mass spectra of synthetic peptide RVGVAGG.

The high energy CID spectrum of RVGVAGG $[M + H]^+$ contains many fragment ion types (Figure 53, top panel). Complete series of a_i- and b_i-type ions are present. Ammonia loss ions for most of these fragments are also present in high relative

abundances. Several C-terminal charge retention products are present in lower abundances, which we attribute to proton migration during fragmentation rather than the charge being located at the C-terminus upon ionization, as these products do not appear in the photofragment ion spectrum. An abundant fragment ion is observed at m/z 433 which does not correspond to a sequence ion, internal fragment, or neutral loss that is common in tandem mass spectra of peptide ions. A few other fragment ions of this nature appear in lower abundance in this CID spectrum. Figure 53 (bottom panel) contains the photofragment ion spectrum of RVGVAGG $[M + H]^+$. Again, carbon-carbon bond dissociations are observed following valine residues (a_2 and a_4) with corresponding valine side chain cleavage products (d_{2a} and d_{4a}). Ammonia losses are observed from the a_1 and a_2 ions, similar to the two photofragment ion spectra shown above. Relative abundances of all other ions are reduced upon substitution of glycine as the sixth amino acid. A single C-terminally charged fragment ion is present in very low relative abundance (y_3).

A complete b_i-type ion series is present in the CID spectrum of HVGVASG $[M + H]^+$ (Figure 54, top panel). An a_i ion is observed for all residues except the glycine in the third position. With the exception of a_1 versus b_1, a_i-type ions appear in lower abundances than b_i-type ions. The majority of the a_i-type ions may arise from secondary fragmentation of b_i-type ions formed with excess internal energy. Several y_i-type ions are observed in this CID spectrum. Since very little abundance of C-terminal charge retention products appears in the photofragment ion spectrum of this peptide, these

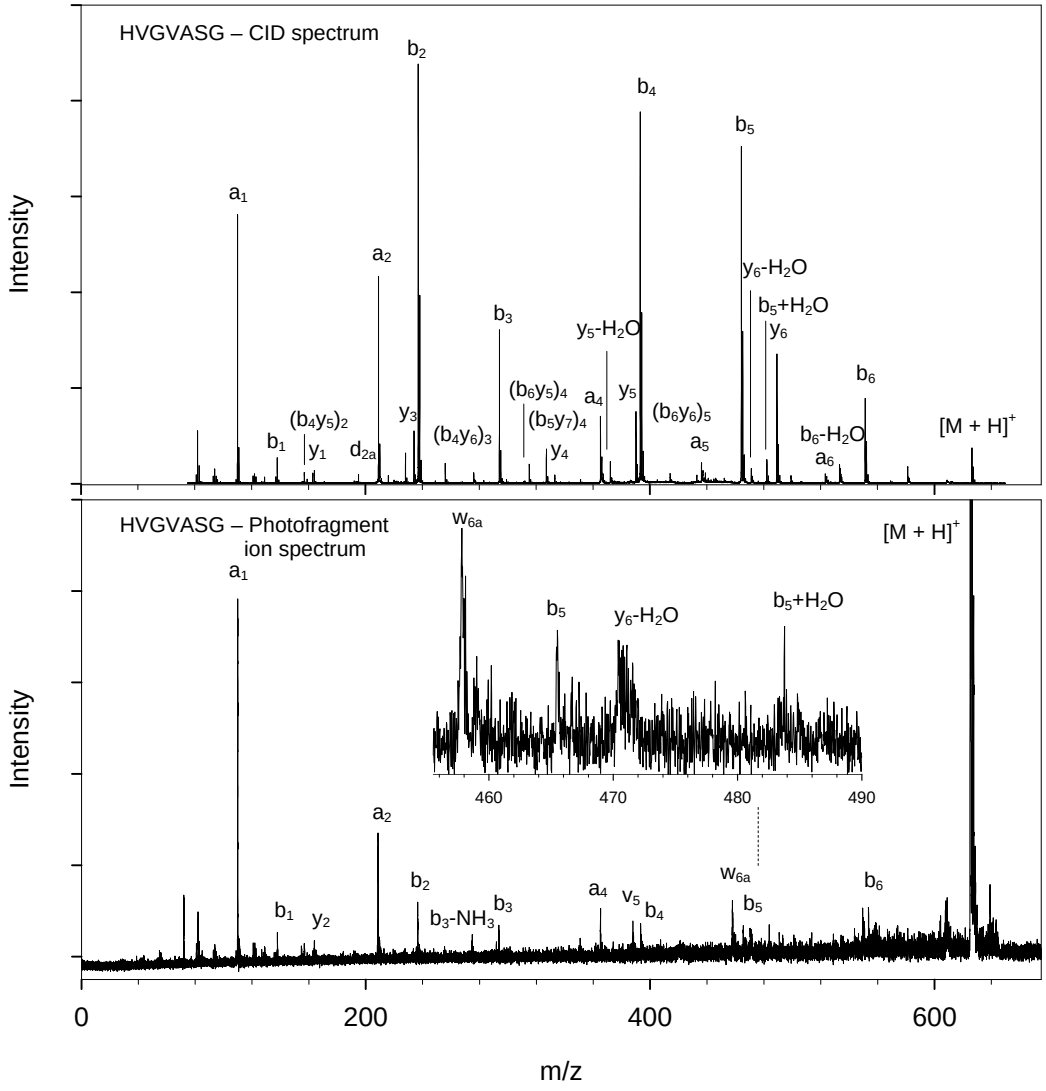

Figure 54. Tandem mass spectra of synthetic peptide HVGVASG.

fragmentation products may be attributable to charge migration during fragmentation. Five internal cleavage product ions are observed in this CID spectrum.

A complete b_i-type ion series is also present in the photofragment ion spectrum of HVGVASG $[M + H]^+$ (Figure 54, bottom panel). This result is uncharacteristic of photofragment ion spectra, and is likely the result of the intrinsic properties of the histidine containing peptide ion. Similar to the other photofragment ion spectra

displayed in this chapter, the a_1 ion appears in high relative abundance, and a_i ions are observed for cleavage after valine residues. Photodissociation of this peptide does not result in d_{ia}-type ions formed at the valine residues; however side chain cleavage products are observed having C-terminal charge retention at the valine residue in the second position (w_{6a}) and at glycine in the third position (v_5). In contrast to the CID spectrum, no internal cleavage products are observed.

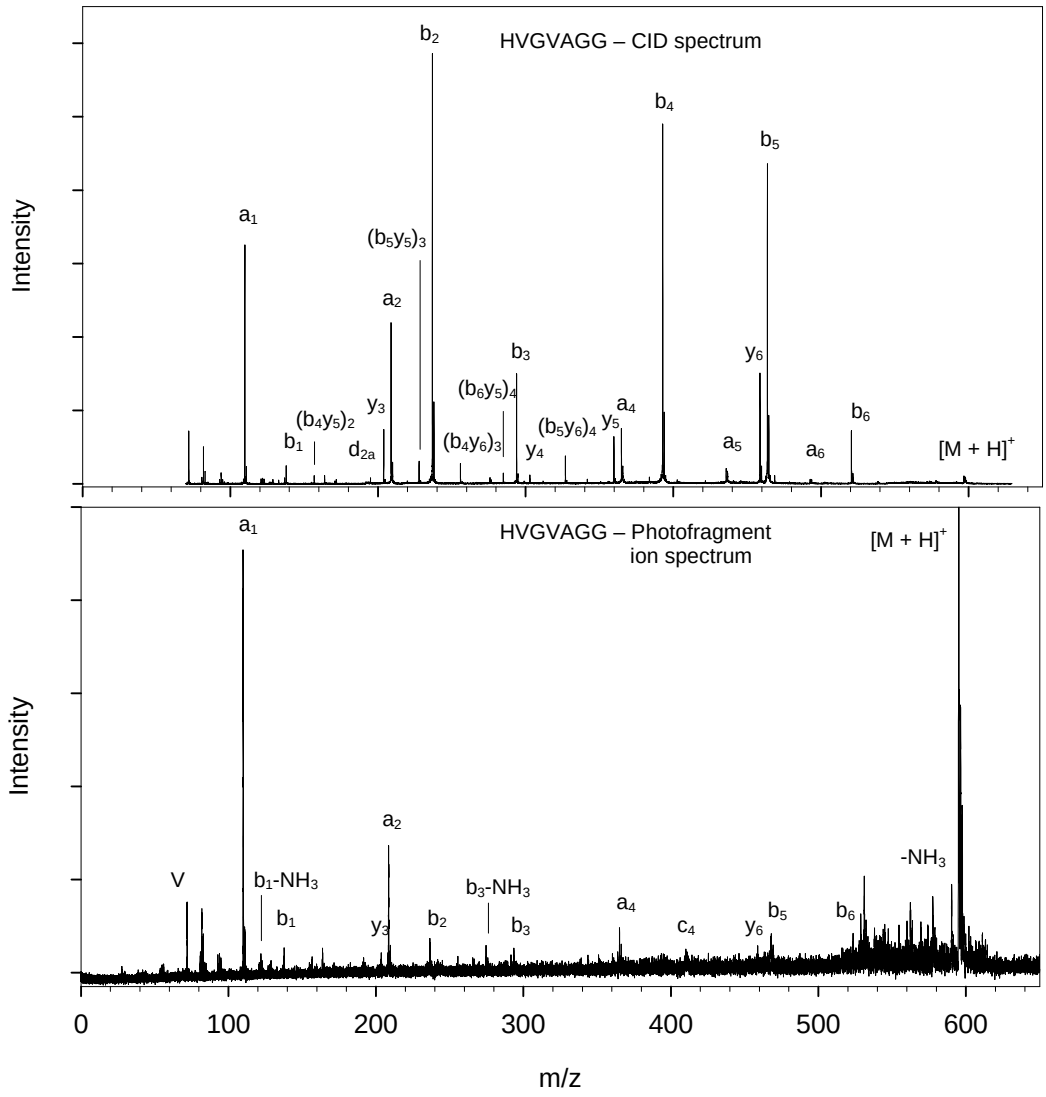

Figure 55. Tandem mass spectra of synthetic peptide HVGVAGG.

The CID spectrum of HVGVAGG $[M + H]^+$ (Figure 55, top panel) contains high abundances of b_i ions, with a complete series present. A complete series of a_i ions is also present, although the a_3 ion appears in very low relative abundance. C-terminal charge retention products are also lower in abundance in the CID spectrum, appearing only as y_i-type ions. Five internal cleavage products are present. Photodissociation of HVGVAGG [M + H]+ (Figure 55, bottom panel) yields b_i ions for all but the fourth amino acid. Similar to the previous N-terminal histidine containing peptide, a_1 is the dominant photofragment ion. Photodissociation after valine residues to produce the a_2 and a_4 ions is also observed in this tandem mass spectrum. The c_4 ion appears in low abundance, as does C-terminal charge retention products y_3 and y_6. Unlike the CID spectrum, no significant abundances of internal cleavage products are present.

Figure 56 (top panel) contains the CID spectrum of KVGVASG $[M + H]^+$. The b_i- and y_i-type ions in this spectrum appear in greater relative abundances than the a_i-type ions. Nine ions resulting from secondary fragmentation to form internal cleavage products or small neutral loss ions are observed in this CID spectrum. The photofragment ion spectrum of KVGVASG $[M + H]^+$ (Figure 56, bottom panel) contains several high m/z ions, resulting from loss of carboxylic acid (a_7), C-terminal amino acid loss (b_6+H_2O), and two ions resulting from side chain loss at lysine with C-terminal charge retention (w_{7a} and v_7). Carbon-carbon bond cleavage following valine residues to form a_2 and a_4 occurs for this peptide ion, similar to the N-terminal arginine and histidine containing moieties. Side chain cleavage products at these residues are lower in relative abundance than those of the peptides containing arginine, while b_i-type ions

for the first three amino acid residues appear in greater relative abundance. In contrast to the other photofragment ion spectra reported, a significant abundance of the y_3 ion is observed. Only one internal cleavage product and one ammonia loss ion is present in this spectrum.

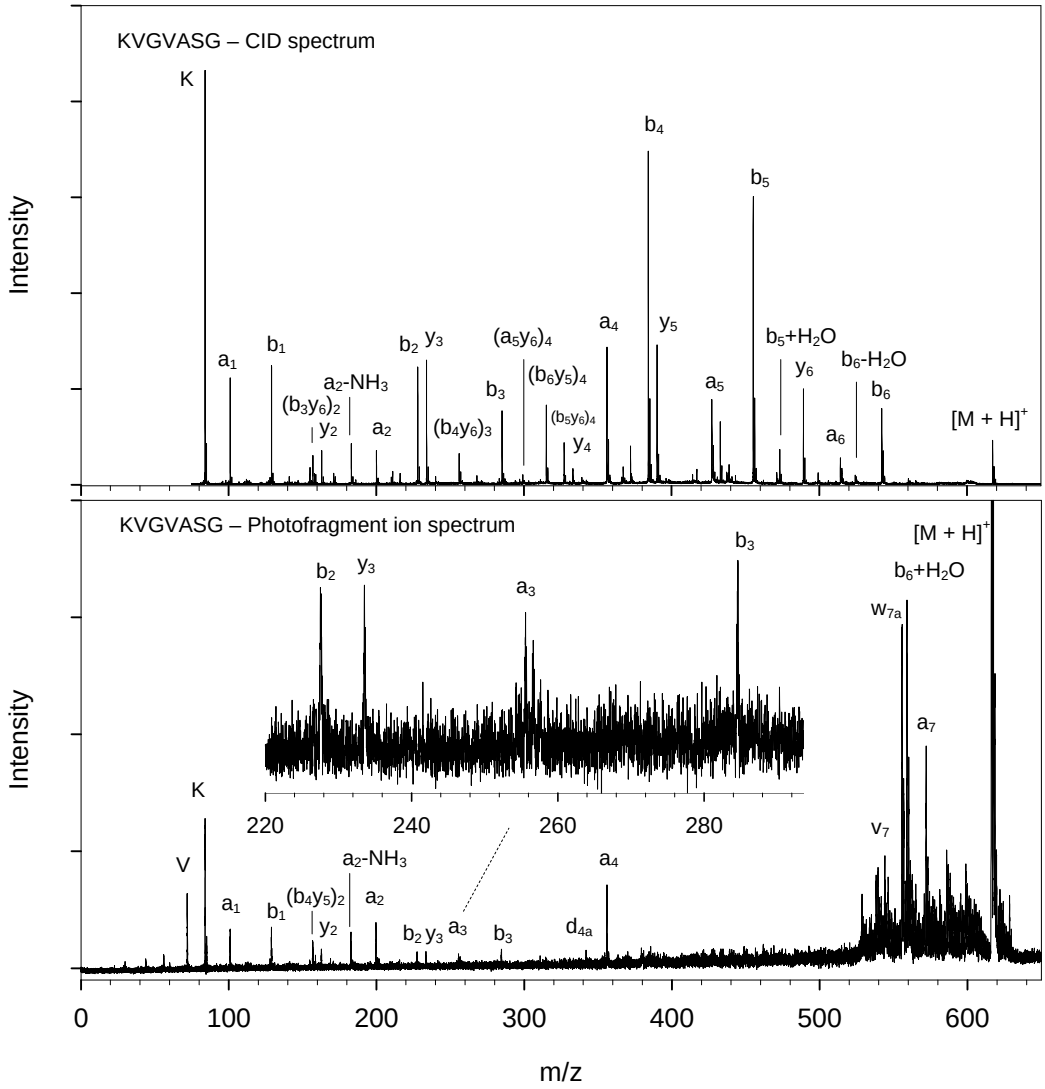

Figure 56. Tandem mass spectra of synthetic peptide KVGVASG.

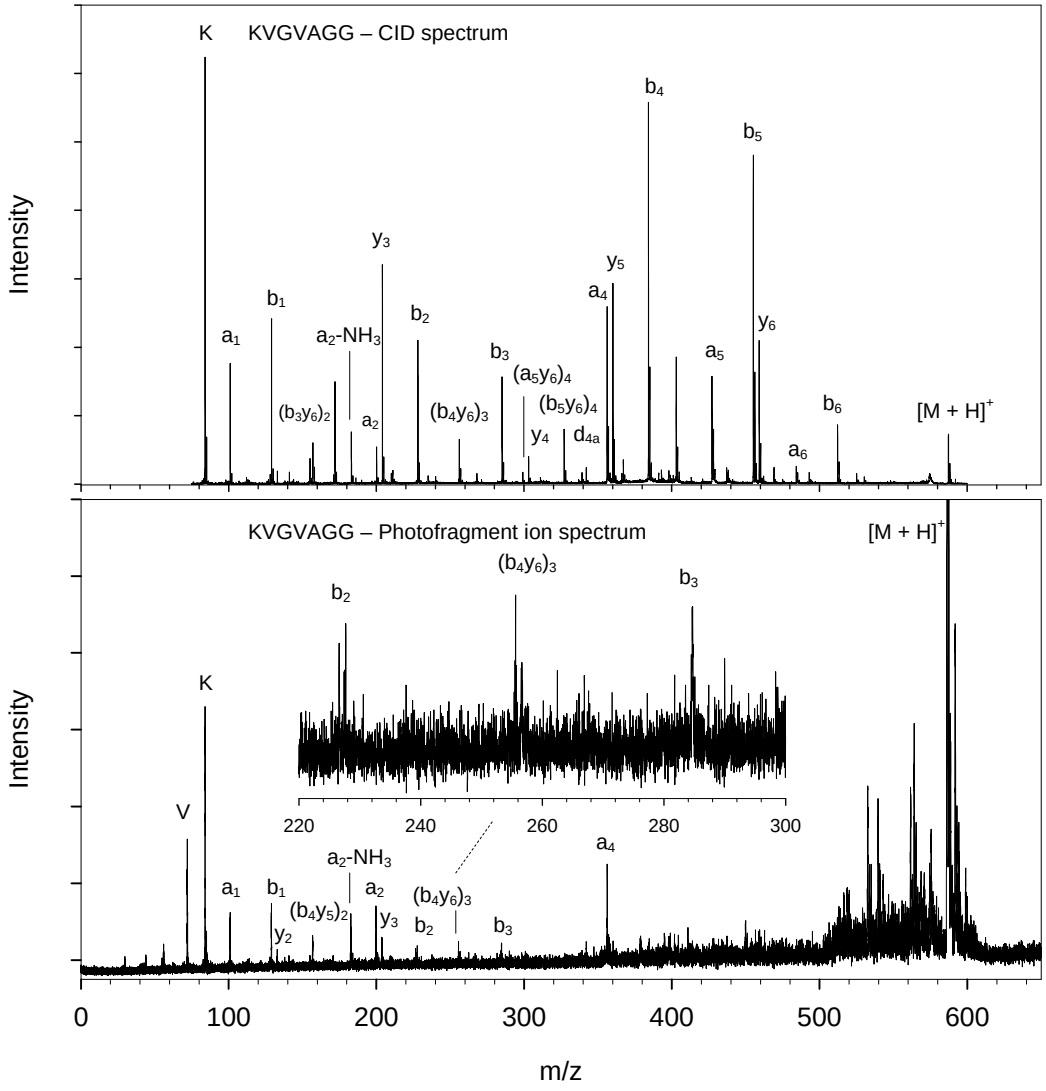

Figure 57. Tandem mass spectra of synthetic peptide KVGVAGG.

The CID spectrum of KVGVAGG $[M + H]^+$ (Figure 57, top panel) contains predominantly b_i- and y_i-type ions, with a few abundant signals from a_i-type ions. Strong signals at m/z 172 and m/z 403 are observed which do not correlate with predicted fragment ions of this peptide. Four internal cleavage products are observed, and one ion resulting from ammonia loss is observed.

The photofragment ion spectrum of KVGVAGG $[M + H]^+$ (Figure 57, bottom panel) contains similar sequence ions to the photofragment ion spectrum of KVGVASG $[M + H]^+$. In addition to these fragments, this spectrum also contains two internal cleavage product ions. Photofragment ions having high m/z in this spectrum do not correlate to predicted peptide fragments, likely because they are formed after ion reacceleration within the field-free drift region of TOF-2. Metastable ions at these m/z's are temporally focused at the detector for the reflectron voltage used. These peaks thus have narrow arrival time distributions but do not have the correct m/z, since they do not represent promptly formed ions.

For the analogous peptides examined in this chapter, 193-nm photofragmentation of carbon-carbon bonds with N-terminal charge retention is preferential, especially following valine residues. N-terminally charged side chain cleavage products (d_{ia} ions) are observed, which are also preferentially formed at the valine residues. Very few C-terminal charge retention products are observed in the photofragment ion spectra of the peptides with basic N-termini, which appear as y_i-type sequence ions and w_{ia}- and v_i-type side chain cleavage ions. The relative abundances of internal cleavage products and small neutral loss ions are lower in photofragment ion spectra versus high energy CID spectra for the peptide ions examined. These results make analysis of prompt 193-nm photodissociation products advantageous for identification of peptides using database searching and for *de novo* primary structure elucidation.

CHAPTER V

COMPARISON OF PHOTODISSOCIATION BY PSD FOCUSING AND TOF-TOFMS

Introduction

Several years ago Tecklenberg *et al*. [53] demonstrated that a change in the timescale allotted for fragmentation in a tandem MS experiment gives rise to differences in the fragment ions that are observed. This effect has recently been demonstrated for 193-nm photodissociation TOFMS [56]. Previously reported photofragment ion spectra obtained in our laboratory utilized the post-source decay (PSD) focusing method for detection of product ions formed over a relatively long timescale (10 μs) [102,114]. Experiments performed recently examine only those product ions formed over a shorter timescale following photoactivation (1 μs). In this chapter, prompt photofragment ion spectra are compared to PSD focusing photofragment ion spectra. Of particular interest are post-translationally modified peptides, containing one or more sites of phosphorylation.

Phosphorylated proteins play important roles in cellular activities, including signaling [148], activation and deactivation of genes for transcription during cellular mitosis [149], and lymphocyte activation [150] to name only a few. The use of mass spectrometry techniques for the characterization of phosphorylated proteins has become commonplace [151-153], however several challenges exist. For example, the natural abundance of phosphoproteins is low relative to their non-phosphorylated counterparts [154] and ionization of phosphopeptides is suppressed in the presence of other analytes

in a positive mode mass spectrometry experiment due to their lower proton affinities [155], often necessitating enrichment of the phosphorylated peptides prior to analysis. Furthermore, loss of the phosphate group in the form of H_3PO_4 or HPO_3 is a facile process, causing difficulty in primary structure determination by tandem MS methods [156-158]. For example, Crowe and Brodbelt [54] have demonstrated that phosphorylated peptides dissociate subsequent to infrared laser activation with relatively short irradiation times, however phosphoric acid loss is the predominant fragmentation pathway and sequence determination is limited because little fragmentation occurs between residues adjacent to the site of phosphorylation. Since fragment ions are trapped in the same volume as parent ions after dissociation, secondary fragmentation to form sequence ions with phosphate loss occurs (e.g. y_i-H_3PO_4). Dissociation of phosphopeptides without phosphate loss has been demonstrated using ECD [159,160]; however, this activation method is not suitable for TOFMS due to the inability to trap low energy electrons without an adverse effect on ion trajectory. Here we demonstrate prompt 193-nm photodissociation of phosphopeptides without the appearance of phosphate loss from fragment ions using TOF-TOFMS.

Experimental

Fibrinopeptide A (ADSGEGDFLAEGGGVR), angiotensin II (DRVYIHPF), angiotensin III (RVYIHPF), bradykinin (RPPGFSPFR), RRApSPVA, phosphorylated angiotensin II (DRVpYIHPF), fructose and α-cyano-4-hydroxycinnamic acid (CHCA) were obtained from Sigma-Aldrich (St. Louis, MO). Phosphorylated peptides KRpTLRR, F(Nle)(Nle)pTPpYVVTR, LKRApYLG-NH_2, and LRRApSLG were

obtained from American Peptide Company (Sunnyvale, CA). All peptides and reagents were used without further purification. Dried droplet MALDI spots were prepared as described in previous chapters. Fructose was added to samples used in PSD focusing photodissociation TOFMS experiments as described by Hettick *et al*. [114,164] to reduce contributions from products of metastable decay [161-164].

Photofragment ion spectra were collected using the PSD focusing method [103] utilizing the instrument shown schematically in Figure 10 (Chapter II) in the absence of the decelerating/accelerating photodissociation cell. An ion source accelerating voltage of 20 kV was used in these experiments. Approximately fifteen reflectron potential settings were used to spatially focus photofragment ions of various m/z at the detector. Each spectrum acquired was calibrated using the standard PSD calibration equation for a single-stage reflectron mass spectrometer (Equation 10) [165].

$$m_f = \left(\frac{\frac{t_f}{t_p} - C_1}{1 - C_1} \right) \left(MirrorRatio - C_3 \left(1 - MirrorRatio\right)^{C_4} \right) \tag{8}$$

In Equation 8, m_f is the m/z of the fragment ion and t_f is its TOF at the mirror ratio used. Constants C_1, C_3, and C_4 are dependent upon the dimensions of the mass spectrometer and the voltages used. Calibrated spectra are truncated and spliced to obtain a complete photofragment ion spectrum. Photodissociation TOF-TOFMS experiments were performed in the same manner as described in Chapter II.

Results

Photofragment ion spectra collected using the PSD focusing method are compared to prompt photofragment ion spectra of the same or similar peptide, which are shown here or in previous chapters. Figure 58 contains the photofragment ion spectra of fibrinopeptide A (ADSGEGDFLAGGGVR). In the PSD focusing photofragment ion

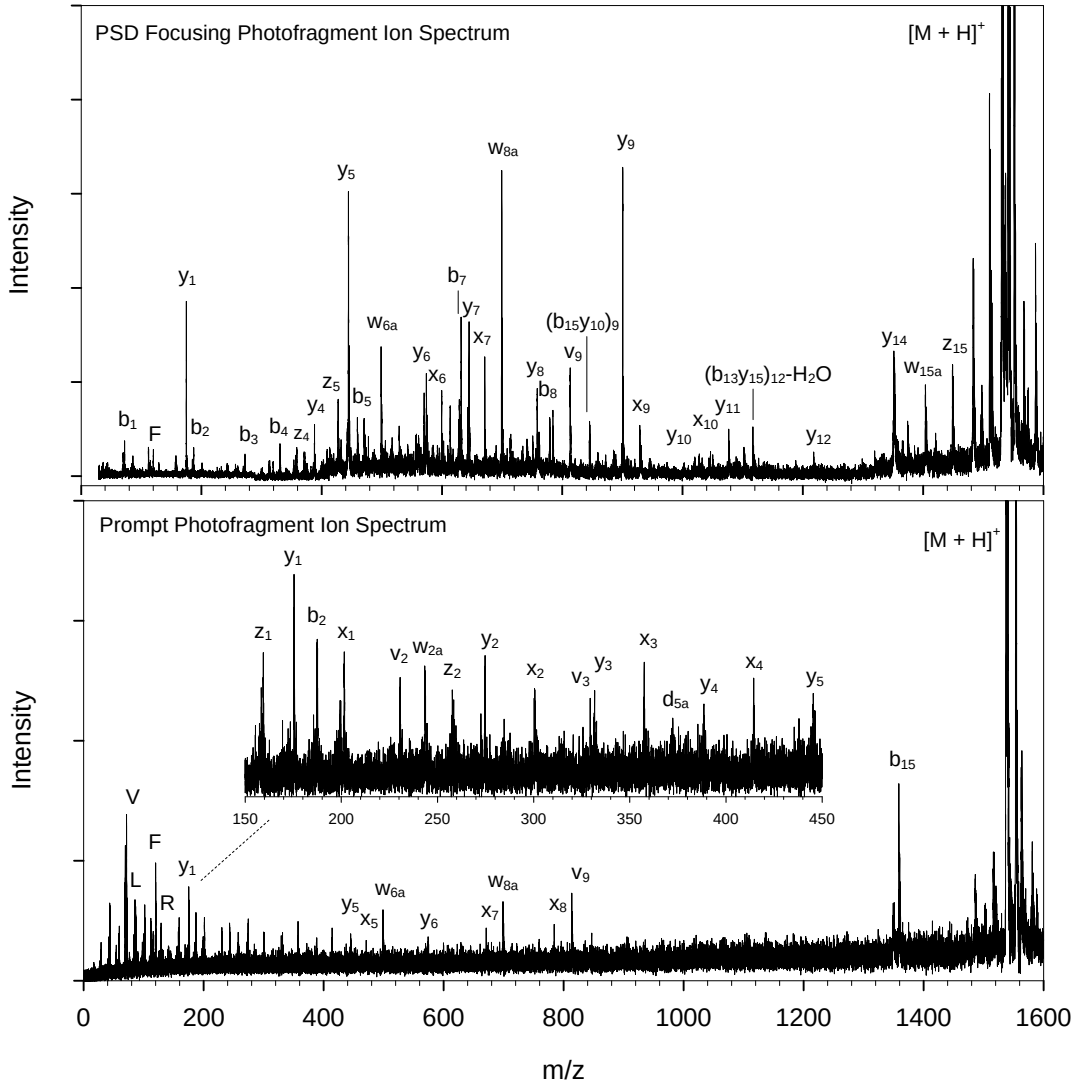

Figure 58. Photofragment ion spectra of fibrinopeptide A (ADSGEGDFLAE-GGGVR). [56] (Reprinted with permission from Elsevier)

spectrum (top panel), the most abundant fragment ions arise from amide bond cleavage near the acidic amino acids (Asp and Glu). An abundant photofragment ion is present resulting from side chain cleavage at leucine (w_{8a}), and a few x_i, z_i, and b_i ions are present in lower relative abundances. Two internal cleavage products are observed.

In the prompt photofragment ion spectrum (bottom panel), relative abundances of y_i ions are lowered, especially for those resulting from cleavage near acidic amino acids. The most abundant product ions of prompt photodissociation are side chain cleavage ions (v_2, w_{2a}, w_{6a}, w_{8a}, and v_9). Fragment ions resulting from cleavage at backbone carbon-carbon bonds (x_i ions) appear with relative abundances similar to or greater than those of y_i ions. Aside from immonium ions, no secondary cleavage products are observed.

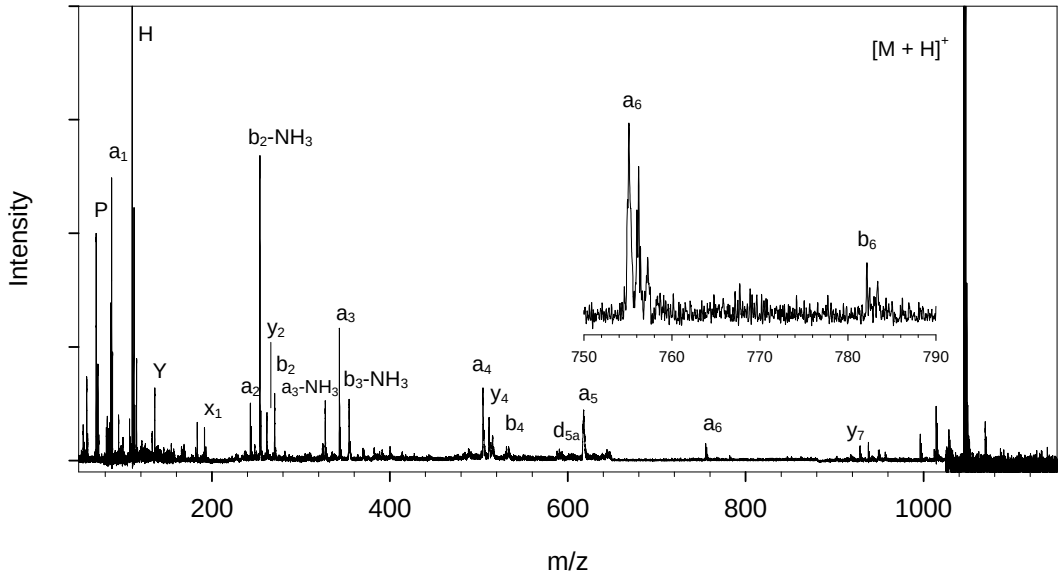

Figure 59. PSD focusing photofragment ion spectrum of angiotensin II (DRVYIHPF).

Figure 59 contains the PSD focusing photofragment ion spectrum of angiotensin II (DRVYIHPF). Similar a_i ions to those observed in the prompt photofragment ion spectrum (Figure 25, Chapter II) appear in this spectrum. Abundances of fragment ion signals decrease with increasing m/z, whereas in the spectrum of promptly formed photofragment ions relative abundances are similar for ions of various m/z. Note that the a_3-NH_3 ion appears in the PSD focusing spectrum, while the prompt photofragment ion spectrum contains the d_{3a} ion instead. The d_{3a} ion serves to confirm valine as the third amino acid; conversely, the a_3-NH_3 ion has very little informative value. The w_{6a} ion is another side chain cleavage product that appears in the spectrum of prompt photofragment ions but is absent from the PSD focusing spectrum.

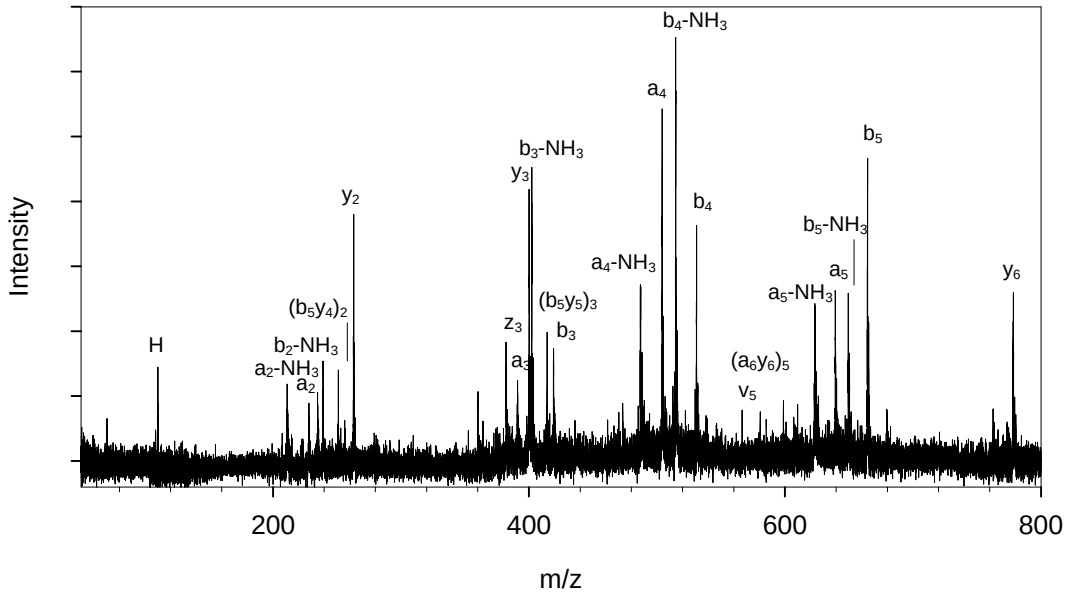

Figure 60. PSD focusing photofragment ion spectrum of angiotensin III (RVYIHPF).

The PSD focusing photofragment ion spectrum of angiotensin III (RVYIHPF) is contained in Figure 60. In contrast to the prompt photofragment ion spectrum (Figure

26, Chapter II), abundant b_i, b_i-NH_3, and a_i-NH_3 ions are present. The y_2 and y_3 ions appear in much greater relative abundances than a_i ions in this mass range. The relative abundance of the a_2 ion is much higher than that of the y_2 ion in the prompt photofragment ion spectrum, and the y_3 and y_6 ions are not present, revealing that extent of charge migration is lowered for a shorter fragmentation timescale. Side chain cleavage products d_{2a} and d_{4a} appear in the prompt photofragment ion spectrum, whereas the PSD focusing spectrum contains only the a_i-NH_3 peaks. The d_{2a} and d_{4a} ions are useful in confirming sequence ion assignments and determining isoleucine, whereas the ammonia loss products are non-sequence informative. Three internal cleavage products are observed in the PSD focusing spectrum while none are observed as products of prompt photodissociation.

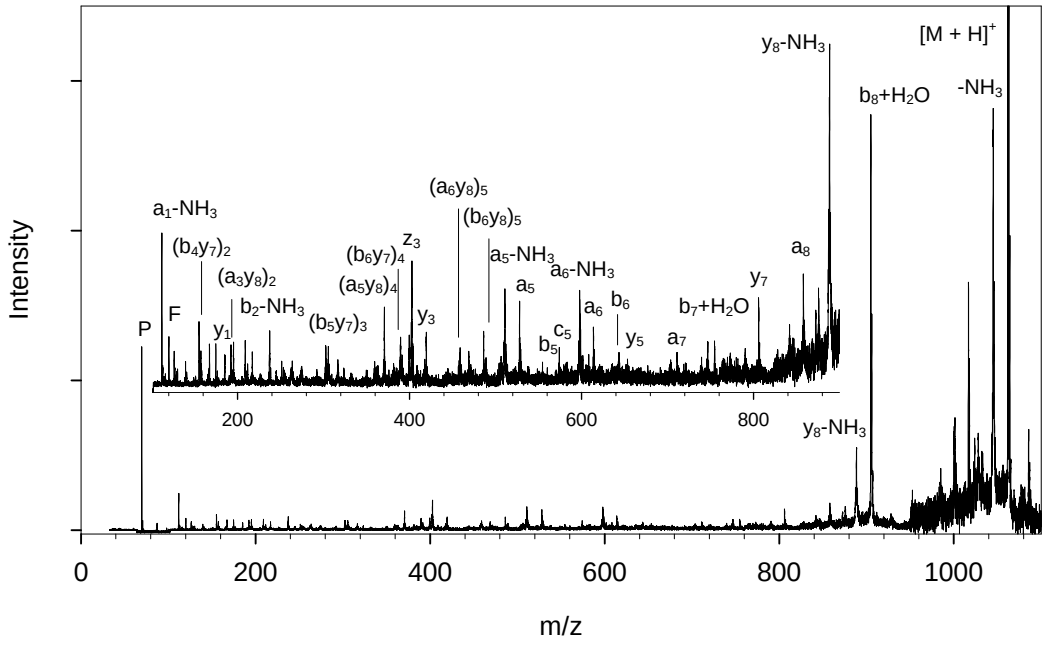

Figure 61. PSD focusing photofragment ion spectrum of bradykinin (RPPGFSPFR).

The PSD focusing photofragment ion spectrum of bradykinin (RPPGFSPFR) (Figure 61) contains twelve peaks arising from internal cleavage or loss of small neutrals and several peaks which do not correspond to fragment ions predicted by the nomenclature. The prompt photofragment ion spectrum of this peptide (Figure 41, Chapter III) contains only five peaks of this nature, and they are in low relative abundance. The PSD focusing photofragment ion spectrum includes a_i, b_i, y_i, and z_i ions, whereas the prompt photofragment ion spectrum includes predominantly the first six a_i ions and the d_{6a} ion. Fragment ions in the prompt photofragment ion spectrum having charge retention by the C-terminus are minute in comparison to the PSD focusing spectrum, again revealing a reduction in ions arising from charge migration over the shorter fragmentation timescale. Both mass spectra contain high relative abundances of $b_8 + H_2O$, which is attributed to the formation of this ion within the field-free drift region of the mass spectrometer between the ionization source and the photodissociation window in both experiments.

The PSD focusing photofragment ion spectrum of phosphorylated peptide RRApSPVA is contained in Figure 62. The most abundant ion signal is from loss of phosphoric acid and an abundant peak is also observed for loss of PO_3. Abundant signals appear for sequence informative ions d_{2a}, a_2, a_3, a_4, and a_6. Many ions of various relative abundances are observed which correspond to sequence ions that have lost the phosphate group or ammonia, or both. These ions complicate primary structure elucidation and may arise from photodissociation of the metastable decay product $[M + H - H_3PO_4]^+$. Another possible explanation for the appearance of these fragment ions is

loss of the phosphate group from sequence informative ions that occurs in the field-free region of the TOFMS between the photoactivation plane and the reflectron entrance.

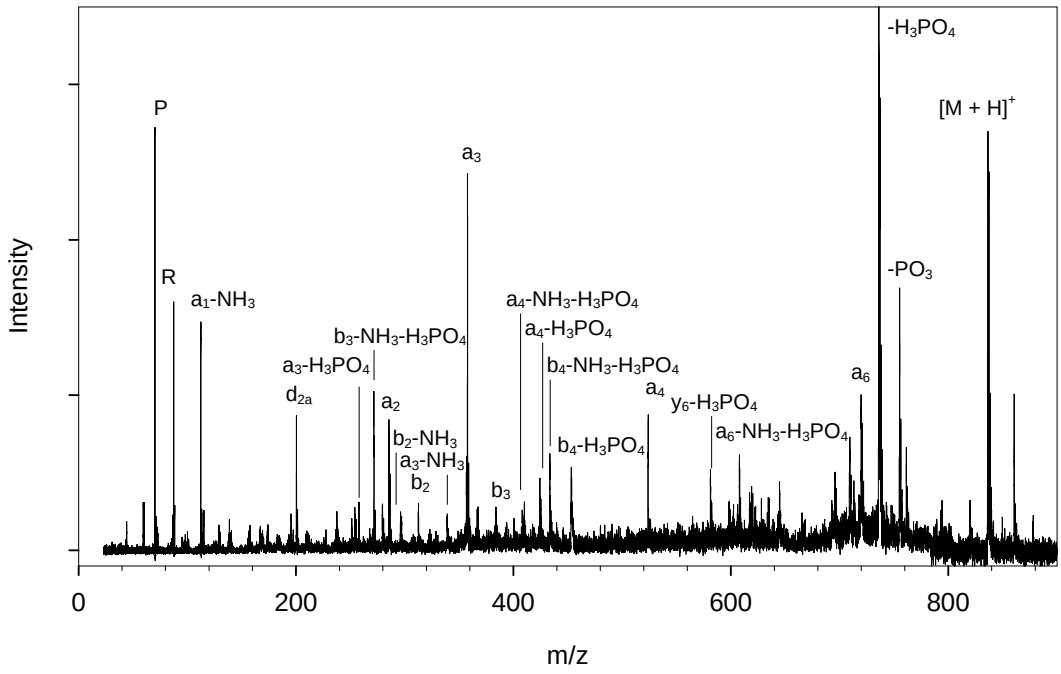

Figure 62. PSD focusing photofragment ion spectrum of phosphorylated peptide RRApSPVA.

Figure 63 contains the prompt photofragment ion spectrum of a similar phosphorylated peptide, RRApSVA. Again, loss of phosphoric acid is the most abundant product ion. The fragment ion corresponding to loss of PO_3 is also present, although it is in lower relative abundance than in the previous example. Note that sequence informative fragment ions also having loss of H_3PO_4 do not appear in this photofragment ion spectrum. Sequence informative ions observed include a_1, c_1, a_2, a_3, and v_6. Only two ammonia loss ions are observed.

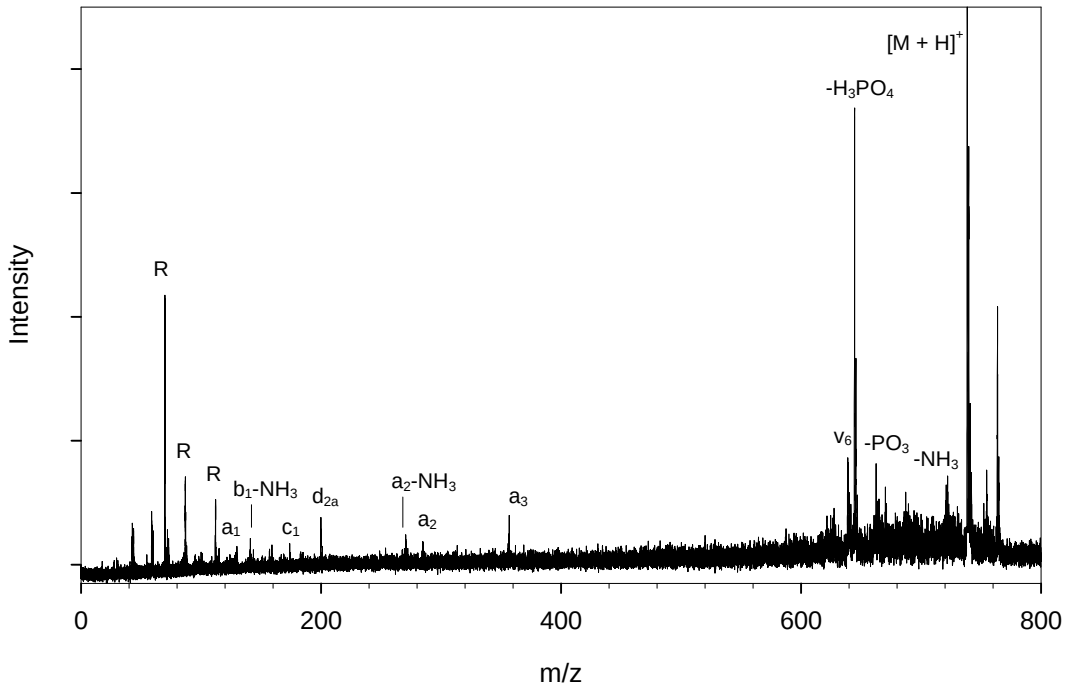

Figure 63. Prompt photofragment ion spectrum of phosphorylated peptide RRApSVA.

The photofragment ion spectra of phosphorylated angiotensin II (DRVpYIHPF) are contained in Figure 64. These two spectra contain very similar fragment ions. Key differences include the appearance of an abundant peak for b_7-H_3PO_4 and lower relative abundances of b_3, y_3, b_4, b_5, and y_5 in the PSD focusing spectrum (top panel). The increased abundances of fragment ions resulting from amide bond cleavage is attributed to the longer timescale of observable fragmentation allotted in the PSD focusing experiment. Both the amino acid sequence and the location of the post-translational modification are easily identified using either of these spectra.

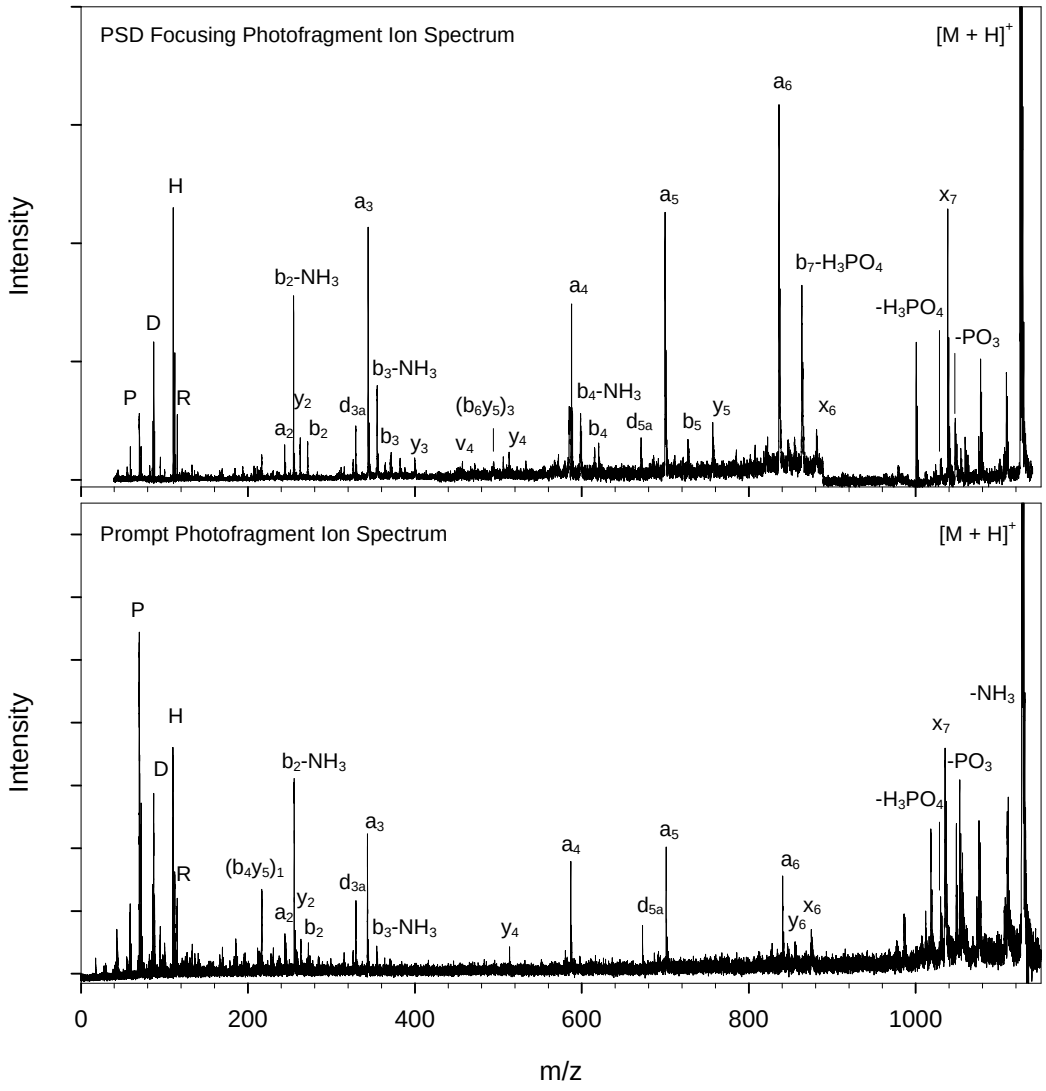

Figure 64. Photofragment ion spectra of phosphorylated angiotensin II (DRVpYIHPF).

An abundant product ion corresponding to arginine side chain loss from the intact parent ion (m_i) is observed in the photofragment ion spectrum of KRpTLRR (Figure 65) owing to the high UV molar extinction coefficient of this amino acid (ε = 13.1 X 10^{-3} at l = 190 nm) [166]. Four of the five sequence informative photofragment

ions present are the result of side chain cleavages. Note that phosphoric acid loss from fragment ions is not observed.

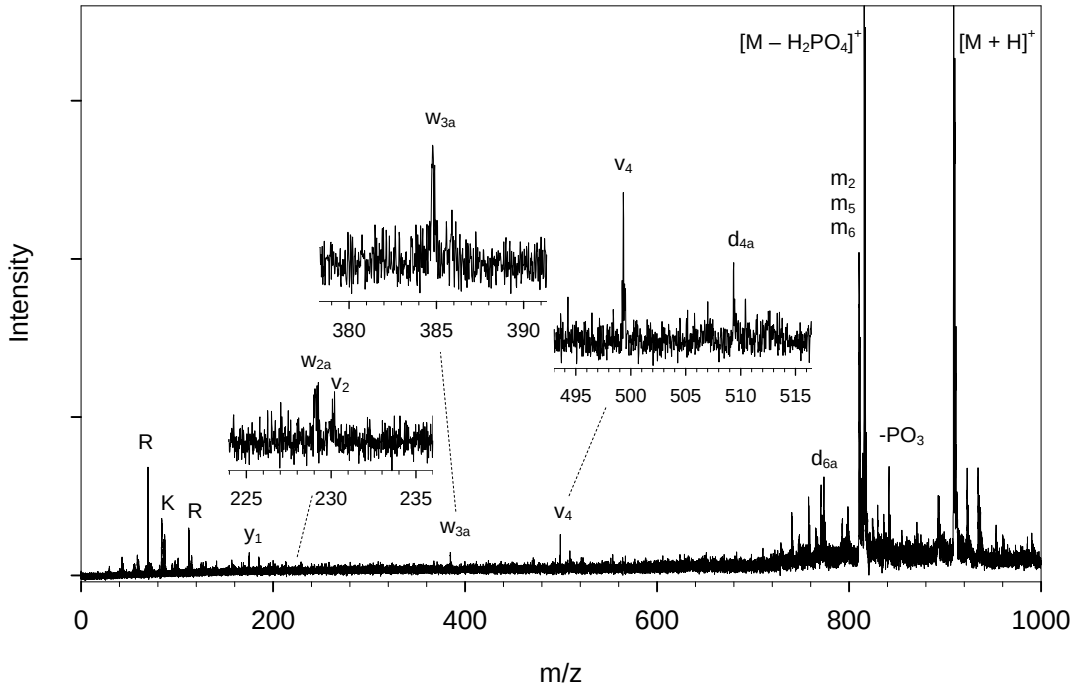

Figure 65. Prompt photofragment ion spectrum of phosphorylated peptide KRpTLRR.

Figure 66 contains the photofragment ion spectrum of a peptide with two sites of phosphorylation, F(Nle)(Nle)pTPpYVVTR. The amino acid Nle is norleucine, an isomer of leucine having no branching. Side chain cleavage products are observed for both norleucine residues (w_{8a} and w_{9a}). Side chain cleavages are also observed at the phosphotyrosine residue (v_5), valine (w_{4a}, v_4, w_{3a}, and v_3), and threonine (w_{2a} and v_2). Two ions are observed for which charge is retained by the N-terminal fragment (a_2 and b_8) and two internal cleavage products are observed. The remaining fragment ions in the spectrum either x_i, y_i, or z_i. Again, no fragment ions are identified that have lost the

phosphate group. Unfortunately, complete primary structure elucidation is complicated by the fact that side chain cleavage products often appear without corresponding backbone cleavage product ions; however, this information can be used to complement that obtained from other tandem MS methods. Only one ion is present resulting from backbone cleavage adjacent to a phosphorylated residue (y_6), thus the two phosphorylated residues could not be identified. Determination of the site of phosphorylation when more than one possible site of phosphorylation is present is especially important to biologists. The factors that influence backbone cleavage at phosphorylated residues should be the focus of future experiments. These factors may include (but are not limited to) the identities of the phosphorylated amino acids, the identities of the adjacent amino acids, and the presence of acidic or basic residues.

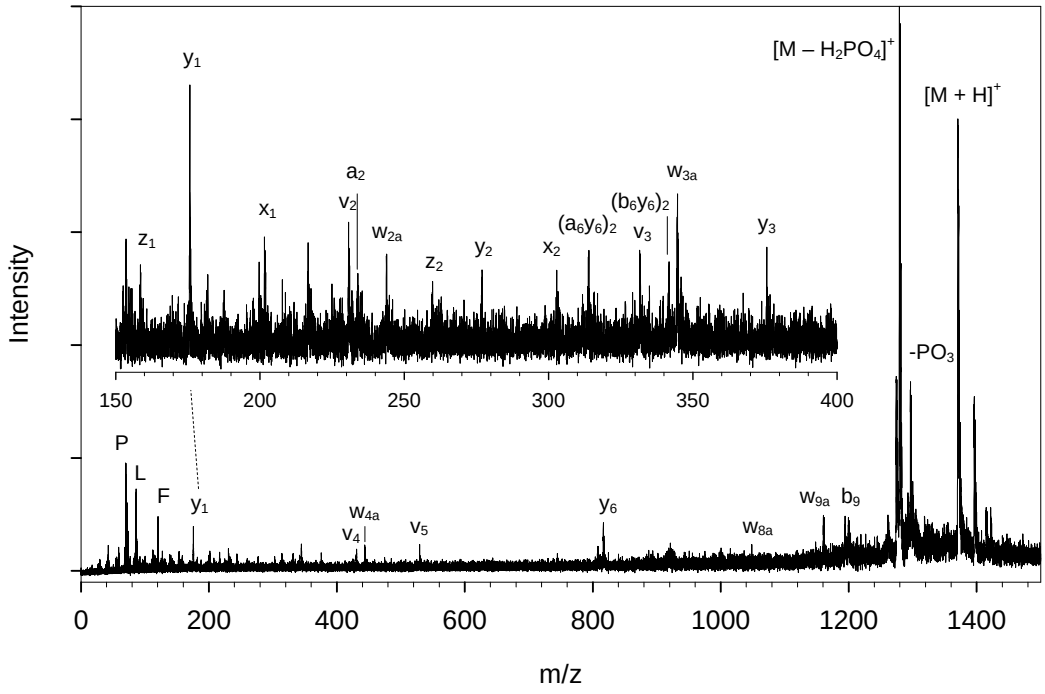

Figure 66. Prompt photofragment ion spectrum of phosphorylated peptide F(Nle)(Nle)pTPpYVVTR.

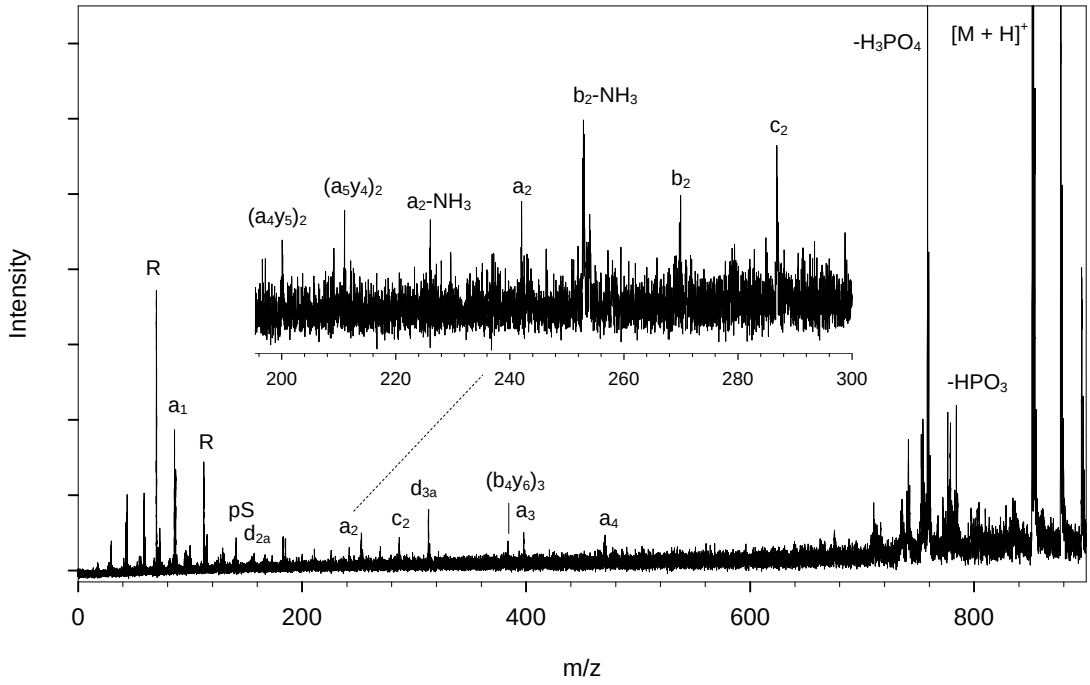

Figure 67. Prompt photofragment ion spectrum of phosphorylated peptide LRRApSLG.

Photodissociation of phosphorylated peptide LRRApSLG (Figure 67) yields a_i ions for the first five amino acids. The most abundant sequence informative ion signal present results from side chain cleavage at the second arginine residue (d_{3a}). Six ions resulting from cleavage at the first arginine are produced, including two ammonia loss ions and a side chain cleavage product (d_{2a}), likely due to the high UV absorbance of this amino acid and its propensity for loss of ammonia from the side chain. A side chain cleavage product is also observed at the leucine residue (d_{6a}) allowing determination of this amino acid over its isomeric counterpart, isoleucine. Four internal cleavage products appear in low relative abundance, including the intact phosphoserine residue. The presence of the phosphoserine immonium ion confirms the identity of the

phosphorylated amino acid, although its position within the peptide cannot be unambiguously determined. The a_i ions for the first four residues does, however, illustrate that the phosphoserine residue occurs within three amino acids from the C-terminus.

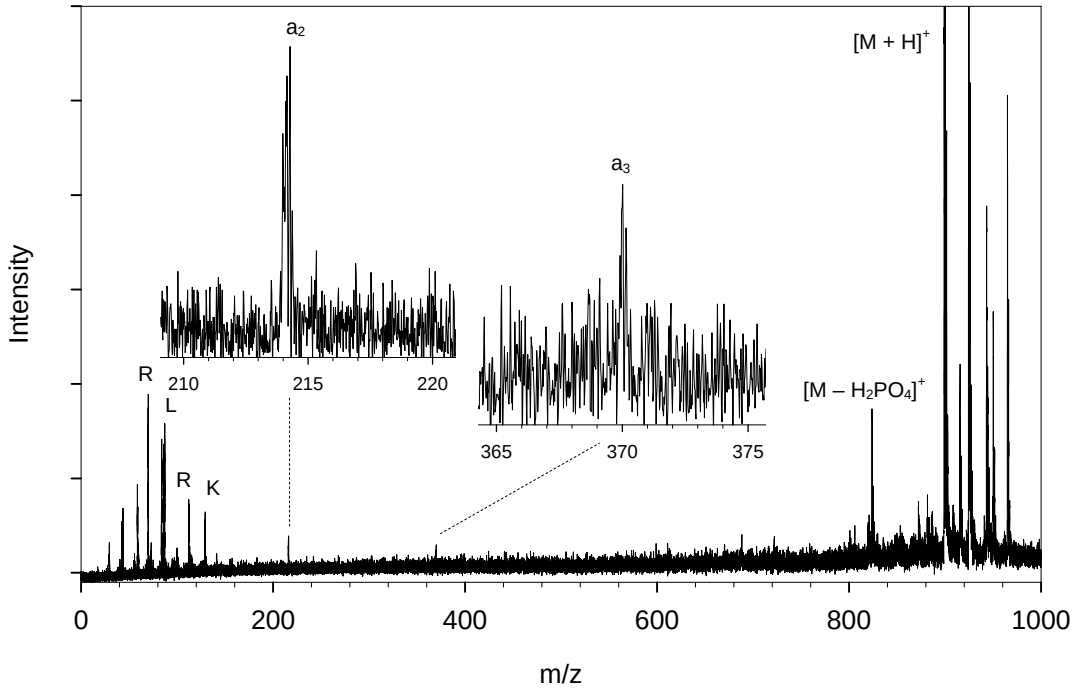

Figure 68. Prompt photofragment ion spectrum of phosphorylated peptide LKRApYLG-NH_2.

Figure 68 contains the photofragment ion spectrum of LKRApYLG-NH_2. Only two sequence ions are observed for this peptide, a_2 and a_3. The most abundant fragment ions present are for the loss of phosphoric acid and immonium ions. The lack of sequence information in this spectrum may be due to the presence of an internal arginine residue. The high relative abundance of immonium ions indicates that perhaps too much laser power was used to photodissociate this peptide ion. A reduction in laser intensity

of the addition of fructose to the sample [114] may increase the sequence information obtained.

Conclusion

Analysis of photofragment ions formed promptly (within 1 μs) after photoactivation greatly reduces the complexity of resulting tandem mass spectra. Contributions from low energy fragmentation processes such as amide bond cleavages are reduced, as well as fragmentations involving migration of the charge carrier within the peptide ion. The experimental results shown in this chapter demonstrate that peptide side chain cleavages occur promptly upon photoactivation, as relative abundances of these ions increase when using TOF-TOFMS versus PSD focusing. Additionally, contributions from secondary fragmentation such as ammonia loss and internal cleavage are reduced when examining only the promptly formed photofragment ions. The most commonly observed promptly-formed sequence informative photofragment ions are those resulting from backbone carbon-carbon bond cleavage, which are x_i ions for C-terminally charged peptides and a_i ions for N-terminally charged peptides.

Photofragment ion spectra of phosphorylated peptides are also simplified by examining only the promptly formed fragments. Use of a short fragmentation timescale does not eliminate phosphoric acid loss from the intact ion, which is a valuable diagnostic tool for determining if a peptide is phosphorylated, but does eliminate phosphoric acid loss from fragment ions, which complicates determination of the site of post-translational modification. In some cases, phosphopeptides promptly photodissociate into predominantly side chain cleavage product ions. This result is

beneficial for confirming sequence assignments made using data obtained by other tandem MS methods, but is detrimental to primary structure elucidation when peptide backbone cleavage products are not present.

CHAPTER VI

SUMMARY, CONCLUSIONS AND FUTURE DIRECTIONS

The initial goal of the research described in this dissertation was to increase instrumental throughput for photodissociation TOFMS experiments. Implementation of a decelerating/accelerating photodissociation cell allowed for acquisition of a complete photofragment ion spectrum for each MALDI event. Photodissociation experiments performed using the PSD focusing method [102] required acquisition of approximately fifteen individual summed spectra at various reflectron voltages to spatially focus photofragment ions at the detector. Acquisition times for these experiments were often in excess of one half hour, depending upon the consistency of ion generation by MALDI and quantities of ions produced. Calibration, truncation, and spectral splicing added another half hour of operator time per photofragment ion spectrum. Use of the TOF-TOFMS instrumentation described herein reduced these times to about fifteen minutes per spectrum acquisition and less than ten minutes for data handling.

Several other advantages to post-source acceleration prior to photoactivation were realized during the course of this research. First, the decelerating field on the source side of the photoactivation plane causes a greater decrease in velocities of products of metastable decay formed in the first field-free region of the mass spectrometer than for the ions of interest. The post-source decay products are thus not activated by excimer laser irradiation, and photodissociation products of these PSD fragments do not appear in the resulting spectra. Secondly, parent ion production may be continuously monitored during the tandem experiment. Parent ions exit through the

rear of the reflectron when using low reflectron voltages in the PSD focusing experiment making determination of the quality of MALDI ion formation impossible. Optimization of signal-to-noise is more easily achieved in the TOF-TOFMS experiment.

Another advantage associated with the decelerating/accelerating photodissociation cell is the decreased ion velocity at the photoactivation plane. Ion velocity is directly proportional to the square root of kinetic energy ($v = (2KE/m)^{1/2}$), thus ions with 7 keV of kinetic energy travel approximately half as fast as ions with 20 keV of kinetic energy. Precise control of the intersection of a 17 ns excimer laser pulse with the ion packet is simplified for slower moving ions.

Finally, observation of only those fragment ions formed promptly after photoactivation results in a simplified tandem mass spectrum. As shown in previous chapters, photodissociation within 1 μs of ion activation yields predominantly products of cleavage at carbon-carbon bonds along the peptide backbone and cleavage at amino acid side chains. Photodissociation over approximately 10 μs (demonstrated in Chapter V) often yields high abundances of secondary fragmentation products such as ammonia loss and internal cleavage ions, as well as a multitude of sequence informative fragment ion types. Reduction of secondary fragmentation is especially important when attempting to determine the site of post-translational modifications. Peptide primary structure is more easily identified through database searching or *de novo* sequencing when a complete series of a single ion type dominates the tandem mass spectrum.

Results presented in Chapter II demonstrate that photodissociation provides complementary information to that obtained from high energy CID. Side chain cleavage

products are enhanced in the prompt photofragment ion spectra, providing confirmation of assignments made using backbone cleavage product ions. For peptides that carry charge at the C-termini, the predominant sequence informative photofragment ions observed are x_i, with some contributions from y_i and z_i. Peptides that carry charge at the N-termini predominantly photodissociate to yield a_i ions. Very few photofragment ions resulting from proton migration are observed, whereas high energy CID TOF-TOF spectra contain many fragment ions that retain charge at both termini. Mass accuracy for fragment ions attained using the novel photodissociation TOF-TOFMS is within 0.25 Da and resolution is sufficiently high to separate ions differing by a single mass unit at the baseline.

Valuable information is obtained through photodissociation of metal cation bound peptides, as shown in Chapter III. Relative abundances of secondary cleavage product ions are reduced for $[M + Na]^+$ ions versus that of $[M + H]^+$. Peptides containing sodium as the charge carrier are easily identified as $[M + Na]^+$ ions by 193-nm photodissociation, as Na^+ is a dominant fragmentation product. The binding energy of Cu^+ to a peptide is higher than the enthalpies of formation of backbone bonds. Sequence informative photofragment ions are observed for $[M + Cu]^+$ ions, and photodetachment of Cu^+ has not been observed. Copper is non-mobile within the peptide ion, so the binding site(s) of the metal atom is easily determined from the photofragment ion spectrum.

Photodissociation holds several benefits over conventional ion activation methods such as CID and SID. Excitation of ions with a photon causes no change in

trajectory or kinetic energy, making photoactivation an attractive alternative for TOFMS experiments. High abundances of side chain cleavage products observed in 193-nm photofragment ion spectra complement information obtained from other tandem mass spectrometry methods. Photon absorption results in a quantized increase in ion internal energy, whereas the excitation energy imparted during a collision is limited by the center of mass. Introduction of an inert buffer gas, a requirement of CID, is not needed for photodissociation experiments. For ions that are close in m/z and may not be resolved by the ion selection optics, precise tuning of the photodissociation laser trigger timing may be employed to only irradiate the ions of interest. These advantages should make photodissociation a permanent tool for mass spectrometrists.

Future experiments utilizing 193-nm photodissociation for the examination of peptide fragmentation chemistry may take multiple directions. Using the instrumentation described in this dissertation, source and photodissociation cell voltages may be adjusted to vary the residence time of photoactivated ions within the cell. Experiments of this nature may be used to determine the rates of fragmentation to yield the various types of peptide fragment ions. Using this knowledge, experimental parameters may be adjusted to obtain optimal tandem mass spectrometry data for proteomic analysis, or parameters may be varied to obtain complementary information. An important aspect of biological mass spectrometry is the determination of post-translational modification. Backbone and side chain fragmentation of phosphorylated peptides via UV photodissociation without the appearance of neutral loss product ions is a significant benefit that should be exploited. Often, however, the intrinsic nature of the

peptide prevents backbone cleavage from occurring at each amino acid, limiting the sequence information that is obtained. Further investigation is needed to determine the factors that influence the utility of the information acquired from the prompt 193-nm photodissociation of phosphorylated peptides.

REFERENCES

1. McLafferty, F. W.; Turaček, F. *Interpretation of Mass Spectra*, 4th Ed. University Science Books: Sausalito, CA, 1993.
2. McLafferty, F. W. *Advances in Mass Spectrometry*, John Wiley & Sons Ltd.: New York, 1985.
3. Johnson, J. V.; Yost, R. A.; Kelley, P. E.; Bradford, D. C. Tandem-in-Space and Tandem-in-Time Mass Spectrometry: Triple Quardupoles and Quadrupole Ion Traps. *Anal. Chem.* **1990**, *62*, 2162-2172.
4. Marshall, A. G.; Hendrickson, C. L.; Jackson, G. S. Fourier Transform Ion Cyclotron Resonance Mass Spectrometry: A Primer. *Mass Spectrom. Rev*. **1998**, *17*, 1-35.
5. March, R. E. Quadrupole Ion Trap Mass Spectrometry. A View at the Turn of the Century. *Int. J. Mass Spectrom.* **2000**, *200*, 285-312.
6. Shevchenko, A.; Chernushevich, I.; Wilm, M.; Mann, M. De Novo Peptide Sequencing by Nanoelectrospray Tandem Mass Spectrometry Using Triple Quadrupole and Quadrupole/Time-of-Flight Instruments. *Meth. Mol. Biol.* **2000**, *146*, 1-16.
7. Matsuo, T. High Performance Sector Mass Spectrometers: Past and Present. *Mass Spectrom. Rev.* **1989**, *8*, 203-236.
8. Sysoev, A. A. Time-of-Flight Analyzers with Sector Fields: Advances and Prospects. *Eur. J. Mass Sepctrom.* **2000**, *6*, 501-513.

9. Laskin, J.; Lifshitz, C. Kinetic Energy Release Distributions in Mass Spectrometry. *J. Mass Spectrom.* **2001**, *36*, 459-478.
10. Mamyrin, B. A. Time-of-Flight Mass Spectrometry (Concepts, Achievements, and Prospects). *Int. J. Mass Spectrom.* **2001**, *206*, 251-266.
11. Katzenstein, H. S.; Friedland, S. S. New Time-of-Flight Mass Spectrometer. *Rev. Sci. Inst.* **1955**, *26*, 324-327.
12. Opsal, R. B.; Owens, K. G.; Reilly, J. P. Resolution in the Linear Time-of-Flight Mass Spectrometer. *Anal Chem.* **1985**, *57*, 1884-1889.
13. Wiley, W. C.; McLaren, I. H. Time-of-Flight Mass Spectrometer with Improved Resolution. *Rev. Sci. Inst.* **1955**, *26*, 1150-1157.
14. Barbacci, D. C.; Edmondson, R. D.; Russell, D. H. Evaluation of the Variables that Affect Resolution in Delayed Extraction MALDI-TOF. *Int. J. Mass Spectrom. Ion Processes*. **1997**, *165/166*, 221-235.
15. Mamyrin, B. A.; Karataev, V. I.; Shmikk, D. V.; Zagulin, V. A. Mass Reflectron. New Nonmagnetic Time-of-Flight High-Resolution Mass Spectrometer. *Zhurnal Eksperimental'noi i Teoreticheskoi Fiziki*. **1973**, *64*, 82-89.
16. Mamyrin, B. A. Time-of-Flight Mass Spectrometry (Concepts, Achievements, and Prospects). *Int. J. Mass Spectrom.* **2001**, *206*, 251-266.
17. Sunner, J.; Morales, A.; Kebarle, P. Mechanism of Formation of FAB Spectra. *Int. J. Mass Spectrom. Ion Processes*. **1988**, *86*, 169-186.

18. Pachuta, S. J.; Cooks, R. G. Mechanisms in Molecular SIMS. *Chem. Rev.* **1987**, *87*, 647-669.

19. Sundqvist, B.; Macfarlane, R. D. Californium-252-Plasma Desorption Mass Spectrometry. *Mass Spectrom. Rev.* **1985**, *4*, 421-460.

20. Della-Negra, S.; Le Beyec, Y. New Method for Metastable Ion Studies with a Time of Flight Mass Spectrometer. Future Applications to Molecular Structure Determinations. *Anal Chem.* **1985**, *57*, 2035-2040.

21. Fenn, J. B.; Mann, M.; Meng, C. K.; Wong, S.F.; Whitehouse, C.M. Electrospray Ionization for Mass Spectrometry of Large Biomolecules. *Science*. **1989**, *246*, 64-71.

22. Karas, M.; Bachmann, D.; Bahr, U.; Hillencamp, F. Matrix-Assisted Ultraviolet Laser Desorption of Non-volatile Compounds. *Int. J. Mass Spectrom. Ion Processes*. **1987**, *78*, 53-81.

23. Tanaka, K.; Waki, H.; Ido, Y.; Akita, S.; Yoshida, Y.; Yoshida, T. Protein and Polymer Analyses up to m/z 100,000 by Laser Ionization Time-of-Flight Mass Spectrometry. *Rapid Commun. Mass Spectrom*. **1988**, *2*, 151-153.

24. Preisler, J.; Hu, P.; Rejtar, T.; Karger, B. L. Capillary Electrophoresis-Matrix-Assisted Laser Desorption/Ionization Time-of-Flight Mass Spectrometry Using a Vacuum Deposition Interface. *Anal Chem.* **2000**, *72*, 4785-4795.

25. Wei, H.; Nolkrantz, K.; Powell, D. H.; Woods, J. H.; Ko, M.; Kennedy, R. T. Electrospray Sample Deposition for Matrix-Assisted Laser Desorption/Ionization

(MALDI) and Atmospheric Pressure MALDI Mass Spectrometry with Attomole Detection Limits. *Rapid Commun. Mass Spectrom.* **2004**, *18*, 1193-1200.

26. Price, D.; Milnes, G. J. The Renaissance of Time-of-Flight Mass Spectrometry. *Int. J. Mass Spectrom. Ion Processes.* **1990**, *99*, 1-39.
27. Pandey, A.; Mann, M. Proteomics to Study Genes and Genomes. *Nature*. **2000**, *405*, 837-846.
28. Russell, D. H.; Edmondson, R. D. High Resolution Mass Spectrometry and Accurate Mass Measurements with Emphasis on the Characterization of Peptides and Proteins by Matrix-Assisted Laser Desorption/Ionization Time-of-Flight Mass Spectrometry. *J. Mass Spectrom.* **1997**, *32*, 263-276.
29. Henzel, W. J.; Billeci, T. M.; Stults, J. T.; Wong, S. C.; Grimley, C.; Watanabe, C. Identifying Proteins from Two-dimensional Gels by Molecular Mass Searching of Peptide Fragments in Protein Sequence Databases. *Proc. Natl. Acad. Sci. U.S.A.* **1993**, *90*, 5011-5015.
30. Yergey, A. L.; Coorssen, J. R.; Backlund, P. S.; Blank, P. S.; Humphrey, G. A.; Zimmerberg, J.; Campbell, J. M.; Vestal, M. L. De Novo Sequencing of Peptides Using MALDI-TOF/TOF. *J.Am. Soc. Mass Spectrom.* **2002**, *13*, 784-791.
31. Eng, J. K.; McCormack, A. L.; Yates, J. R. An Approach to Correlate Tandem Mass Spectral Data of Peptides with Amino Acid Sequences in a Protein Database. *J. Am. Soc. Mass Spectrom.* **1994**, *5*, 976-989.

32. Roepstorff, P.; Fohlman, J. Proposal for a Common Nomenclature for Sequence Ions in Mass Spectra of Peptides. *Biomed. Mass Spectrom.* **1984**, *11*, 601.

33. Biemann, K. Nomenclature for Peptide Fragment Ions (Positive Ions). *Methods in Enzymology*. **1990**, *193*, 886-887.

34. Biemann, K. Mass Values for Amino Acid Residues in Peptides. *Methods in Enzymology*. **1990**, *193*, 888.

35. Biemann, K. Sequencing Peptides by Tandem Mass Spectrometry and High-Energy Collision-Induced Dissociation. *Methods in Enzymology*. **1990**, *193*, 455-479.

36. Wankenne, H.; Carprace, G.; Mornigny, J. Unimolecular Decay of Metstable Ions in Formaldehyde. *Int. J. Mass Spectrom. Ion Processes*. **1984**, *57*, 149-158.

37. Standing, K. G.; Ens, W.; Beavis, R. Time-of-Flight Measurements of Metastable Decay. *Springer Ser. Chem. Phys.* **1983**, *25*, 107-110.

38. Shukla, A. K.; Futrell, J. H. Tandem Mass Spectrometry: Dissociation of Ions by Collisional Activation. *J. Mass Spectrom.* **2000**, *35*, 1069-1090.

39. Jennings, K. R. The Changing Impact of the Collision-Induced Decomposition of Ions on Mass Spectrometry. *Int. J. Mass Spectrom.* **2000**, *200*, 479-493.

40. Grill, V.; Shen, J.; Evans, C.; Cooks, R. G. Collisions of Ions with Surfaces at Chemically Relevant Energies: Instrumentation and Phenomena. *Rev. Sci. Inst.* **2001**, *72*, 3149-3179.

41. McLafferty, F. W. Neutralization-Reionization Mass Spectrometry. *Int. J. Mass Spectrom. Ion Processes*. **1992**, *118/119*, 221-235.

42. Zubarev, R. A.; Kelleher, N. L.; McLafferty, F. W. Electron Capture Dissociation of Multiply Charged Protein Cations. A Nonergodic Process. *J. Am. Chem. Soc.* **1998**, *120*, 3265-3266.

43. Kruger, N. A.; Zubarev, R. A.; Carpenter, B. K.; Kelleher, N. L.; Horn, D. M.; McLafferty, F. W. Electron Capture Versus Energetic Dissociation of Protein Ions. *Int. J. Mass Spectrom.* **1999**, *182/183*, 1-5.

44. Cooper, H. J.; Hakansson, K.; Marshall, A. G. The Role of Electron Capture Dissociation in Biomolecular Analysis. *Mass Spectrom. Rev.* **2005**, *24*, 201-222.

45. McFarland, M. A.; Chalmers, M. J.; Quinn, J. P.; Hendrickson, C. L.; Marshall, A. G. Evaluation and Optimization of Electron Capture Dissociation Efficiency in Fourier Transform Ion Cyclotron Resonance Mass Spectrometry. *J. Am. Soc. Mass Spectrom.* **2005**, *16*, 1060-1066.

46. Iavarone, A. T.; Paech, K.; Williams, E. R. Effects of Charge State and Cationizing Agent on the Electron Capture of a Peptide. *Anal Chem.* **2004**, *76*, 2231-2238.

47. Mihalca, R.; Kleinnijenhuis, A. J.; McDonnell, L. A.; Heck, A. J. R.; Heeren, R. M. A. Electron Capture Dissociation at Low Teperatures Reveals Selective Dissociations. *J. Am. Soc. Mass Spectrom.* **2004**, *15*, 1869-1873.

48. Silvira, O. A.; Kjeldsen, F.; Ivonin, I. A.; Zubarev, R. A. Electron Capture Dissociation of Polypeptides in a Three-Dimensional Quadrupole Ion Trap: Implementation and First Results. *J. Am. Soc. Mass Spectrom.* **2005**, *16*, 22-27.

49. Leymarie, N.; Costello, C. E.; O'Connor, P. B. Electron Capture Dissociation Initiates a Free Radical Reaction Cascade. *J. Am. Chem. Soc.* **2003**, *125*, 8949-8958.

50. Turaček, F.; Syrstad, E. A. Mechanisms and Energetics of Intramolecular Hydrogen Transfer in Amide and Peptide Radicals and Cation-Radicals. *J. Am. Chem. Soc.* **2003**, *125*, 3353-3369.

51. Syrstad, E. A.; Turaček, F. Toward a General Mechanism of Electron Capture Dissociation. *J. Am. Soc. Mass Spectrom.* **2004**, *16*, 208-224.

52. Cui, W.; Hu, Y.; Lifshitz, C. Time Resolved Photodissociation of Small Peptide Ions. *Eur. Phys. J. D.* **2002**, *20*, 565-571.

53. Tecklenburg, R. E.; Miller, M. N.; Russell, D. H. Laser Ion Beam Photodissociation Studies of Model Amino Acids and Peptides. *J. Am. Chem. Soc.* **1989**, *111*, 1161-1171.

54. Crowe, M. C.; Brodbelt, J. S. Infrared Multiphoton Dissociation (IRMPD) and Collisionally Activated Dissociation of Peptides in a Quadrupole Ion Trap with Selective IRMPD of Phosphopeptides. *J. Am. Soc. Mass Spectrom.* **2004**, *15*, 1581-1592.

55. Keller, K. M.; Brodbelt, J. S. Collisionally Activated Dissociation and Infrared Multiphoton Dissociation of Oligonucleotides in a Quadrupole Ion Trap. *Anal. Biochem.* **2004**, *326*, 200-210.

56. Morgan, J. W.; Hettick, J. M.; Russell, D. H. Peptide Sequencing by MALDI 193-nm Photodissociation TOF MS. *Meth. Enzymol.* 2005, *402*. (In press)

57. Laskin, J.; Futrell, J. H. Collisional Activation of Peptide Ions in FT-ICR Mass Spectrometry. *Mass Spectrom. Rev.* **2003**, *22*, 158-181.

58. Johnson, R. S.; Martin, S. A.; Biemann, K. Collision-Induced Fragmentation of $[M+H]^+$ Ions of Peptides. Side Chain Specific Sequence Ions. *Int. J. Mass Spectrom. Ion Processes*. **1988**, *86*, 137-154.

59. Biemann, K.; Martin, S. A. Mass Spectrometric Determination of the Amino Acid Sequence of Peptides and Proteins. *Mass Spectrom. Rev.* **1987**, *6*, 1-76.

60. Nuwaysir, L. M.; Wilkins, C. L. Photodissociation of Laser Desorbed Ions as a Structure Determination Tool. *Anal. Chem.* **1989**, *61*, 689-694.

61. Bradley, C. D.; Curtis, J. M.; Derrick, P. J. Collisional Activation of Large Ions. Energy Losses and an Impulsive Collision Theory of Energy Transfer. *J. Chem. Soc. Faraday Trans.* **1994**, *90*, 239-247.

62. Uggerud, E.; Derrick, P. J. Z. Mechanism of Energy Transfer in Collisional Activation of Kiloelectronvolt Macromolecular Ions. *Naturforsch A*: *Phys. Sci.* **1989**, *44*, 245-246.

63. Dongré, A. R.; Somogyi, Á.; Wysocki, V. H. Surface-Induced Dissociation: An Effective Tool to Probe Structure, Energetics and Fragmentation Mechanisms of Protonated Peptides. *J. Mass Spectrom.* **1996**, *31*, 339-350.

64. Morris, M. R.; Riederer, D. E.; Winger, B. E.; Cooks, R. G.; Ast, T.; Chidsey, C. E. D. Ion/Surface Collisions at Functionalized Self-Assembled Monolayer Surfaces. *Int. J. Mass Spectrom. Ion Processes*. **1992**, *122*, 181-217.

65. Burroughs, J. A.; Wainhaus, S. B.; Hanley, L. Impulsive Excitation of $Cr(CO)_6^+$ During Surface-Induced Dissociation at Organic Monolayers. *J. Phys. Chem.* **1994**, *98*, 10913-10919.

66. Yata, M.; Uesugi-Saitow, Y. Activated Dissociation via a Trapping Precursor: O_2/Cu(001)-(2√2 X √2)-O. *J. Chem. Phys.* **2002**, *116*, 3075-3082.

67. Chirsten, W.; Even, U.; Raz, T.; Levine, R. D. The Transition from Recoil to Shattering in Cluster-Surface Impact: An Experimental and Computational Study. *Int. J. Mass Spectrom. Ion Processes*. **1998**, *174*, 35-52.

68. Christen, W.; Even, U. Cluster Impact Chemistry. *J. Phys. Chem. A.* **1998**, *102*, 9420-9426.

69. Hanley, L.; Lim, H.; Schultz, D. G.; Garbis, S.; Yu, C.; Ada, E. T.; Wijesundara, M. B. J. Energetics, Timescales, and Chemistry of Low Energy Molecular Ion-Organic Surface Collisions. *Nuc. Inst. Meth. Phys. Res. B.* **1999**, *157*, 174-182.

70. Laskin, J.; Bailey, T. H.; Futrell, J. H. Shattering of Peptide Ions on Self-Assembled Monolayer Surfaces. *J. Am. Chem. Soc.* **2003**, *125*, 1625-1632.

71. Hendell, E.; Even, U.; Raz, T.; Levine, R. D. Shattering of Clusters Upon Surface Impact: An Experimental and Theoretical Study. *Phys. Rev. Lett.* **1995**, *75*, 2670-2673.

72. Schultz, D. G.; Hanley, L. Shattering of SiMe3+ During Surface-Induced Dissociation. *J. Chem. Phys.* **1998**, *109*, 10976-10983.

73. Meroueh, S. O.; Wang, Y.; Hase, W. L. Direct Dynamics Simulations of Collision- and Surface-Induced Dissociation of N-Protonated Glycine. Shattering Fragmentation. *J. Phys. Chem. A.* **2002**, *106*, 9983-9992.

74. Dunbar, R. C. Photodissociation of the CH_3Cl^+ and N_2O^+ Cations. *J. Am. Chem. Soc.* **1971**, *93*, 4354-4358.

75. Kramer, J. M.; Dunbar, R. C. Photodissociation of Gaseous Olefinic Cations. *J. Chem. Phys.* **1973**, *59*, 3092-3100.

76. Dunbar, R. C. Photodissociation of Toluene Parent Cations. *J. Am. Chem. Soc.* **1973**, *95*, 472-476.

77. Freiser, B. S.; Beauchamp, J. L. Gas Phase Ion Chemistry and Photochemistry of Ions Generated from Perfluoropropylene. Photodissociation of the Perfluoroallyl Cation. *J. Am. Chem. Soc.* **1974**, *96*, 6260-6266.

78. Little, D. P.; Speir, J. P.; Senko, M. W.; O'Connor, P. B.; McLafferty, F. W. Infrared Multiphoton Dissociation of Large Multiply Charged Ions for Biomolecule Sequencing. *Anal. Chem.* **1994**, *66*, 2809-2815.

79. Flora, J. W.; Muddiman, D. C. Determination of the Relative Energies of Activation for the Dissociation of Aromatic Versus Aliphatic Phosphopeptides by ESI-FTICR-MS and IRMPD. *J. Am. Soc. Mass Spectrom.* **2004**, *15*, 121-127.

80. Duley, W. W. *CO2 Lasers: Effects and Applications*. Academic Press: New York, 1976.

81. Gauthier, J. W.; Trautman, T. R.; Jacobson, D. B. Sustained Off-Resonance Irradiation for Collision-Activated Dissociation Involving Fourier Transform Mass Spectrometry. Collision-Activated Dissociation Technique that Emulates Infrared Multiphoton Dissociation. *Anal. Chem. Acta* **1991**, *246*, 211-225.

82. Boering, K. A.; Brauman, J. I. Collisional Relaxation of Vibrational Excitation: Effects of Bath Gas Structure. *J. Chem. Phys.* **1992**, *97*, 5439-5450.

83. Carlson, D. G. Dynamics of a Repetitively Pump-Pulsed Neodymium:Yttrium-Aluminum Garnet Laser. *J. App. Phys.* **1968**, *39*, 4369-4374.

84. Ewing, J. J.; Brau, C. A. Laser Action on the 2Σ1/2+ → 2Σ1/2+ Bands of Krypton Fluoride (KrF) and Xenon Chloride (XeCl). *App. Phys. Lett.* **1975**, *27*, 350-352.

85. Rokni, M.; Mangano, J. A.; Jacob, J. H.; Hsia, J. C. Rare Gas Fluoride Lasers. *IEEE J. Quantum Elect.* **1978**, *14*, 464-481.

86. McCusker, M.; Brau, C. A.; Gallagher, A. *Excimer Lasers*, 2nd Ed. Rhodes, C. K., Ed.; Springer-Verlag: New York, 1984.

87. Duley, W. W. *UV Lasers: Effects and Applications in Materials Science*. Cambridge University Press: Cambridge, UK, 1996.

88. Hunt, D. F.; Shabanowitz, J.; Yates, J. R. Peptide Sequence Analysis by Laser Photodissociation Fourier Transform Mass Spectrometry. *J. Chem. Soc., Chem. Commun.* **1987**, *8*, 548-550.

89. *CRC Handbook of Biochemistry and Molecular Biology,* 3rd Ed. *Proteins, Vol. I*. Fasman, G. D., Ed.; CRC Press: Cleveland. 1978.

90. Preiss, J. W.; Setlow, R. Spectra of Some Amino Acids, Peptides, Nucleic Acids, and Protein in the Vacuum Ultraviolet. *J. Chem. Phys.* **1956**, *25*, 138-141.

91. Streitwieser, A.; Heathcock, C. H. *Introduction to Organic Chemistry,* 3rd Ed. Macmillan Publishing Company: New York. 1985.

92. Warneck, P. *Chemistry of the Natural Atmosphere*. Academic Press, Inc.: San Diego. 1988.

93. Houston, P. L. *Chemical Kinetics and Reaction Dynamics*. McGraw Hill: New York. 2001.

94. Diau, E. W.; Herek, J. L.; Kim, Z. H.; Zewail, A. H. Femtosecond Activation of Reactions and the Concept of Nonergodic Molecules. *Science* **1998**, *279*, 847-851.

95. McNaught, A. D.; Wilkinson, A. *IUPAC Compendium of Chemical Terminology* 2nd Ed. Blackwell Scientific: Oxford. 1996.

96. Maier, J. P. Open-Shell Organic Cations: Spectroscopic Studies by Means of the Radiative Decay in the Gas Phase. *Acc. Chem. Res.* **1982**, *15*, 18-23.

97. Griffin, L. L.; McAdoo, D. J. The Effects of Ion Size on Rate of Dissociation: RRKM Calculations on Model Large Polypeptide Ions. *J. Am. Soc. Mass Spectrom.* **1993**, *4*, 11-15.

98. Steinfeld, J. I.; Francisco, J. S.; Hase, W. L. *Chemical Kinetics and Dynamics*, 2nd Ed. Prentice Hall: Upper Saddle River, NJ. 1999.

99. Gimon-Kinsel, M. E.; Kinsel, G. R.; Edmondson, R. D.; Russell, D. H. Photodissociation of High Molecular Weight Peptides and Proteins in a Two-Stage

Linear Time-of-Flight Mass Spectrometer. *J. Am. Soc. Mass Spectrom.* **1995**, *6*, 578-587.

100. Gimon-Kinsel, M. E. *Fundamental Studies of the Photodissociation of Large Molecules*. Ph. D. Dissertation, Department of Chemistry, Texas A&M University, College Station, TX, 1996.
101. Barbacci, D. C. *Photodissociation of Peptide Ions in a Matrix-Assisted Laser Desorption Ionization Reflectron Time-of-Flight Mass Spectrometer*. Ph. D. Dissertation, Department of Chemistry, Texas A&M University, College Station, TX, 2000.
102. Barbacci, D. C.; Russell, D. H. Sequence and Side-Chain Specific Photofragment (193 nm) Ions from Protonated Substance-P by Matrix Assisted Laser Desorption Ionization Time-of-Flight Mass Spectrometry. *J. Am. Soc. Mass Spectrom.* **1999**, *10*, 1038-1040.
103. Spengler, B.; Kirsch, D.; Kaufmann, R. Fundamental Aspects of Postsource Decay in Matrix-Assisted Laser Desorption Mass Spectrometry. 1. Residual Gas Effects. *J. Phys. Chem.* **1992**, *96*, 9678-9684.
104. Vestal, M. L., Juhasz, P.; Martin, S. A. Delayed Extraction Matrix-Assisted Laser Desorption Time-of-Flight Mass Spectrometry. *Rap. Commun. Mass Spectrom.* **1995**, *9*, 1044-1050.

105. Brown, R. S.; Lennon, J. J. Mass Resolution Improvement by Incorporation of Pulsed Ion Extraction in a Matrix-Assisted Laser Desorption/Ionization Linear Time-of-Flight Mass Spectrometer. *Anal. Chem.* **1995**, *67*, 1998-2003.

106. Edmondson, R. D.; Russell, D. H. High-Resolution Mass Spectrometry and Accurate Mass Measurements of Biopolymers Using MALDI-TOF. In *Mass Spectrom. Biol. Materials*, Dekker: New York, 1998.

107. Bienvenut, W. V.; Déon, C.; Pasquarello, C.; Campbell, J. M.; Sanchez, J.; Vestal, M. L.; Hochstrasser, D. F. Matrix-Assisted Laser Desorption/Ionization-Tandem Mass Spectrometry with High Resolution and Sensitivity for Identification and Characterization of Proteins. *Proteomics*. **2002**, *2*, 868-876.

108. Rejtar, T.; Chen, H.; Andreev, V.; Moskovets, E.; Karger, B. L. Increased Identification of Peptides by Enhanced Data Processing of High-Resolution MALDI TOF/TOF Mass Spectra Prior to Database Searching. *Anal. Chem.* **2004**, *76*, 6017-6028.

109. Mann, M.; Hoejrup, P.; Roepstorff, P. Use of Mass Spectrometric Molecular Weight Information to Identify Proteins in Sequence Databases. *Biol. Mass Spectrom.* **1993**, *22*, 338-345.

110. Fenyo, D.; Qin, J.; Chait, B. T. Protein Identification Using Mass Spectrometric Information. *Electrophoresis*. **1998**, *19*, 998-1005.

111. Zhang, W.; Chait, B. T. ProFound: An Expert System for Protein Identification Using Mass Spectrometric Peptide Mapping Information. *Anal. Chem.* **2000**, *72*, 2482-2489.

112. Schlosser, A.; Lehmann, W. D. Five-Membered Ring Formation in Unimolecular Reactions of Peptides: A Key Structural Element Controlling Low-Energy Collision-Induced Dissociation of Peptides. *J. Mass Spectrom.* **2000**, *35*, 1382-1390.

113. Tecklenburg, R. E.; Russell, D. H. An Evaluation of the Analytical Utility of the Photodissociation of Fast Ion Beams. *Mass Spectrom. Rev.* **1990**, *9*, 405-451.

114. Hettick, J. M.; McCurdy, D. L.; Barbacci, D. C.; Russell, D. H. Optimization of Sample Preparation for Peptide Sequencing by MALDI-TOF Photofragment Mass Spectrometry. *Anal. Chem.* **2001**, *73*, 5378-5386.

115. Bowers, W. D.; Delbert, S. S.; McIver, R. T. Consecutive Laser-Induced Photodissociation as a Probe of Ion Structure. *Anal. Chem.* **1986**, *58*, 969-972.

116. Thompson, M. S.; Cui, W.; Reilly, J. P. Mass Spectrometry: Fragmentation of Singly Charged Peptide Ions by Photodissociation at λ = 157 nm. *Angew. Chem. Int. Ed.* **2004**, *43*, 4791-4794.

117. Cui, W.; Thompson, M. S.; Reilly, J. P. Pathways of Peptide Ion Fragmentation Induced by Vacuum Ultraviolet Light. *J. Am. Soc. Mass Spectrom.* **2005**, *16*, 1384-1398.

118. Li, L.; Lubman, D. L. Ultraviolet-Visible Absorption Spectra of Biological Molecules In the Gas Phase Using Pulsed Laser-Induced Volatilization Enhancement In a Diode Array Spectrophotometer. *Anal. Chem.* **1987**, 2538-2541.

119. Harrison, A. G. The Gas-Phase Basicities and Proton Affinities of Amino Acids and Peptides. *Mass Spectrom. Rev.* **1997**, *16*, 201-217.

120. Paizs, B.; Suhai, S. Towards Understanding the Tandem Mass Spectra of Protonated Oligopeptides. 1: Mechanism of Amide Bond Cleavage. *J. Am. Soc. Mass Spectrom.* **2004**, *15*, 103-113.

121. Shevchenko, A.; Jenson, O. N.; Podtelejnikov, A. V.; Sagliocco, F.; Wilm, M.; Vorm, O.; Mortensen, P.; Shevchenko, A.; Boucherie, H.; Mann, M. Linking Genome and Proteome by Mass Spectrometry: Large-scale Identification of Yeast Proteins from Two Dimensional Gels. *Proc. Natl. Acad. Sci. USA*. **1996**, *93*, 14440-14445.

122. Henzel, W. J.; Watanabe, C.; Stults, J. T. Protein Identification: The Origins of Peptide Mass Fingerprinting. *J. Am. Soc. Mass Spectrom.* **2003**, *14*, 931-942.

123. Dongré, A. R.; Jones, J. L.; Somogyi, Á.; Wysocki, V. Influence of Peptide Composition, Gas-Phase Basicity, and Chemical Modification on Fragmentation Efficiency: Evidence for the Mobile Proton Model. *J. Am. Chem. Soc.* **1996**, *118*, 8365-8374.

124. Zhao, H.; Adams, J. Mechanisms of Fragmentation of Cationic Peptide Ions. *Int. J. Mass Spectrom. Ion Processes*. **1993**, *125*, 195-205.

125. Baer, T.; Hase, W. L. *Unimolecular Reaction Dynamics: Theory and Experiments*. Oxford University Press: New York, 1996.

126. Gebelica, V.; De Pauw, E. Internal Energy and Fragmentation of Ions Produced in Electrospray Sources. *Mass Spectrom. Rev.* **2005**, *24*, 566-587 and references therein.

127. Lakowicz, J. R. *Principles of Fluorescence Spectroscopy*, Plenum Press: New York, 1983.

128. Hettick, J. M. *Optimization and Utilization of MALDI 193-nm Photofragment Time-of-Flight Mass Spectrometry for Peptide Sequencing*. Ph. D. Dissertation, Department of Chemistry, Texas A&M University, College Station, TX, 2003.

129. Cui, W.; Thompson, M. S.; Reilly, J. P. Pathways of Peptide Ion Fragmentation Induced by Vacuum Ultraviolet Light. *J. Am. Soc. Mass Spectrom.* **2005**, *16*, 1384-1398.

130. Tomer, K. B.; Deterding, L. J.; Guenat, C. Collisionally Activated Dissociation Spectra of Sodiated Peptides and Peptide Amides. *Biol. Mass Spectrom.* **1991**, *20*, 121-129.

131. Cerda, B. A.; Cornett, L.; Wesdemiotis, C. Probing the Interaction of Alkali and Transition Metal Ions with Bradykinin and its des-Arginine Derivatives via Matrix-assisted Laser Desorption/Ionization and Postsource Decay Mass Spectrometry. *Int. J. Mass Spectrom.* **1999**, 205-226.

132. Teesch, L. M.; Adams, J. Fragmentations of Gas-Phase Complexes between Alkali Metal Ions and Peptides: Metal Ion Binding to Carbonyl Oxygens and Other Neutral Functional Groups. *J. Am. Chem. Soc.* **1991**, *113*, 812-820.

133. Bluhm, B. K.; Shields, S. J.; Bayse, C. A.; Hall, M. B.; Russell, D. H. Determination of Copper Binding Sites in Peptides Containing Basic Residues: A Combined Experimental and Theoretical Study. *Int. J. Mass Spectrom.* **2001**, *204*, 31-46.

134. Shields, S. J.; Bluhm, B. K.; Russell, D. H. Fragmentation Chemistry of $[M+Cu]^+$ Peptide Ions Containing an N-terminal Arginine. *J. Am. Soc. Mass Spectrom.* **2000**, *11*, 626-638.

135. Macht, M.; Asperger, A.; Deininger, S. Comparison of Laser-Induced Dissociation and High-Energy Collision-Induced Dissociation Using Matrix-Assisted Laser Desorption/Ionization Tandem Time-of-Flight (MALDI-TOF/TOF) for Peptide and Protein Identification. *Rapid Commun. Mass Spectrom.* **2004**, *18*, 2093-2105.

136. Shields, S. J.; Bluhm, B. K.; Russell, D. H. Novel Method for $[M+Cu]^+$ Ion Formation by Matrix-Assisted Laser Desorption Ionization. *Int. J. Mass Spectrom.* **1999**, *182/183*, 185-189.

137. Sawyer, H. A.; Marini, J. T.; Stone, E. G.; Ruotolo, B. T.; Gillig, K. J.; Russell, D. H. The Structure of Gas-Phase Bradykinin Fragment 1-5 (RRPGF) Ions: An Ion Mobility Spectrometry and H/D Exchange Ion-Molecule Reaction Chemistry Study. *J. Am. Soc. Mass Spectrom.* **2005,** *16*, 893-905.

138. Thorne, G. C.; Ballard, K. D.; Gaskell, S. J. Metastable Decomposition of Peptide $[M + H]^+$ Ions via Rearrangement Involving Loss of the C-Terminal Amino Acid Residue. *J. Am. Soc. Mass Spectrom*. **1990**, *1*, 249-257.

139. Grese, R. P.; Cerny, R. L.; Gross, M. L. Metal Ion-Peptide Interactions in the Gas Phase: A Tandem Mass Spectrometry Study of Alkali Metal Cationized Peptides. *J. Am. Chem. Soc*. **1989**, *111*, 2835-2842.

140. Grese, R. P.; Gross, M. L. Gas-Phase Interactions of Lithium Ions and Dipeptides. *J. Am. Chem. Soc.* **1990**, *112*, 5098-5104.

141. Ballard, K. D.; Gaskell, S. J. Intramolecular [^{18}O] Isotopic Exchange in the Gas Phase Observed during Tandem Mass Spectrometric Analysis of Peptides. *J. Am. Chem. Soc.* **1992**, *114*, 64-71.

142. Fang, S.; Takao, T.; Satomi, Y.; Mo, W.; Shimonishi, Y. Novel Rearranged Ions Observed for Protonated Peptides Via Metastable Decomposition in Matrix-Assisted Laser Desorption/Ionization Time-of-Flight Mass Spectrometry. *J. Am. Soc. Mass Spectrom.* **2000**, *11*, 345-351.

143. Cann, J. R.; Liu, X.; Stewart, J. M.; Gera, L.; Kotovych, G. A CD and an NMR Study of Multiple Bradykinin Conformations in Aqueous Trifluoroethanol Solutions. *Biopolymers* **1994**, *34*, 869-78.

144. Sawyer, H. A. *Investigation of the Effect of Intra-Molecular Interactions on the Gas-Phase Conformation of Peptides as Probed by Ion Mobility-Mass Spectrometry, Gas-Phase Hydrogen/Deuterium Exchange, and Molecular*

Mechanics. Ph. D. Dissertation, Department of Chemistry, Texas A&M University, College Station, TX, 2004.

145. Renner, D.; Spiteller, G. Linked Scan Investigation of Peptide Degradation Initiated by Liquid Secondary Ion Mass Spectrometry. ***Biomed. Environ. Mass Spectrom.*** **1988**, *15*, 75-77.
146. Chan, W. C.; White, P. D. *Fmoc Solid Phase Peptide Synthesis: A Practical Approach*. Hames, D. B., Ed.; Oxford: New York, 2000.
147. London, R. E.; Matwiyoff, N. A.; Stewart, J. M.; Cann, J. R. 13C Nuclear Magnetic Resonance Study of the Cis-Trans Isomerism in X-Pro-Pro Tripeptides. ***Biochem.*** **1978**, *17*, 2277-2283.
148. Hervé, J. C.; Sarrouilhe, D. Modulation of Junction Communication by Phorphorylation: Protein Phosphatases, the Missing Link in the Chain. ***Biol. Cell*** **2002**, *94*, 423-432.
149. Straight, A. F.; Shou, W.; Dowd, G. J.; Turck, C. W.; Deshaies, R. J.; Johnson, A. D.; Moazed, D. Net1, a Sir2-Associated Nucleolar Protein Required for rDNA Silencing and Nucleolar Integrity. *Cell* **1999**, *97*, 245-256.
150. Krebs, E. G. The Growth of Research on Protein Phosphorylation. ***Trends Biochem. Sci.*** **1994**, *19*, 439.
151. Mann, M.; Jensen, O. N. Proteomic Analysis of Post-Translational Modifications. ***Nat. Biotech.*** **2003**, *21*, 255-261.

152. Ruotolo, B. T.; Verbeck, G. F.; Thompson, L. M.; Woods, A. S.; Gillig, K. J.; Russell, D. H. Distinguishing Between Phosphorylated and Nonphosphorylated Peptides with Ion Mobility-Mass Spectrometry. *J. Proteome Res.* **2002**, *1*, 303-306.

153. Ruotolo, B. T.; Gillig, K. J.; Woods, A. S.; Egan, T. F.; Ugarov, M. V.; Schultz, J. A.; Russell, D. H. Analysis of Phosphorylated Peptides by Ion Mobility-Mass Spectrometry. *Anal. Chem.* **2004**, *76*, 6727-6733.

154. Yan, J. X.; Packer, N. H.; Gooley, A. A.; Williams, K. L. Protein Phosphorylation: Technologies for the Identification of Phosphoamino Acids. *J. Chromatogr. A* **1998**, *808*, 23-41.

155. McLachlin, D. T.; Chait, B. T. Analysis of Phosphorylated Proteins and Peptides by Mass Spectrometry. *Curr. Opinion Chem. Biol.* **2001**, *5*, 591-602.

156. Mann, M.; Hendrickson, R. C.; Pandey, A. Analysis of Proteins and Proteomes by Mass Spectrometry. *Ann. Rev. Biochem.* **2001**, *70*, 437-473.

157. Carr, S. A.; Huddleston, M. J.; Annan, R. S. Selective Detection and Sequencing of Phosphopeptides at the Femtomole Level by Mass Spectrometry. *Anal. Biochem.* **1996**, *239*, 180-192.

158. Annan, R. S.; Carr, S. A. Phosphopeptide Analysis by Matrix-Assisted Laser Desorption Time-of-Flight Mass Spectrometry. *Anal. Chem.* **1996**, *68*, 3413-3421.

159. Chalmers, M. J.; Håkansson, K.; Johnson, R.; Smith, R.; Shen, J.; Emmett, M. R.; Marshall, A. G. Protein Kinase A Phosphorylation Characterized by Tandem

Fourier Transform Ion Cyclotron Resonance Mass Spectrometry. *Proteomics* **2004**, *4*, 970-981.

160. Chalmers, M. J.; Kolch, W.; Emmett, M. R.; Marshall, A. G.; Mischak, H. Identification and Analysis of Phosphopeptides. *J. Chromatog. B* **2004**, *803*, 111-120.
161. Beavis, R. C.; Linder, J.; Grotemeyer, J.; Schlag, E. W. Sample-Matrix Effects in Infrared Laser Neutral Desorption, Multiphoton-Ionization Mass Spectrometry. *Chem. Phys. Lett.* **1988**, *146*, 310-314.
162. Gusev, A. I.; Wilkinson, W. R.; Proctor, A.; Hercules, D. M. Improvement of Signal Reproducibility and Matrix/Comatrix Effects in MALDI Analysis. *Anal. Chem.* **1995**, *67*, 1034-1041.
163. Preston, L. M.; Murray, K. K.; Russell, D. H. Reproducibility and Quantitation of Matrix-Assisted Laser Desorption Ionization Mass Spectrometry: Effects of Nitrocellulose on Peptide Ion Yields. *Biol. Mass Spectrom.* **1993**, *22*, 544-550.
164. Koomen, J. M.; Russell, W. K.; Hettick, J. M.; Russell, D. H. Improvement of Resolution, Mass Accuracy, and Reproducibility in Reflected Mode DE-MALDI-TOF Analysis of DNA Using Fast Evaporation-Overlayer Sample Preparations. *Anal. Chem.* **2000**, *72*, 3860-3866.
165. Cotter, R. J. *Time of Flight Mass Spectrometry Instrumentation and Applications in Biological Research*. American Chemical Society: Washington DC, 1997.

166. *CRC Handbook of Biochemistry and Molecular Biology. Proteins – Volume I* 3rd Ed. Fasman, G. D., Ed.; CRC Press: Cleveland, OH, 1976.

APPENDIX A

SIMION RENDERINGS

RENDERING Page

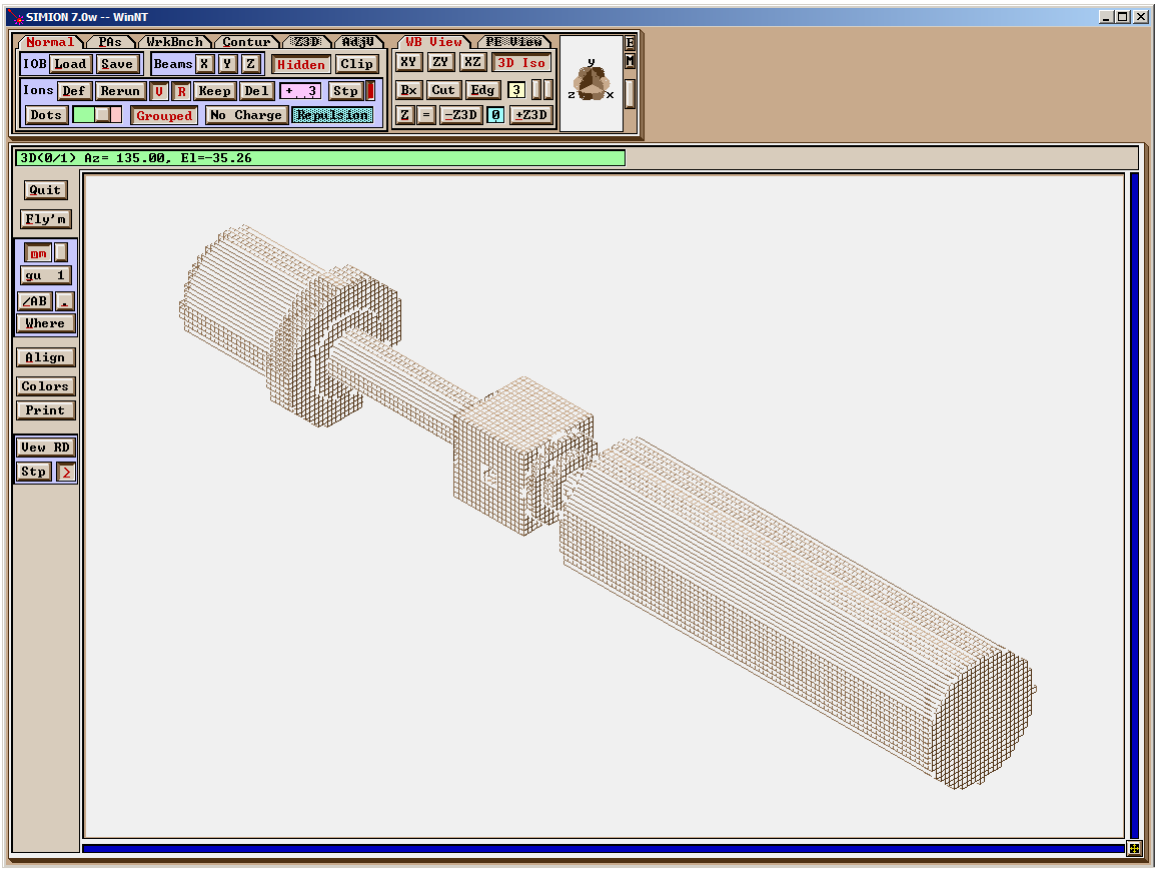
SIMION 7.0w -- WinNT
Normal
PAs
WrkBnch
Contur
Z3D
AdjU
VB View
PE View
IOB
Load
Save
Beams
X
Y
Z
Hidden
Clip
Ions
Def
Rerun
U
R
Keep
Del
Stp
Dots
Grouped
No Charge
Repulsion
XY
ZY
XZ
3D Iso
Bx
Cut
Edg
Z
=
-Z3D
+Z3D
3D<0/1> Az= 135.00, El=-35.26
Quit
Fly'm
gu 1
Where
Align
Colors
Print
Vew RD
Stp

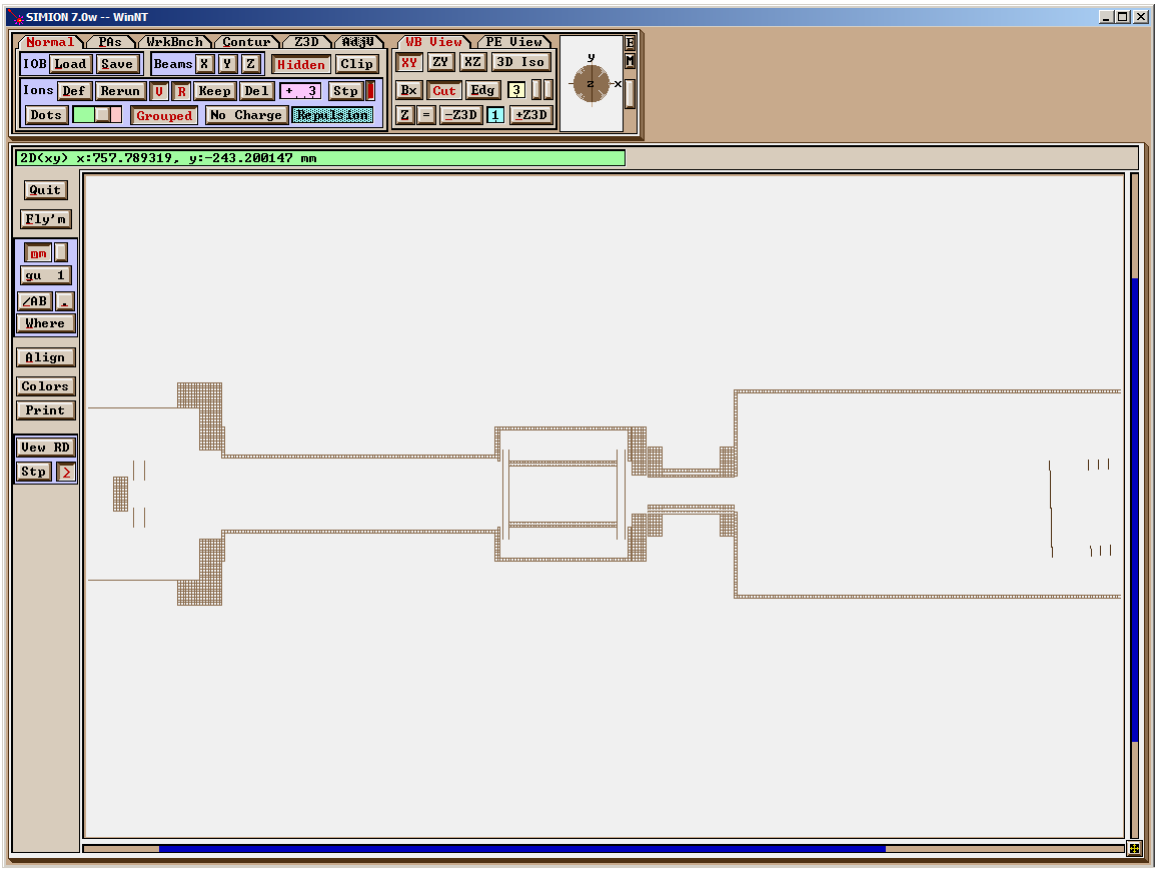
SIMION 7.0w -- WinNT
Normal
PAs
WrkBnch
Contur
Z3D
AdjU
WB View
PE View
IOB
Load
Save
Beams
X
Y
Z
Hidden
Clip
Ions
Def
Rerun
U
R
Keep
Del
Stp
Dots
Grouped
No Charge
Repulsion
XY
ZY
XZ
3D Iso
Bx
Cut
Edg
Z
=
-Z3D
+Z3D
2D(xy) x:757.789319, y:-243.200147 mm
Quit
Fly'm
mm
gu 1
∠AB
Where
Align
Colors
Print
Vew RD
Stp

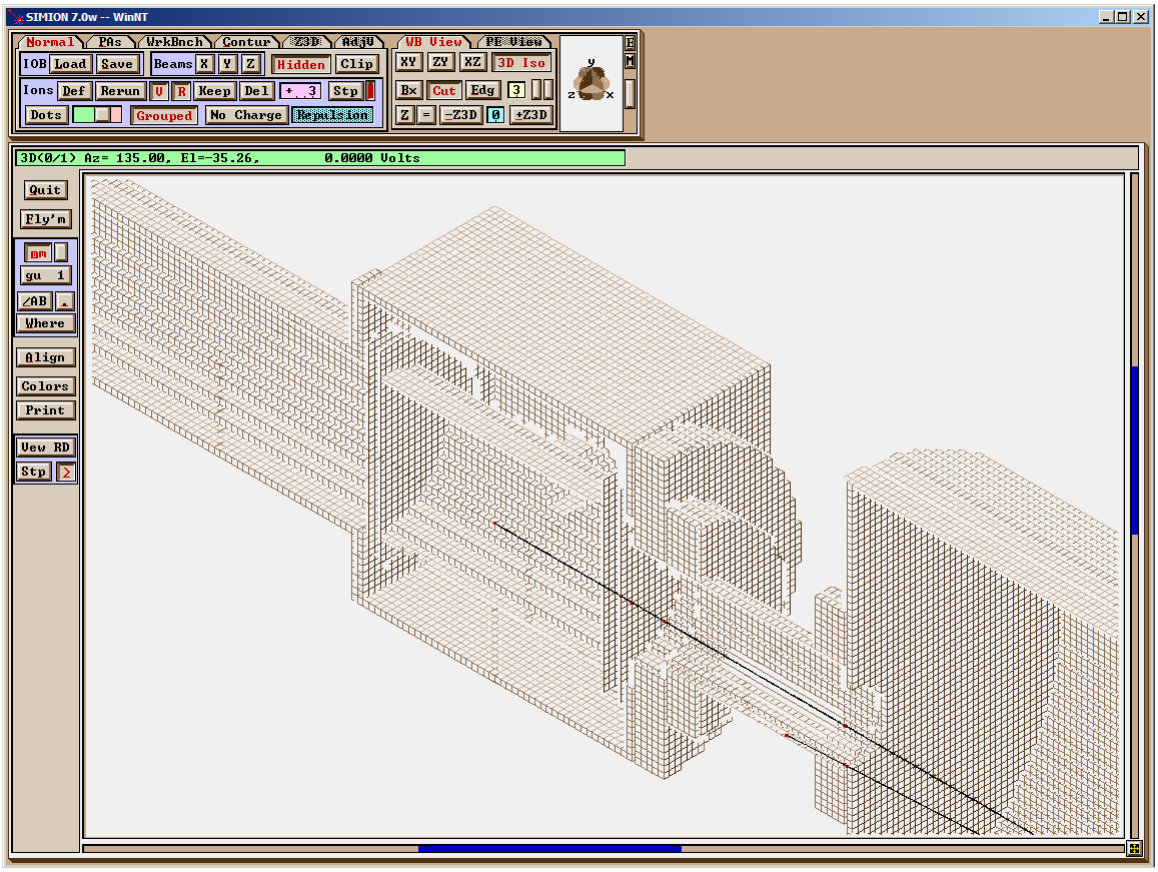
SIMION 7.0w -- WinNT
Normal
PAs
WrkBnch
Contur
Z3D
AdjU
VB View
PE View
IOB
Load
Save
Beams
X
Y
Z
Hidden
Clip
Ions
Def
Rerun
U
R
Keep
Del
Stp
Dots
Grouped
No Charge
Repulsion
XY
ZY
XZ
3D Iso
Bx
Cut
Edg
-Z3D
+Z3D
3D<0/1> Az= 135.00, El=-35.26,
0.0000 Volts
Quit
Fly'm
gu 1
Where
Align
Colors
Print
Vew RD
Stp

APPENDIX B

INSTRUMENT DRAWINGS

DRAWING Page

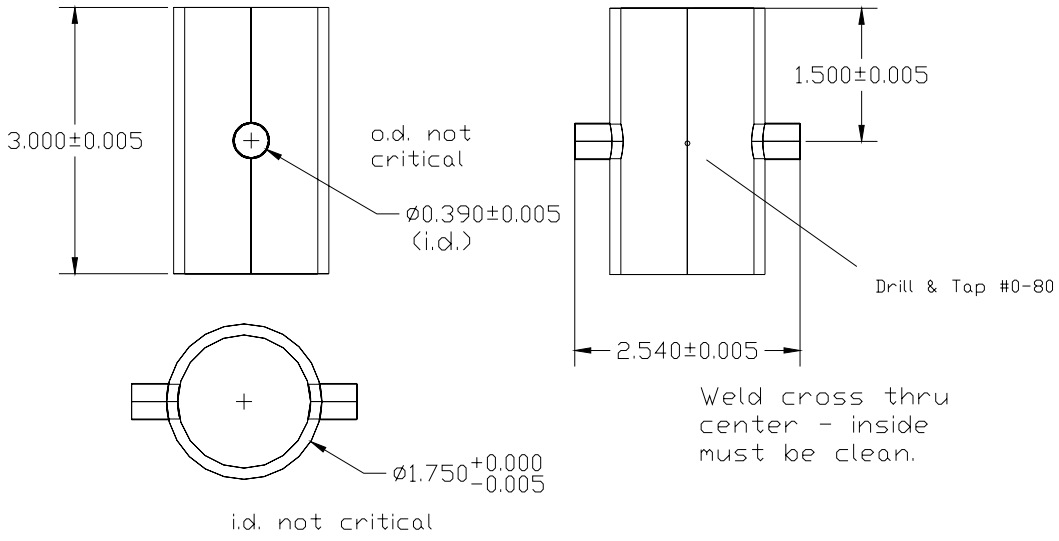
3.000±0.005
o.d. not
critical
ø0.390±0.005
(i.d.)
1.500±0.005
Drill & Tap #0-80
2.540±0.005
Weld cross thru
center - inside
must be clean.
ø1.750 +0.000 −0.005
i.d. not critical

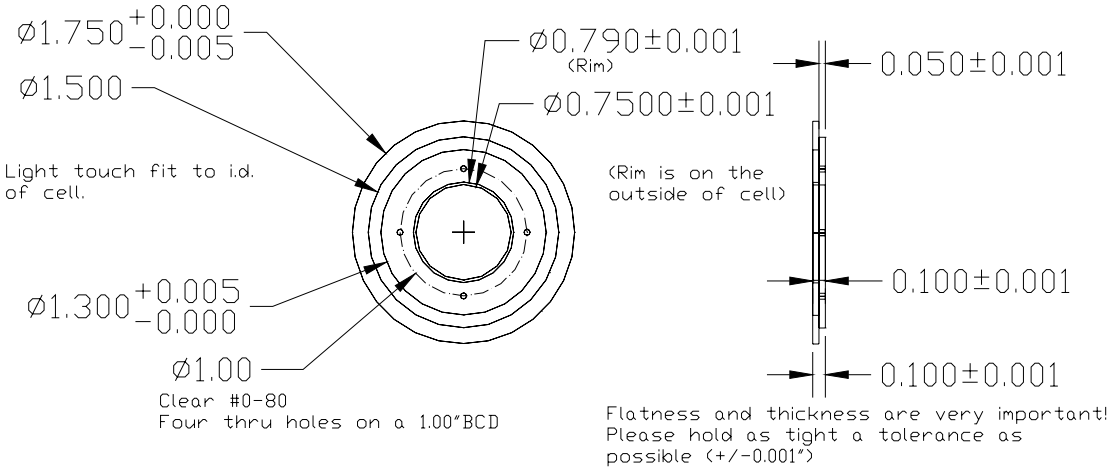
Ø1.750 +0.000 −0.005
Ø1.500
Light touch fit to i.d. of cell.
Ø1.300 +0.005 −0.000
Ø1.00
Clear #0-80
Four thru holes on a 1.00"BCD
Ø0.790±0.001
(Rim)
Ø0.7500±0.001
(Rim is on the outside of cell)
0.050±0.001
0.100±0.001
0.100±0.001
Flatness and thickness are very important!
Please hold as tight a tolerance as possible (+/-0.001")

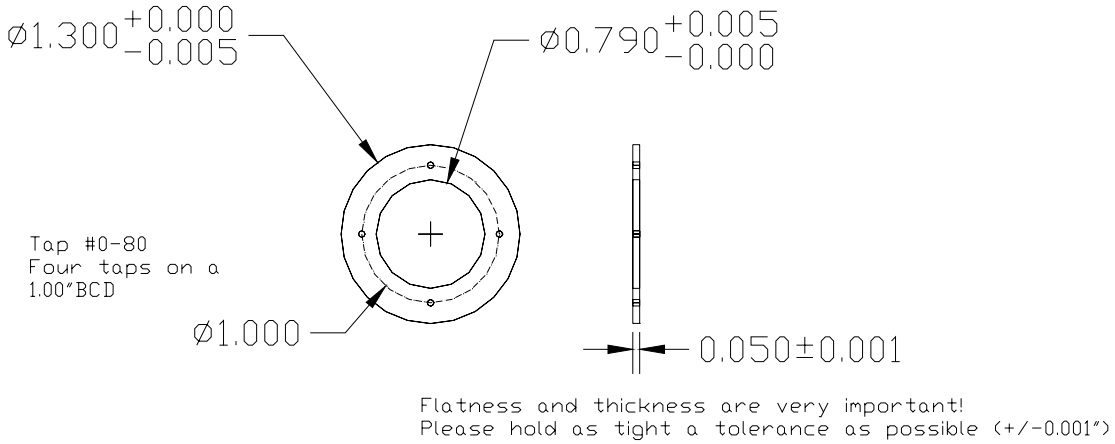
Ø1.300 +0.000 −0.005
Ø0.790 +0.005 −0.000
Tap #0-80
Four taps on a
1.00"BCD
Ø1.000
0.050±0.001
Flatness and thickness are very important!
Please hold as tight a tolerance as possible (+/-0.001")

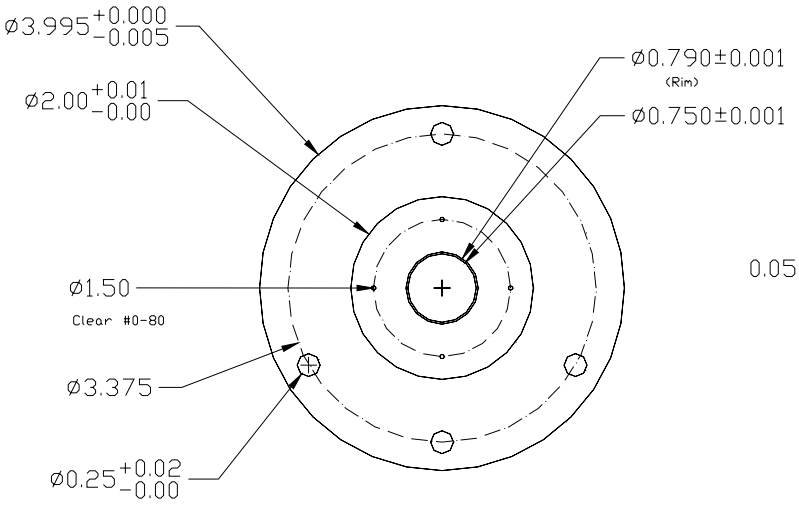

Three 1/4" thru holes on a 3.3.75"BCD,
and a fourth bisecting two others.

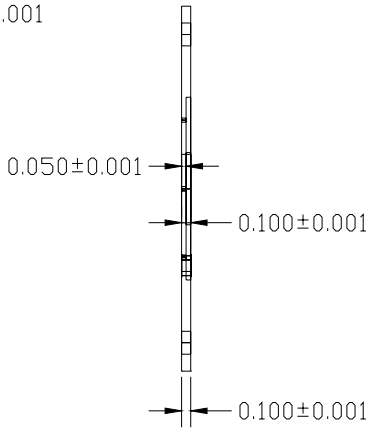

Flatness and thickness are very important!
Please hold as tight a tolerance as possible (+/-0.001")

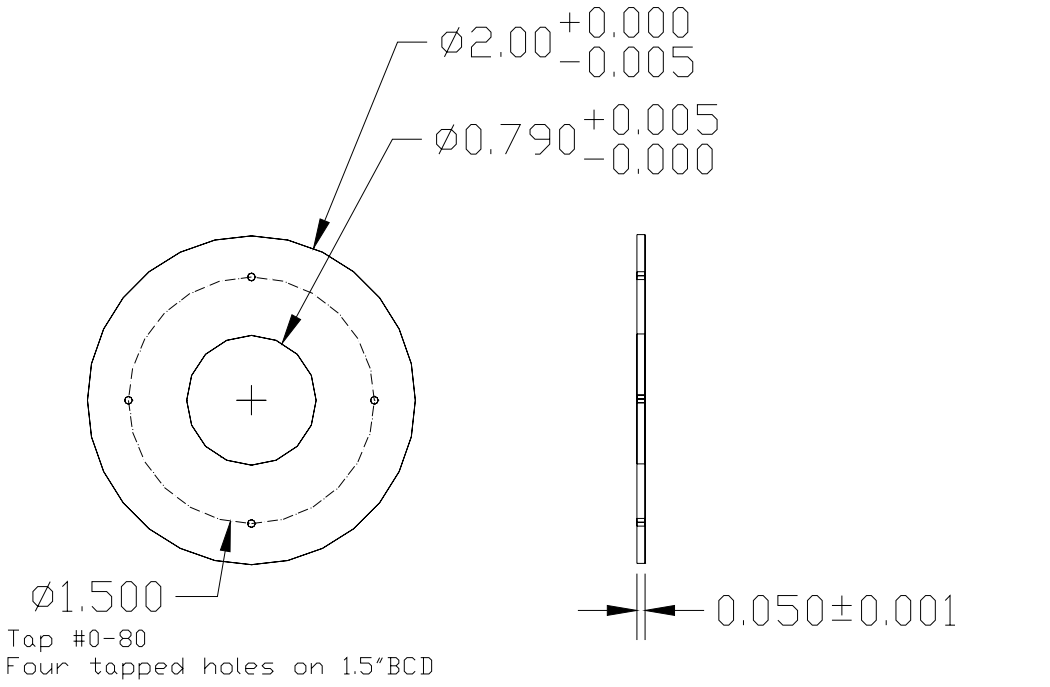

Tap #0-80
Four tapped holes on 1.5"BCD

Flatness and thickness are very important!
Please hold as tight a tolerance as possible (+/-0.001")

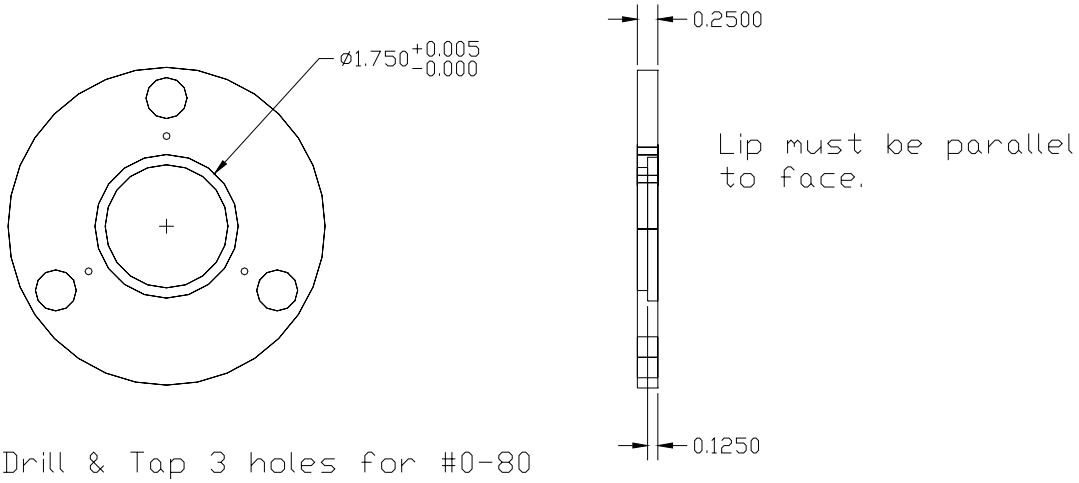

Drill & Tap 3 holes for #0-80 on 2.200" BCD on part provided.

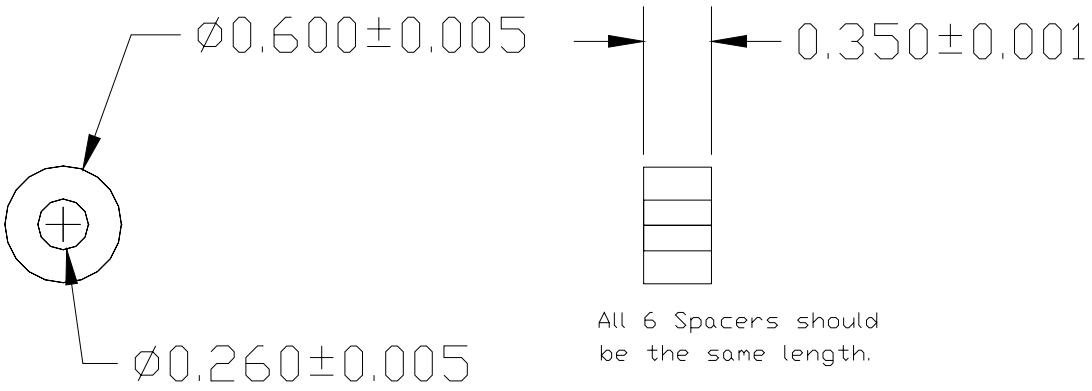
Ø0.600±0.005
0.350±0.001
Ø0.260±0.005
All 6 Spacers should
be the same length.

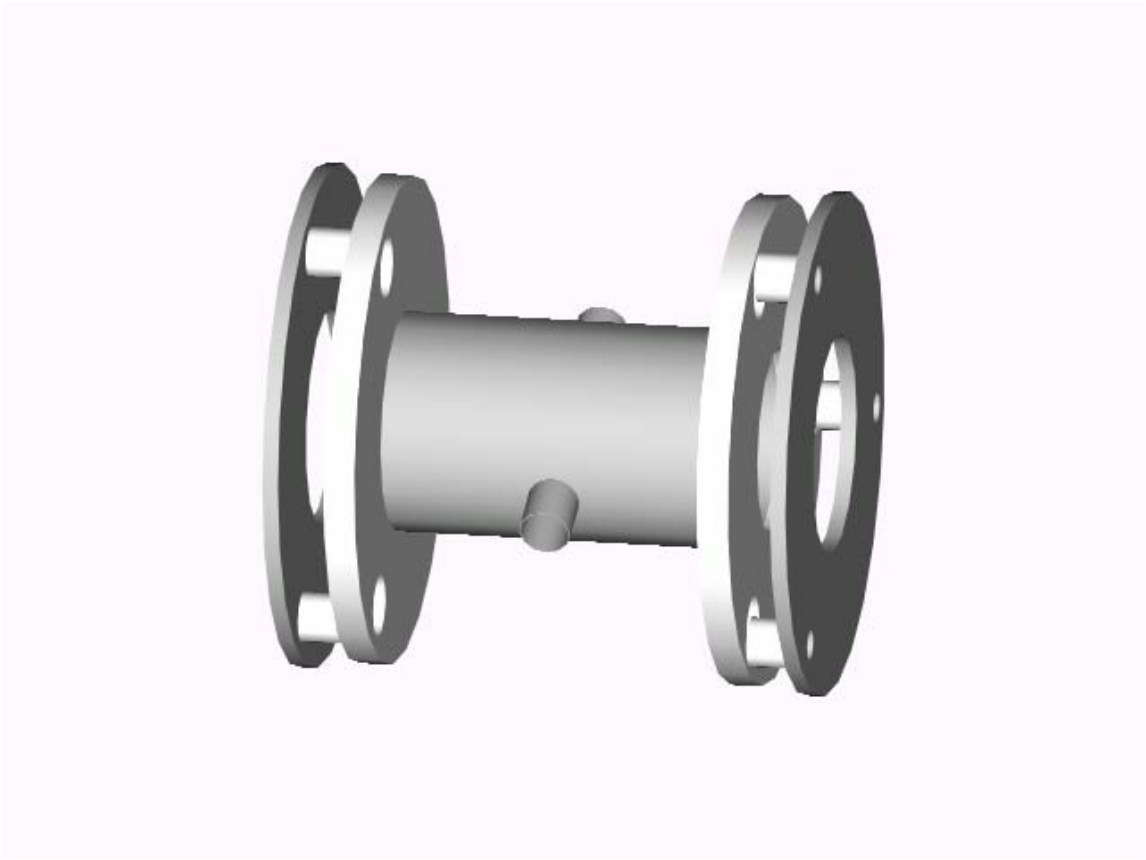

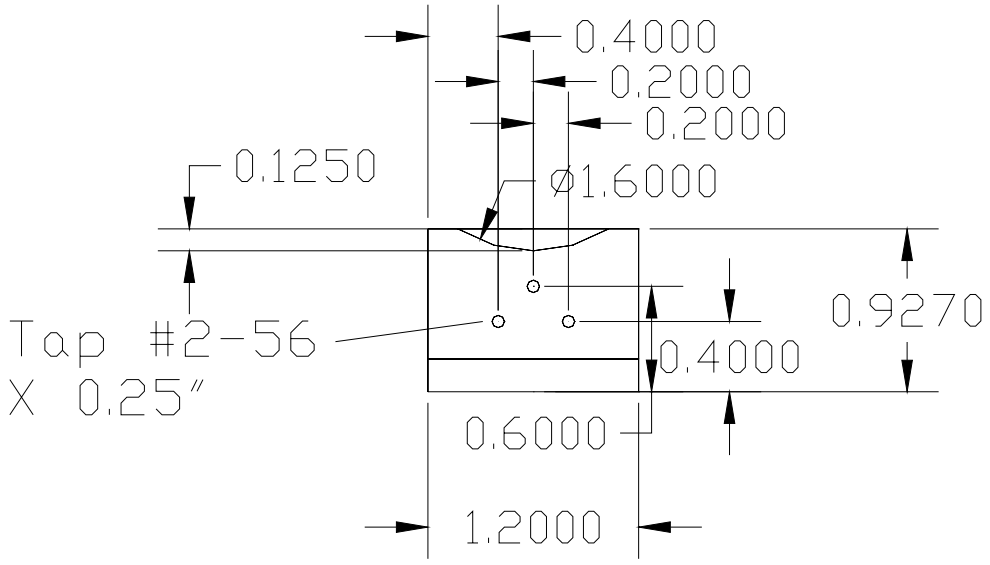

Front view

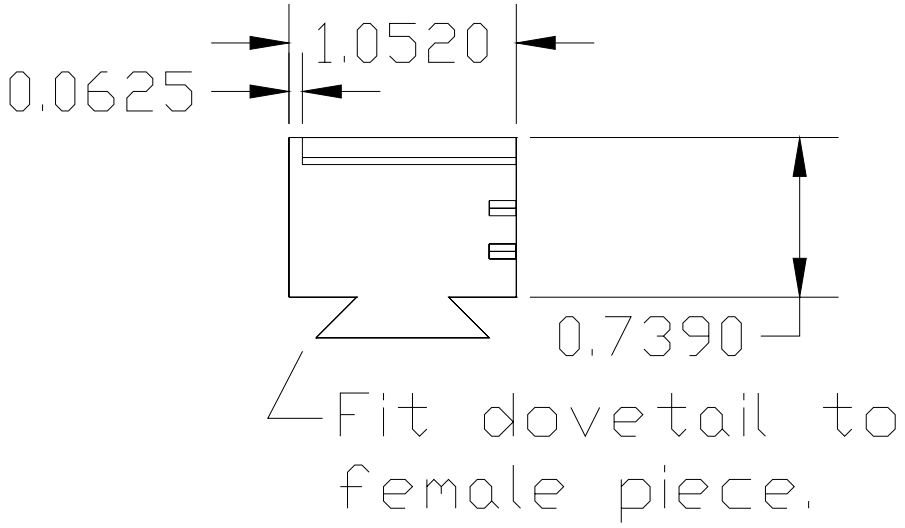

Side view

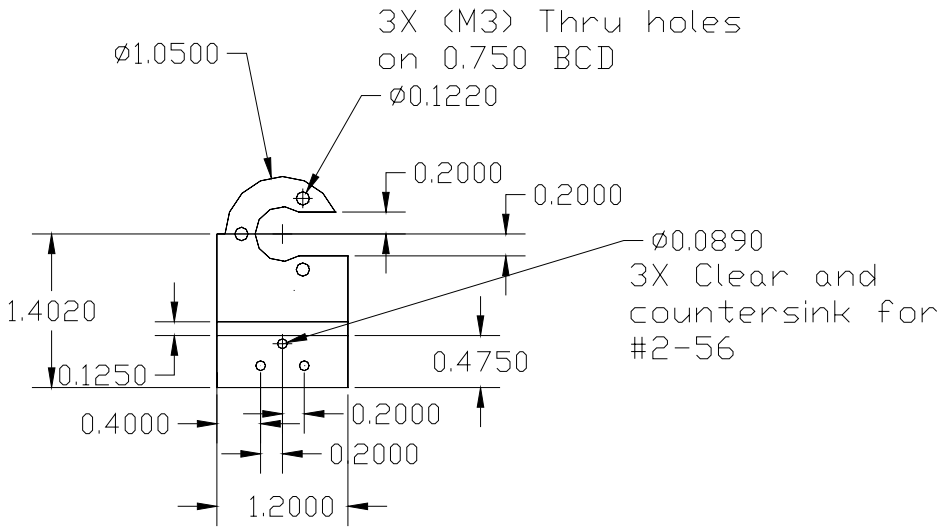

Front view

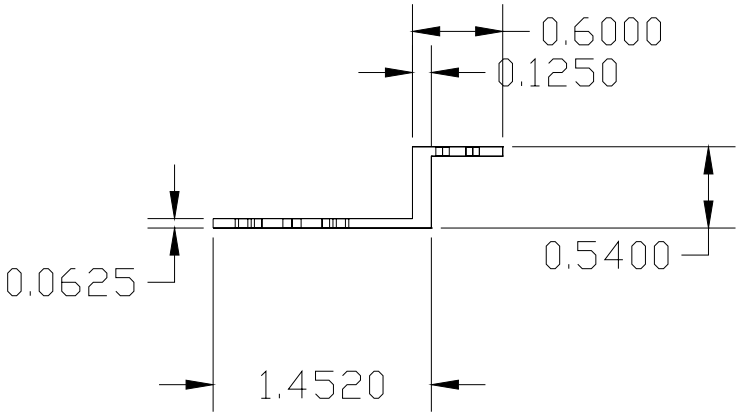

Side view

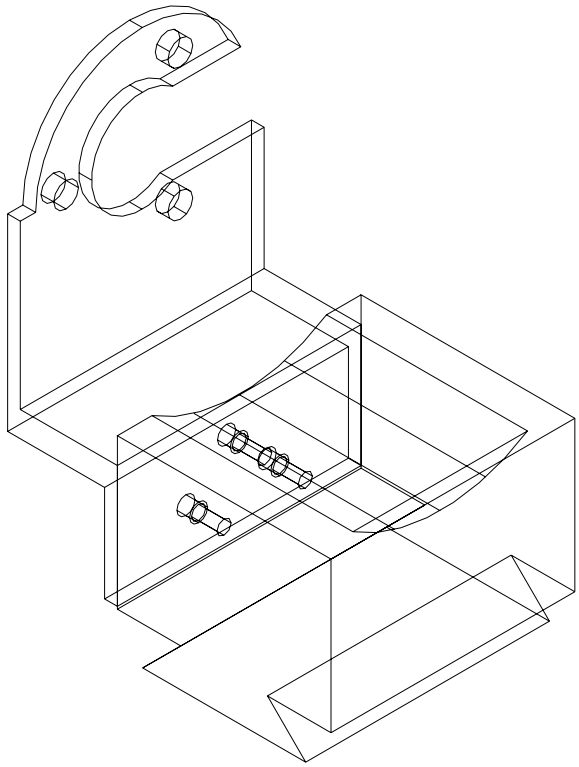

APPENDIX C

To Whom It May Concern:

I am a doctoral student at Texas A&M University and am writing for permission to include in my dissertation part of the material from Methods in Enzymology Volume 402, Chapter 6. The dissertation will be made available to the public on the Web through Texas A&M University Libraries.

In addition the dissertation will be microfilmed by UMI Dissertation Publishing (ProQuest Information and Learning), and copies of the dissertation will be sold on demand. Please supply a signed letter granting me permission to use the work. You can email the permission to jmorgan@mail.chem.tamu.edu.

Thank you for your help.

Sincerely,

Joseph W. Morgan
Department of Chemistry
Texas A&M University

Dear Mr. Morgan

We hereby grant you permission to reprint the material mentioned below at no charge **in your thesis, in print and on the Texas A&M University web site** subject to the following conditions:

1. If any part of the material to be used (for example, figures) has appeared in our publication with credit or acknowledgement to another source, permission must also be sought from that source. If such permission is not obtained then that material may not be included in your publication/copies.
2. Suitable acknowledgment to the source must be made, either as a footnote or in a reference list at the end of your publication, as follows:

   > "Reprinted from Publication title, Vol number, Author(s), Title of article, Pages No., Copyright (Year), with permission from Elsevier".

3. Reproduction of this material is confined to the purpose for which permission is hereby given.
4. This permission is granted for non-exclusive world **English** rights only. For other languages please reapply separately for each one required.
5. Should your thesis be published commercially, please reapply for permission. This includes permission for UMI to supply single copies, on demand, of the complete thesis. Should your thesis be published commercially, please reapply for permission.

Yours sincerely

Helen Gainford
Rights Manager

VITA

Joseph William Morgan
1014 Sunset Strip
Excelsior Springs, MO 64024
(816) 630-1931

EDUCATION

2000-2005	Ph.D. (12/2005), Texas A&M University, College Station, TX Chemsitry, GPA: 3.85/4.00
1996-2000	B.S. (05/2000), Truman State University, Kirksville, MO Chemistry (ACS Certified), GPA: 3.41/4.00

PUBLICATIONS

Morgan, J. W.; Hettick, J. M.; Russell, D. H. Peptide Sequencing by MALDI 193-nm Photodissociation TOF MS. *Meth. Enzymol.* 2005, *402*. (In press)

SELECTED PRESENTATIONS

Joseph W. Morgan, J. Garrett Slaton, and David H. Russell, "Prompt 193-nm Photodissociation of Analogous Synthetic Peptides by MALDI TOF-TOF," 53rd ASMS Conference on Mass Spectrometry and Allied Topics, San Antonio, TX, 2005.

Joseph W. Morgan and David H. Russell, "Novel MALDI Tandem Time-of-Flight Instrumentation for 193-nm Photodissociation of Peptides," 52nd ASMS Conference on Mass Spectrometry and Allied Topics, Nashville, TN, 2004.

Joseph W. Morgan, Justin M. Hettick, J. Garrett Slaton, and David H. Russell, "Photodissociation Time-of-Flight Mass Spectrometry: A Tool for Proteomics," 15th Sanibel Conference on Mass Spectrometry, Sanibel Island, FL, 2003.